Republic of Iraq
Ministry of Higher Education
and Scientific Research
University of Babylon
College of Sciences for women

study of Random Laser Action Parameters of Compound Cavity

A Thesis
Submitted to the Council of the College of Sciences for Women,
University of Babylon
In Partial Fulfillment of the Requirements for the Degree of
Doctor of Philosophy in Laser Physics and its Applications

By

Majid Flayeh Haddawi

B. Sc. Physics 2001
M. Sc. Physics 2017

Supervised by

Prof. Dr. Jassim Mohammed **Prof. Dr. Mahri Hamidi**

2023 A.D. 1445 A.H.

بِسْمِ اللَّهِ الرَّحْمَنِ الرَّحِيمِ

وَالرَّاسِخُونَ فِي الْعِلْمِ يَقُولُونَ آمَنَّا بِهِ كُلٌّ مِّنْ عِندِ رَبِّنَا

صَدَقَ اللهُ العَظيم

سورة آل عمران الاية (7)

Supervisor Certification

We certify that this thesis entitled **(study of Random Laser Action Parameters of Compound Cavity) was prepared by Majid Flayeh Haddawi** under our supervision at laser physics department, college of sciences for women, university of Babylon as a partial fulfillment of the requirements for the degree of doctor of philosophy in laser physics and its applications.

Signature:
Name: **Dr. Jassim Mohammed Jassim**
Title: Professor
Address :Dept. of laser physics, College of sciences for women, University of Babylon
Date: / /2023

Signature:
Name: **Dr .S. M. Hamidi**
Title: Professor
Address : Head of magneto-plasmonic lab of Laser and Plasma Research Institute, Shahid Beheshti University, Tehran.
Date: / /2023

In view of the available recommendations, I forward this thesis for debate by the examination committee.
Signature:
Name: **Prof. Dr. Jinan Ali Abd**
Title: Head of the department
Address: Dept. of laser physics, College of sciences for women, University of Babylon.
Date: / /2023

Dedication

To those who left us and I know That their soul always beside me my mother, father, and brother.

To my brothers and sisters .

To my dearest wife ,

To the pleasure of my heart, My sons ,Ahmed ,Moamal ,Mayar, to say thanks. All of you in the folds of my heart.

Acknowledgments

At first, praise is to Allah, the Lord of all worlds, for who I am. May Allah's Blessings and Peace be upon the most honored of Messengers, our prophet Muhammad, His Pure Immediate family.

Then, I would like to extend my thanks and gratitude tomy supervisors Prof. Dr. Jassim Mohammed Jassim and Prof. Dr .S. M. Hamidi, For their valuable contribution, continuous help, encouragement ,and precious time that they provided during the research period

All thanks and gratitude are to the head of the Department of Laser physics and its applications, Prof. Dr. Jinan Ali Abd .

I also extend my thanks and gratitude to all the professors of the Department of Laser Physics and its applications for their scientific efforts and their unlimited support, whether in the study or research stage.

My thanks and appreciation are to the my brother Dr. Saddam Flayeh Haddawi, and the Dr. Nizar Salem Shannan, Dr. Ahmed Kazem Khudairi and Mr. Rafea Tuama Ahmed, for their unlimited support for me throughout the research period.

Abstract

In this study, to prepare liquid and solid random laser emission media in the form of composite cavities on the performance of random laser systems has been addressed, in particular the intensity of their emission spectrum, the width of the emission spectrum (FWHM), and the laser threshold.

In the first part of the work, the effect of liquid composite cavities the performance of random lasers have been studied .The first factor discussed the thermal blooming phenomena by using a CW laser with a wavelength of 405 nm and an optical power of 100 mW vertically focused on a quartz cuvette containing dye solution with different nanoparticles, to generate thermal cavitation. We observed that SPM-typical far-field loops suddenly shifted into a completely different diffraction pattern when the dye solution was heated beyond self-phase modulation (SPM) ,this change in new diffraction patterns is generated by the formation of bubbles . In addition, we observed the effect of (Ag, Fe_2O_3 and Ag: Fe_2O_3) NPs on the speed of formation of the bubbles and their number increases with the increase the concentration of nanomaterials . After that, the effects of thermal cavity on random laser properties were studied ,the results showed that the properties of the random laser are affected by thermal cavity significantly, also was studied films for Au nanoparticles diffused in a glass substrate ,using the physical vapor deposition and with spin coating with the three different concentrations ,(10^{-3} ,10^{-4} ,10^{-5}) M of Rhodamine 6G dye mixture and PVP polymer. The results showed that the dye's active media with a middle concentration (10^{-4})had the best effect and multi wavelength separate lasing compared with low and high concentrations due to solid coupling appearing in the median concentration. This led to enhanced peak intensity and reduced lasing threshold and FWHM,

After that, Red and green lasers was attained by a multi-layered 2D structure onto a curved glass substrate and a gold nanostructure with rhodamine dye. For this purpose, a layer of Kapton tape was attached to the CCD by applying pressure to get a two-dimensional structure and transfer onto the glass, then the gold nanostructure was covered inside that glass substance. The properties of the random laser were studied on different sides, The results showed an efficient coherent random, and the result of the convex surface inward was better than the outside in terms of intensity and pulse width, as well as the laser threshold from 0.85 to 0.35mJ. This indicates that the photons are scattered from the inner surface and this is a clear indication of the increase in the gain in this medium. Further, this improvement in laser output is attributed to a change in the 2D periodic square pattern, causing reduced distance between them, so that photons can stay in the medium as long as possible.

The cavity consists of new FeB based two dimensions' magneto-plasmonic structure which cover by gold thin film and Rhodamine 6G from the bottom and top respectively propose as new kind of random laser substance under the external magnetic field. The results showed a higher intensity in the emission spectra with a lower lasing threshold and full width at half maximum (FWHM) according to the effects of the external magnetic field on the sample ,observed enhancement in the output emission spectra with decreased laser threshold from 0.66 mJ to 0.35 mJ, and also the FWHM decreased from 7.8 to 4 nm.

The toroidal resonator was fabricated on a glass base to form composite cavities. A silica glass material with a thickness of (2 mm) was used, a circular hole with a diameter of (9 mm) and a depth of (2 mm) was drilled, then this toroidal resonator was placed on a glass substrate to form a cavity.

. Then this annular cavity was coated with gold using a dip-coating method in a nano solution consisting of (water + gold) 10 times. Then this annular cavity was filled with a dye (RhB) dissolved in pure water with a polymer (pvp) with Ag at different concentrations. It was found that an increase In the emission intensity (from 19141 to 39420.64), the decrease in laser threshold (from 0.68 to 0.34 mJ), and the decrease in FWHM (from 7.4 to 3 nm) with increasing Ag wire concentration.

Table of Contents

LIST OF SYMBOLS

Symbol	Description	Unit
σ_{SR}	Scattering cross section for Rayleigh approximation	cm^2
λ_0	Wavelength of incident photon	m
R	Particle radius	m
n_p	Refractive index of nanoparticle	---
n_m	Refractive index of surrounding medium	---
α_n	Scattering coefficient	---
l_t	Transport mean free path	
$k = 2\pi/\lambda$	Wave vector	m^{-1}
l_G	Generation length	m
l_P	Mean path length	m
γ	Spatial coherence	---
n	Average photon number	---
l_g	Gain length	---
l_s	Scattering mean free path	m
ρ	Particle density	cm^{-3}
σ_s	Scattering cross section	m^2
W	Full width at half maximum of backscattering cone	---
θ	Scattering angle	---
l_{amp}	Amplification length	m
n_g	The density of gain molecules	cm^{-3}
σ_e	Emission cross section	cm^{-2}
$\Delta\lambda$	FWHM	nm
n_{eff}	the effective refractive index of the waveguide	---
Λ	the period of the corrugation	---
C	Light velocity	m/s
τ	The lifetime of the upper level of random laser	S
φ	excitation spot beam diameter	m
σ_a	Absorption cross section	cm^2
l	Cuvette thickness	Mm
I_0	transmitted intensity through pure solvent without gain or scatterers	---
I	transmitted intensity through pure solvent with gain and scatterers	---
N_{th}	Threshold of population inversion	m^3
E_{th}	Threshold of pumping energy	Joule
h	Plank's constant	J.s
ν_p	Frequency of pumping photon	Hz

g_{th}	Gain coefficient	m^{-1}
A_{21}	spontaneous emission rate	s^{-1}
a.u.	Arbitrary unit	---
l_a	Absorption length	m
λ_{peak}	Wavelength of peak emission	nm
τ_r	Residence time of photon inside random medium	S

LIST OF ABBREVIATION

Abbreviations	Description
NPs	Nanoparticles
(RGB)	red-green blue
FWHM	Full width at half maximum
Ag	Silver
Au	Gold
LSPR	localized surface plasmon resonance
Rh6G	Rhodamine 6G
Al	Aluminum
ZnO	Zinc oxide
SiO_2	Silicon dioxide
Si	Silicon
PDMS	Polydimethylsiloxane
DP	dye-doped polymer
NSs	Nanostars
NRs	Nanorods
RhB	Rhodamine B
Al_2O_3	Aluminum oxide
FRET	Fluorescence resonance energy transfer
NTs	Nanotubes
$AgNO_3$	Silver nitrate
NaOH	Sodium hydroxide
PVP	Polyvinylpyrrolidone
RL	Random laser
PMMA	Polymethylmethacrylate
GFs	graphene flakes
PVA	Polystyrene
LEDs	Light emitting diodes
ASE	Amplified spontaneous emission
MNPs	Metallic nanoparticles
SPR	Surface plasmon resonance
FeB	Iron boron
(PVD)	Physical vapor deposition
(IC)	integrated circuit

DBR	Distributed Bragg resonators
DFB	Distributed Feed Back
Fe_2O_3	iron oxide
0D	Zero dimension
1D	One dimension
2D	Two dimension
SEM	Scanning electron microscopy
TEM	Transmission electron microscopy

LIST OF TABLES

LIST OF FIGURES

Chapter One

Introduction

1.1 Introduction

The random laser is a unique form of laser that relies on the light scattering phenomena derived from diverse disordered media, including dyesolutions containing suspended nanoparticles (NPs) [1], polymer doped dye films with nanoparticles and semiconductor nano-powders [3], etc. In these types of lasers, the dye can play an essential role because it has a broad fluorescence spectrum, and its efficiency can be enhanced several times when it is mixed with NPs [4]. There are many kinds of random lasers such as multi-wavelength red-green blue (RGB) random laser [5], optofluidic random laser [6], tunable random lasers [7] and plasmonic random lasers [8,9]. The scattered NPs electric field near the can be significantly enhanced by utilizing novel metal NPs such as gold and silver. Many researches have shown that such enhancement is essential to produce a very effective excitation state for NP active, effective centers to provide high lasing gain [10, 11]. The multiple scattering in a random laser system serves as a feedback mechanism for supporting the stimulated emission of radiation, while it was considered a loss in normal laser[12]. Thus, the scattering has been turned from an annoyance in the conventional laser to a tool in random laser systems. The incident light on a random system is experiencing multiple scattering before leaving that system. The random paths of the photons inside the laser medium due to this multiple scattering lead to a delay in the stay of the photon inside the gain medium and thus increasing the likelihood of it being amplified, and when the gain exceeds the loss, it can be obtained the so-called random laser [13]. Random laser systems have many features in common with conventional lasers, such as a

threshold of lasing action and narrow frequency. Despite these common characteristics, the main difference between this type of laser and the rest of the lasers remains in the mechanism of confining the light within the active medium [14]. Where the process of confining light within the active media in known lasers is by means of the reflection process and this is done by using two external mirrors with high reflectivity while in random lasers the process of confining is carried out by the multiple scattering in random systems and this is done by scattering centers that are implanted within the active media [15]. There are two main techniques to get random lasing, the first is using a thin film (solid), while the second is using a liquid medium. But the optical confinement, repeatability, and stability in solid-state random lasers are sometimes better than that of dye random lasers [16 ,17] [16, 17]. For this reason, the scientists are drifted to use semiconductor based nanoparticles (NPs) like metal/ semiconductor in the dye media. [18].

Depending on the feedback mechanism, Random lasers can be categorized into incoherent (non-resonant) and coherent (resonant). In the incoherent feedback type, scattering increases the paths of light and feedback is provided by an increase of the photon lifetime in the system. In the coherent feedback type, interference effects appear evidently where the photon returns to its first position forming a closed path [19].

Nowadays, there is a tunable random laser based on liquid crystals[20 ,21], which possesses the special features of tunability or flexible controllability in their lasing characteristics (e.g., energy threshold or lasing wavelength) by thermal .electric and optical [22-25]. approaches. By adding the liquid crystals into the disordered nanostructures, the wavelength of random lasing can be tuned by heat or electricity, which also, enables us to bring the random laser above and below its threshold by temperature tuning of the diffusion constant. This phenomenon

happens because the liquid crystal behaves as a normal isotropic liquid [26]. Thus, the refractive index can be tuned by changing the temperature and the electric field [27 ,28], However, all of them are in the middle or high threshold power. There is an open question until now about the low threshold power and tunable lasing in these areas

Experimental studies conducted on random lasers have demonstrated the importance of selecting nanomaterials that act as dispersal centers because of their significant impact on the performance and operation of this type of laser[29]. Therefore, in this work, great emphasis will be given to the experimental aspect, where the effect of choosing the liquid and solid composite cavity, and their influence on the random laser properties for choosing the appropriate medium for this system will be studied. This effect on emission spectrum intensity, laser threshold, FWHM, the appearance of spikes and number will be discussed as well as its effect on other factors . In addition to studying the effect of nanomaterials on the work of random lasers, which is considered the main player in this study, some determinants that affect the performance of random lasers will also be discussed and studied, As well as the use of two lasers at the same time pulsed and continuous. The effect of the concentration of the nanomaterial (scattering centers) on the random laser output and the factors that affect its occurrence will be discussed, as the scattering centers are divided into two types: weak and strong based on the amount of nanomaterial added to the same dye concentration. The transition from incoherent random laser to coherent random laser by composite cavity and increasing the concentration of scattering centers of the same nanomaterial in terms of as well as the blending process between two nuclear materials will also be discussed.

1.2 Literature Review

In recent periods, random lasers have been widely studied by many researchers and authors, where a group of them studied the working principle of this type of laser while others studied its characteristics and applications, and another group discussed the outputs of this type of laser. while the fourth group went to use different random modes These studies will be dealt with in some detail, especially those related to our work

In 2010, Murai, Shunsuke, *et al*. [30]. Focused on scattering characteristics of noble NPs, one of the memorable lineaments related to localized surface Plasmon resonance, and depict the NPs application as components of a cavity random laser, and confirm the advantages of scatterers in metallic NPs compared to dielectric NPs, emphasizing an excellent scattering efficiency compared to dielectric NPs. The silver (Ag) and gold (Au) have (LSPR) in the visible range, for this reason, attention to only noble metals. The author also sumed up the highlight on a recently explained surface plasmon-based nanolaser, in which a single NPs acts as a cavity.

In 2011, Liling Yang *et al.* [31]. studied the effect of dye concentration and nanoparticle concentration on random laser behavior in a rhodamine 6G (R6G) dye dissolved in ethylene glycol solution with nanoparticles (Al) as scatterers. The dye concentration was chosen to be from 0.02M to 0.08M while the concentration of Al NPs was from 0.0015M to 0.009M. The pumping energy was changing from 0.05 mJ to 3.6 mJ. They have noticed that when the pumping energy is 0.05 mJ, the emission spectrum is broadband fluorescence, but when the pumping energy has been increased to reach 0.6 mJ, the spikes begin to appear accompanied by a decrease in

the value of the FWHM. When the pumping was increased above the lasing threshold the emission intensity continued to increase while the FWHM was kept at a constant. They also observed when the dye concentration was increased to 0.008 M with the Al NPs is fixed at 0.0015M, the number of spikes increased with pumping energy compared to the first state when dye concentration was 0.002 M. Also the influence of various Al concentrations with kept dye concentration at 0.005M is studied. The maximum of the emission peak as a function of the pump energy, low lasing threshold, and narrowed FWHM can be observed with increasing the Al NPs concentrations .

In 2011, Zhai, Tianrui, *et al*. [32] prepared a new kind of active waveguide by using grating structures to distributed optical feedback arrangement for polymer random lasing. The thin film of a typical light-emitting polymer poly [(9,9-dioctylfluorenyl-2,7-diyl)-alt-co-(1,4-benzo-{2,1',3} thiadiazole)] acts both as a waveguide and the random gain medium. The grating structures are synthesis separately on top of the polymer film through interference lithography. The waveguide layer of the gain medium with high-quality provides laser emission with a narrow line width. Experimental and theoretical analysis investigation implies the possibly excellent performance of the organic distributed feedback random lasers based on the active waveguide grating structures configuration.

In 2012, Lin, Ming C., *et al*. [33]. conducted a study where they utilized atomic layer deposition to prepare cavities from ZnO films on a silicon substrate with a SiO2 layer, followed by rapid thermal annealing. They observed low threshold lasing in ZnO thin films on SiO2/Si substrates. The study found that as the thickness of the ZnO film decreased or the post-annealing duration increased, the stimulated emission shifted towards

shorter wavelengths and the lasing threshold increased. These results were attributed to inter-diffusion between ZnO and SiO_2, leading to modifications in the bandgap renormalization of ZnO.

In 2012, Chahar, *et al*. [34] conducted a study where they chemically doped a synthesized PMMA matrix with Kiton red-620 laser dye. Spectral investigations of the Kiton red-620 doped PMMA matrix were performed ,using FTIR, UV-visible, and photoluminescence spectrophotometers. The FTIR study revealed that the absorption band region between 1800 and 1000 cm^{-1} became sharper as the dye concentration in the PMMA matrix increased. UV-visible and photoluminescence studies demonstrated a slight shift in the absorption and emission spectra, as well as changes in the intensity of emission peaks, with increasing dye concentration in the PMMA matrix.

In 2013, Heydari, Esmaeil, *et al.* [35] studied the possibility emission enhancement of the intensity and reduction threshold of the random lasing by gold nanoparticle-based wave guided, exploiting the (LSPS) excitation. Experimental findings have indicated that optimizing the thickness of the spacer layer between the gold nanoparticles and the gain layer improves the performance of the random laser. This adjustment fine-tunes the interaction between the gain polymer and the gold nanoparticles, preventing the undesired emission quenching that occurs when they are in close proximity. This proximity-induced quenching is recognized as a major source of loss in the present laser system.

In 2014, Tianrui Zhai *et al*. [36].fabricated a tunable random laser based on a waveguide Plasmonic gain channel. This laser had been constructed by adding silver nanowires to the rhodamine 6G organic dye-doped with polydimethylsiloxane (PDMS) and then had been deposited onto a silicone rubber slab. The excellent overlap of the Plasmon resonance peak of the

silver nanowires with both the pump wavelength and the photoluminescence spectrum provides the low threshold and tuning properties of the random laser. They prove that the emission spectrum wavelength can be tuned from 565 to 558 nm when the amount of stretching increases from 0 mm to 6 mm. The tunability originates from the blue shift and narrowing of the Plasmon resonance of Ag nanowires, which is determined by the reorientation and uniform length distribution of Ag nanowires after stretching .

Also In 2014, Zhaona Wang *et al.* [37]. chose silver (Ag) nanowires as scattering centers in diameter of 120 nm and micrometers dozens in length at constant particle density of ($\rho = 7.31 \times 10^{7}\mathrm{cm}^{-3}$) with different concentrations of Rhodamine 6G (R6G) dye (With four different concentrations), which were dissolved in methanol to study the transition from incoherent to coherent emission. When they compared their results for these four cases of dye concentration pumped with different power intensities, they found that the dye concentration does not only determine the position of emission peak but also affects the feedback mechanism in random systems with the same scatterer concentration. They attributed that to the fact that the gain length decreases with increasing the concentration of the dye, in addition the scattering mean free path is an unchanged

In 2015, Johannes Ziegler *et al*. [38]. conducted a study revealing the superior performance of gold nanostars (NSs) compared to conventional nanogold shapes, such as spherical nanoparticles (NPs) and nanorods (NRs), as scattering centers in random lasers composed of R6G-doped polymer thin films. They found that nanostars, provide broadband plasmon resonances that overlap with the emission spectrum of R6G and, further extremely high electric field enhancements strongly localized at their spiky

lips. Their experiment demonstrated that the nanostar-based random laser is operating at a threshold lasing in the range of 0.9 mJ/cm^2, showing multiple lasing modes with FWHM of 0.2 nm or even below.

In 2016, Tianrui Zhai, *et al.* [39] successfully created an ultrathin plasmonic random laser using a simple lift-off process. This laser was constructed by incorporating Ag nanoparticles into a free-standing polymer membrane. embedded with Ag nanoparticles. Upon optical pumping of the 200-nanometer-thick membrane device, the researchers observed low-threshold random lasing. This phenomenon can be attributed to the remarkable plasmonic feedback and high-quality waveguide confinement facilitated by the silver nanoparticles and the polymer membrane, respectively. The exceptional flexibility and transplantability of the free-standing polymer membrane enable its attachment to an optical fiber end face, thereby achieving random lasing. .Consequently, this fabrication technique offers a promising avenue for realizing plasmonic random lasing on surfaces with arbitrary shapes.

Also In 2017, Shuya Ning, *et al.* [40].analyzed the effect of the size of the nanomaterial on the properties of the random laser. Different sizes of Ag NPs were prepared according to the seed-mediated growth method by citrate reduction of silver nitrate ($AgNO_3$) with $NaBH_4$ as a strong reducing agent. The diameters of Ag NPs were 20, 40, 60, 80, and 100 nm respectively. The device structure was glass/Ag film (50 nm)/ SiO_2 (10 nm)/Ag NPs/LiF (5 nm)/ PS:BMT-TPD. For comparison, the gain medium deposited on glass was also prepared as reference (Glass/LiF (5 nm)/PS:BMT-TPD). They found when the Ag NPs are small (diameter$\leq$40 nm) the enhanced localized electric field plays the major role for enhanced lasing. With the increasing of Ag NPs size (diameter$\geq$40 nm) for hybrid

structure, the enhanced localized electric field and scattering play an important role in the enhanced lasing. When the Ag NPs size becomes greater than 80 nm, the effect of scattering compared to the enhanced localized electric field is the deciding factor in the enhanced laser. The best results for the random laser properties are achieved due to both the enhanced localized electric field and the scattering effect.

Also In 2018, Lü, Hao, *et al.* [41] conducted a study on enhancing plasmonic random lasing using dye-doped polymer with dispersed gold nanoparticles (DP@Au NPs). The researchers fabricated gold nanoparticles through simple and convenient sputtering and thermal annealing processes. These nanoparticles were then used as scatterers in a PMMA film doped with DCJTB. By adjusting the sputtering time and annealing temperature, the researchers were able to create randomly arranged and nearly spherical gold nanoparticles. These particles played a crucial role in generating random lasing emissions through multiple scattering phenomena. The researchers observed the random lasing emission in the DP@Au NP system and studied its dependence on detection polarization and pump beam power. Their findings demonstrated polarization dependence and low-threshold lasing.

In 2019, Zhang, Shuai, *et al*. [42] controlled the threshold and polarization of distributed feedback polymer random laser by modifying the cavity coupling. Fabricated cavity structure of distributed feedback polymer random laser consisted of two gratings using a two-beam multi-exposure holographic method. By changing the angle between the two gratings achieve tuned coupling strength of the cavity modes. The threshold random lasing decreased with reducing the coupling strength of the cavity modes at the lowest coupling strength observed minimum random lasing threshold.

Furthermore, the output of azimuthally polarized polymer lasers has been modified by changing the cavity coupling.

Also in 2019, Zhi Ren, *et al.*, [43]. fabricated a wavelength-tunable random laser, and the film was constructed by R6G, PVP and Au NRs, using the silicon rubber slab as a substrate. This silicon slab has an excellent mechanical stretching property. If the stretching amount increases from 0-12 mm, then the central wavelength of the laser emission moves towards the shorter wavelengths (blue shift) from (592 to 585) nm. Also, the presence of gold nanoparticles provides the surface plasmon resonance, which greatly increases the light absorbed by the dye molecules. Accordingly, the fluorescence of the dye molecules should be greatly increased, which may lead to a decrease in the random laser the threshold of about 9.8 mJ/cm^2. Around threshold, the FWHM decreases from 40 nm to 3 nm.

In 2020, S.F. Haddawi, *et al*. [44] conducted a study where they incorporated silver nanowires into a polyvinyl-pyrrolidone polymer to create cavities between three different light-emitting polymers. The researchers evaluated the sample, which consisted of a five-layer system, using a plasmonic imaging system with a high numerical aperture objective lens. They also assessed its nonlinearity using the Z Scan technique. The lasing emissions from the sample were collected in a transmission setup.To achieve multi-wavelength random laser emissions, the samples were pumped with a nanosecond green laser. The resulting lasing was a result of the nonlinearity of the layers, the surface plasmon resonance of the nanowires, and their scattering. The emitted light was collected by a spectrometer positioned vertically. The results demonstrated broadband emission near the green wavelength and coherent lasing in the blue region.

This coherence was achieved by enhancing the nonlinearity of the structure by a factor of two. Additionally, the threshold for lasing was reduced to its minimum value, while the maximum emission intensity was observed in two wavelength regions.

In 2020, Naming Zhang *, et al*. [45] reported a significant improvement in the performance of random lasing through the use of a plasmonic hybrid structure called (Au core)-(Agshell) nanorods deposited on an Ag film ((Au@Ag NRs-Ag film)). The study demonstrated that this hybrid structure, consisting of Au@Ag NRs-Ag film, exhibited more effective enhancement of lasing properties compared to independent Au@AgNRs or Ag film alone. Furthermore, when compared to hybrid structures comprising Ag film with either Au nanorods or Au nanospheres, the gain medium deposited on the Au@Ag NRs-Ag film demonstrated the lowest lasing threshold, amounting to only 12.5% of that observed in the neat gain medium. The unique plasmonic hybrid nanostructure, Au@Ag NRs-Ag film, showcased a stronger localized electrical field and scattering effect in comparison to hybrid structures comprising Ag film with regular Au nanoparticles.This can be attributed to the broader and more robust plasmonic absorption of Au@Ag NRs, as well as the stronger plasmonic coupling between the localized surface plasmons of Au@Ag NRs and the delocalized surface plasmon polariton of Ag film. The findings of this study offer a simple approach to effectively mitigate the negative effects of metal films while achieving a lower pumped threshold.

In 2020, Gummaluri *et al.* [46].succeeded in preparing a random laser system using Au nano-urchins acting as scatterers. These nanomaterials were distributed in polymer films doped with rhodamine 6G dye. The authors compared this system with another one with the same

specifications, except that the scatterer was Au nanospheres instead of Au nano-urchins. To evaluate lasing performance, finite-difference time-domain simulation was used, taking into account the following three aspects: the local field enhancement, absorption cross-section, and scattering cross-section. The field intensity magnitude for nano-urchins was observed to be 2 times higher than that of nanospheres. At the pump wavelength, the authors monitored a higher scattering cross-section and a low absorption cross-section for nano-urchins compared to those for nanospheres. This, in turn, indicated that materials with nano-urchin structure can be better scatterer candidates than spheres with isotropic structure when it comes to enhanced random lasing performance.

In 2021, Rodrigo Sato, *et al*. [47] they worked the formation of microbubbles, in use random lasing in optically pumped solutions of plasmonic nanoparticles (NPs) combined with organic dye molecules. They proposed an alternative mechanism that does not rely on plasmon resonance directly. To observe the photophysical dynamics of the NPs in solution, high-speed confocal microspectroscopy was employed. By applying laser pulses, microbubbles were formed, surrounding and encapsulating the NPs. Subsequently, sharp peaks with a width of less than 1.0 nm were observed, which corresponded to the spectral signature of random lasing. Electromagnetic simulations indicated that ensembles of microbubbles may form optical corrals containing standing wave patterns that are sufficient to sustain coherent optical feedback in a gain medium. These findings collectively demonstrated that plasmonic-induced bubble ensembles have the potential to generate optical feedback and random

in 2021 Pramanik , *et al.* [48] addressed a significant challenge in the design of efficient random lasers (RLs). Their study focused on the

demonstration of a random laser utilizing a 4-(dicyanomethylene)-2-methyl-6-(4-dimethylaminostyryl)-4H-pyran (DCM) dye. The researchers employed an innovative adaptive feedback mechanism by exploiting the phenomenon of total internal reflection of light within microbubbles. These microbubbles were generated in the presence of graphene flakes (GFs) through photothermal means. Notably, the GFs served a dual role as passive scatterers and catalysts for the in situ generation of microbubbles within the liquid suspension of dye molecules. Through a simple pump-probe photography experiment, the researchers demonstrated that photon transport during RL emission occurred through weak scattering in GFs, followed by total internal reflection on microbubbles. As a result, they successfully achieved RL emission at a wavelength of 638.4 nm, with a remarkably low lasing threshold.

In 2022, S.F. Haddawi, *et al*. [49] conducted an experimental and theoretical study to demonstrate a flexible and finely-tuned random laser utilizing a two-face double grating plasmonic structure made of polydimethylsiloxane (PDMS). The PDMS material was fabricated using nanoimprint lithography and coated with a 35 nm-thick gold layer using a physical vapor deposition (PVD) device. Additionally, a light-emitting polymer (F8PT) was applied to enhance the scattering and efficiency of the random laser. The researchers employed a plasmonic gold grating as the substrate and compared the simulation results for both the upper and lower sides of the plasmonic double grating structure. The results showed an improvement in light transmission. Through experimental analysis, a comparison was made between normal plasmonic double grating samples and symmetric and asymmetric double grating-based nanostructures with varying thicknesses of 200, 400, and 600. The findings indicated that

samples with thinner spaces exhibited better random lasing properties due to the coupled mode effects. Specifically, the intensity increased while the lasing threshold decreased from 22 μJ in the normal double grating to 16 μJ in the thinnest double grating structure.

in 2023 Songtao , *et al*. [50] utilized a chemical reduction method to create a core-shell structure of silver (Ag) spheres. These Ag spheres were then mixed with Rhodamine 6G, Polyvinyl Alcohol (PVA), and spin-coated onto a silicone slab. After solidification, a film containing the core-shell structure Ag spheres was fabricated. The Ag spheres served as scattering particles, while the film composed of R6G and PVA acted as the active material layer.When irradiated by a pump beam, the film exhibited random laser emission with a threshold of approximately 12.55 ml/cm². The chemical reduction method employed by the researchers offered a cost-effective approach to fabricating Ag spheres, which in turn enhanced the potential applications of random lasers.

1.3 Random Laser Applications

It is possible to employ random lasers in many fields owing to their distinctive characteristics such as operating at a specific wavelength. Alternatively, the fabrication cost of these lasers is low, and they have flexible shape with substrate compatibility [51]. Redding et al. [52] has indicated the applicability of the random lasers in bioimaging, producing speckle-free light with high intensities. In this way, one can be able to fabricate an integrated on-chip random spectrometer device [53]. For image quality tests, random lasers have also shown promising results, outperforming all the other sources of light. In this regard, the proof of concept was provided by comparing between the performances of random lasers and other light sources for speckle generation, image quality, and

contrast-to-noise ratio tests. Notably, for the speckle generation tests, non-speckle patterns were formed by the random laser and light-emitting diodes (LEDs), whereas they produced higher contrast-to-noise ratios after performing the corresponding tests. When it comes to medical area, random laser are capable of detecting tumor and performing photodynamic therapy [54]. In addition, Song et al. reported the applicability of random lasers for sensing purposes, light with a wavelength of 690 nm has been utilized to excite bone specimens soaked with a dye emitting at a wavelength of 800 nm. Thus, it has been possible to detect nanoscale structural stacks in a mechanical biosensor, resulting from the random lasing characteristics in the bone specimens [55]. On the other hand, Wan Ismail et al. has provided evidence on applicability of the aggregation of gold NPs for the measurement of an extremely low concentration of dopamine. This was enhanced by Cu ions for random lasers, having incoherent feedback. In this regard, emission peak linewidth, emission peak shift, lasing threshold and signal-to-noise ratio were affected, so that a dopamine detection limit of ~1 $\times 10^{-7}$ M was obtained as the detection indicator [56]. Furthermore, under mechanical tests, emission peak wavelength of the random lasers shifted by pressuring the bone specimens. According to Vardeny et al. [57], human tissues can have strong scattering, allowing for the support of the random lasing when penetrated with a laser dye solution with a high concentration. It has also been possible to employ random lasers in order to map cancerous tissues. This was achieved by portraying the affected spectral emission for both the healthy and cancerous tissues. In this respect, the tissues were separately immersed in Rhodamine 6G dye, followed by flattening them between the slides of the microscope. By pumping the specimens using Nd: YAG laser (532 nm, 100 ps, and 800 Hz), emission spectra were obtained.

1.4 Overview of the thesis structure

In this aspect, we will present the most important topics that will be included in this message as follow

The first chapter deals with an introduction to the random laser and its most important features in addition to its applications, as well as experimental studies and research that dealt with the subject of random lasers, in particular those that focused on compound cavities in improving the random laser work.

The second chapter includes a reference to the most important topics related to random lasers, such as the theoretical side of random lasers, types of random lasers, the effect of surface plasmon resonance, as well as how the transition from incoherent to coherent, Optical properties of the used nanomaterials, Thin Film Deposition Techniques, , and the types of random media used in random laser systems are the most important factors that affect the occurrence of Random laser.

The third chapter deals with the practical aspect of this thesis, and the most important materials used in this work will be indicated and an exposure to their characteristics and composition. Next, we address the techniques used to prepare some nanomaterials. And then prepare the random media that will be used to test the performance of the random laser. As well as will be indicated some of the schemes or experimental devices that were used in this work.

The fourth chapter includes presentation and discussion of the results obtained from all measurements.

Chapter Five presents the most important conclusions of our work and suggest for the future.

1-5 Aim of the Work

The main objective of this research is to prepare the different cavities individually or jointly and study their effect on the behavior and properties of the random laser, represented by emission intensity, bandwidth, power threshold, and the transition from incoherent to coherent operating modes. To achieve this, the following composite cavities were constructed: First is thermal cavity is create by a constant-wave (CW) laser beam and a liquid medium with nanoparticles. The second is a fabricated waveguide cavity with a thin layer of gold NPs based on dye and glass as substrate. The third is fabricated as a multi-layered 2D structure onto a curved glass substrate and a gold nanostructure with rhodamine dye. The fourth is fabricated as a magneto-optical cavity by an external magnetic field on a new FeB-based two-dimensional magneto-plasmonic structure covered by gold thin film and Rhodamine 6G. The fifth cavity is a triple optical cavity that consists of external, ring, and fundamental resonators.

Chapter two

This chapter introduces the theory of Random Laser

2.1 Introduction

In this chapter, topics directly related to structure and action of random laser will be covered, as the types of random lasers will be studied and how the transformation from one type to another takes place. The important parameters relate with the random laser as (spontaneous emission seeding in cavity, light amplification, laser threshold, random laser action, the parameters controlled random lasing and types active medium of random lasers) what is the difference between the active type and the passive .The composite cavities of the random laser and its output will be the main topic in this chapter.

2.2 Theory of Random Laser

Understanding the random lasers in the best possible way requires basic knowledge of conventional lasers since both systems have many features in common, for example, the working principle is the same where the emitted photons induce other photons to be emitted by the stimulated emission process, and when the gain exceeds the losses, the lasing process occurs [58]. The only exception is the difference indicated earlier, which is that the random laser has no optical cavity in the sense of a conventional laser and this function which was being performed by mirrors, is now achieved by multiple scattering centers and that the resulting spectrum random lasing is typically emitted in all directions [59].

As we know, a conventional laser has three main components: the pumping source, the active medium, and the optical resonator. The pumping source is responsible for the occurring the population inversion

[60]. The resonator, which in its simplest form consists of two parallel mirrors, one highly reflective and the other partially reflecting light, are responsible for the occurrence of the feedback when the photon has been trapped within the active medium [61]. The active medium which represents the laser core can be any kind of matter: solid, liquid, gas. This medium emitted coherent radiation or exhibited again as a result of the transition of excited atoms or molecules from higher energy level to lower energy level by the stimulated emission process. It is pumped by an external source, and the amplification of light is performed there. Then, when the gain overcomes the total cavity losses, the lasing occurs [62]. In addition, when designing lasers, consideration is given to reducing the process of scattering which causes removing the photon from the cavity of conventional laser [63]. The loss of photons due to the scattering process requires higher pumping energies to overcome these losses and reach the lasing threshold, thus lower laser efficiency [64]. This is why optical scattering is considered a detrimental process in conventional lasers[65].

Unlike the conventional laser, in random laser, the scattering process plays a crucial role in the optical feedback mechanism [66]. Here the scattering particles form an optical cavity instead of the conventional mirrors [67]. Therefore, if there are many centers of scattering, then the light in the gain medium will change its direction thousands of times randomly until it can leave the medium [68]. Thus; the multiple scattering that the photon will encounter within the sample will increase the time it remains in the gain medium and thus increase its amplification time [69]. Through this process, the scattering centers act as a resonator to trap the light in the gain medium [70]. Accordingly, it became not necessary to add reflectors to retain the light inside the medium because the scatterers

perform this function very efficiently. Thus, the term of random laser is used to describe the system that includes these disorders introduced to the gain medium [71]. The random laser occurrence can be regarded as a two-stage integrative process: the first is to re-propagate emitted photons from the scattering centers, and then these photons are amplified by the stimulated emission process in the gain medium as a second stage [72]. There are two basic parameters of length that are associated with the random laser. One is mean path length. It is the average distance a photon travels in the gain medium before leaving it. The second one is generation length. It is the average distance that a photon travels before generating another photon by stimulated emission [73]. Let's imagine photon propagates in the gain medium, when the mean free path is larger than the generation length, every photon generates a new photon before escaping the medium [74]. This scenario leads to a chain reaction in which one photon generates two photons, the two photons generate four photons, and so on. So that, the number of photons depends on the time the photon spends within the medium and the length of period time depends in turn on the strength of the scattering centers [75]. Fig.(2.1) shows the main difference between the traditional laser and random laser.

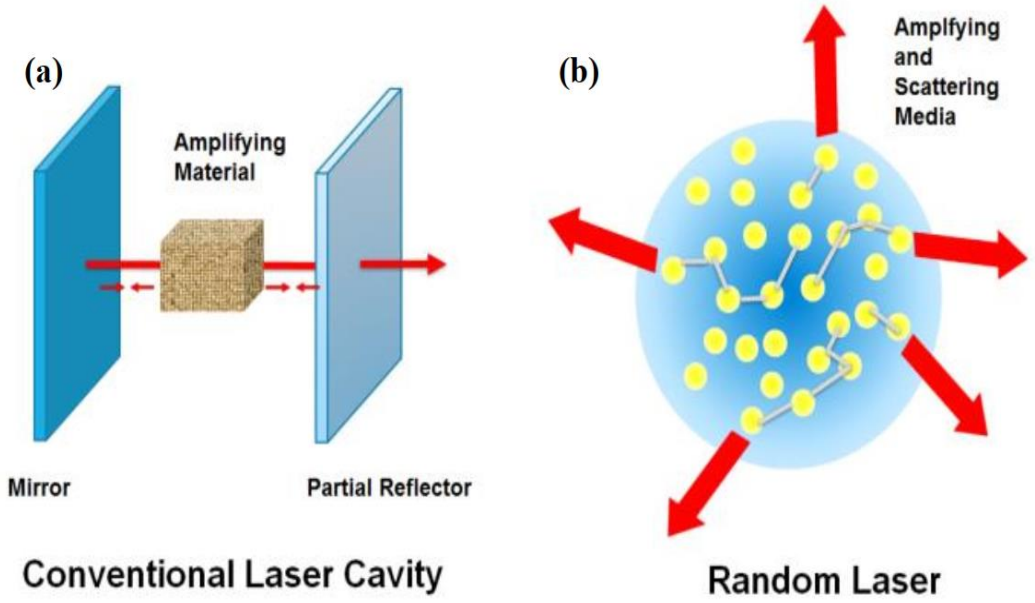

Fig. (2- 1) Schematic diagram of (a) conventional laser and (b) random laser [76].

2.3 Random laser classification

It is clear that the process of amplifying light in random laser is done by stimulated emission and that this process would not have continued had it not been for the feedback provided by multiple scattering of light [67]. Depending on the type of this feedback, the random laser can be divided into two types: (i) random lasers with incoherent (non-resonant) feedback (ii) random lasers with coherent (resonant) feedback [78]. In the case of incoherent random lasers, the intensity feedback can occur but it is not sensitive for phase (incoherent) and an independent frequency (non-resonant), while in the case of a coherent random laser, field or amplitude feedback can be provided where the phase is sensitive (coherent) and the frequency is a dependent (resonant) [79]. These two types will be discussed in more detail.

2.3.1 Incoherent feedback

Let us imagine a light wave is incident on weakly scattered medium or even strongly scattered medium but the area of pumping pulsed is small [80], what will happen? of course, the photons will experience multiple scattering but not for a long time, and then, some of them may escape through the front window into space, while the rest will leave the active volume to un-pumped volume. After a short period and because of the random directionality, a portion of these photons that are still within the disordered medium may return to the effective volume for more amplification [81]. This return process provides intensity or energy feedback. In this case, the trajectory of light is open, which means that the scattered photon does not return to the original position of its scattering, for this reason, the phase of scattered light in this type of random laser does not take into consideration, therefore, it can be called a non-resonant random laser and the photons are emitted as amplified spontaneous emission process [82].

When increasing the pumping rate, the photon intensity grows rapidly, and a narrowed emission peak within few nanometers is produced on broad fluorescence background at the center of the gain spectrum at the threshold [83]. In this type of random laser the scattering mean free path (l_s) which represents the average distance between two successive scattering events is much greater than the wavelength of the emitted photon but is much smaller than the sample thickness L $(L > l_s > \lambda)$ [3]. As a result of the resonance feedback absence, the system sends a stable spectrum with a fixed number of modes (usually one or two) and a bandwidth that is narrowed by about an order of magnitude (typically reaching 25-35 nm). Accordingly, the output spectrum is a smooth narrowed amplified

spontaneous emission (ASE) [84]. So that this model does not involve interference effects and explain the peaks in the diffusive scenario, which involves non-resonant feedback and the distribution of photons satisfies the Bose-Einstein distribution [85].

$$P(n) = \frac{\langle n \rangle^n}{[1+\langle n \rangle]^{n+1}} \quad \ldots\ldots\ldots\ldots\ldots (2.1)$$

Where n is the average photons number.

2.3.2 Coherent feedback

The spectral characteristics of this type of random laser differ significantly from the first type [86]. Under certain conditions of pumping and gain, the spectra of the samples show several very narrow peaks (bandwidth FWHM~ 0.1 nm) installed on an incoherent base. These very narrow modes are temporarily coherent and fluctuate strongly in both frequency and intensity [87]. In this type of feedback, the strong scattering in the active medium plays an important role where the multiple scattering increases the path length and thereby increasing the dwell time of light in the gain medium, and thus enhancing the light amplification by the stimulated emission process [88], also, the strong scattering increases the possibility of light returning to the position of its first scattering [89]. This means after series of multiple scattering, the light returns to its first scattering position, forming a closed-loop that serves as a ring cavity for light and thus providing coherent feedback for lasing oscillation [90]. Interference along this closed-loop leads to standing wave patterns with a high degree of light trapping which means this kind of random laser, enables spatial coherence [91]. In this laser the scattering mean free path (l_s) is equal or less than the reciprocal wave-vector $kl_s \leq 1$ ($l_s \leq \lambda$) which is known as the Ioffe-Regel criterion [92]. This system produces photon

localization, which is equivalent to Anderson's localization proposed by Philip Anderson to interpret conductor-dielectric transitions in electronic transport [93]. In this type, the photon number distribution $P(n)$ satisfies the Poisson distribution [82].

$$P(n) = \frac{\langle n \rangle e^{-\langle n \rangle}}{n!} \quad \ldots\ldots\ldots\ldots\ldots\ldots \quad (2.2)$$

where $\langle n \rangle$ is the average photon number. The laser spikes in the emission spectrum are the main characteristic of this type of random laser. These spikes, which are very narrow spectral features, are caused by the recurrent modes occurring in the random medium of this system. One can be distinguished between a coherent random laser and a non-coherent random laser through the emission spectrum containing spikes in the coherent laser while the incoherent laser is a single spectrum. Fig.(2.2) shows the difference between these two types of random laser, and also compares them with the conventional laser.

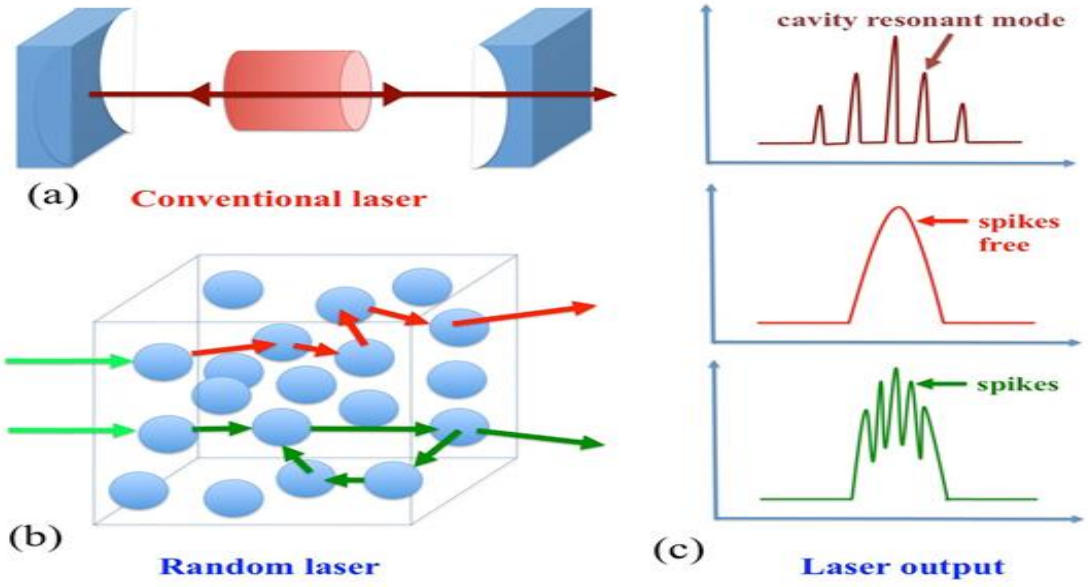

Fig.(2.2) (a) Conventional laser cavity,(b) random laser cavity illustrating the incoherent feedback (red arrows) and coherent feedback (green arrows), (c) illustration of spectral outputs of a conventional laser and a random laser [65]

2.4 Characteristics of random laser

2.4.1 Optical Gain

In addition to multiple light scattering, optical gain plays a crucial role in the random lasing system. The gain material becomes active when it is excited by a high-energy pump source. As light propagates through the medium, it interacts with the amplifying or gain material. For lasing action to occur, the light must be sufficiently amplified before it exits the system, with the gain overcoming any losses [94]. In an amplifying disordered medium, the light waves undergo multiple scattering and amplification. The amplification process is mathematically described by Eq (2.3)

$$l_{amp} = \sqrt{l_t l_g}/3 \quad \text{..... (2. 3)}$$

The terms "l_g" and "l_{amp}" represent the gain length and amplification length, respectively. The amplification length is defined as the average distance between the starting and ending points of paths with a length of l_g, while the gain length is the distance over which the intensity is amplified by a factor of e [95]. As light travels in a straight line in a medium without scattering, the Eq. (2.4) states that the amplification length should be equal to the gain length.

$$l_{amp} = l_g \quad \text{..... (2. 4)}$$

For random lasing to be effective, it relies on two key factors: ample scattering and strong amplification of the scattered light to counterbalance any losses as it exits the gain medium. The emitted photons propagate and undergo amplification within the active gain region until they ultimately escape from it. To ensure that the light is adequately amplified before it escapes the medium, Equation (2.5) represents the essential condition for random lasing [95]

$$l_s \geq l_g \quad \text{..... (2. 5)}$$

2.4.2 Lasing threshold:

The threshold, a significant parameter in lasing, has been the subject of extensive research. In the case of random lasers, the threshold is influenced by the scattering mean free path of photons within the random medium and the luminescence efficiency of the gain medium. Typically, the threshold is reached when the pump transition becomes bleached or saturated. This bleaching effect enhances the penetration of the pump and leads to an increased scattering mean free path [[96]. Notably, the threshold power can be significantly reduced when the scattering mean free path is equal to or smaller than the stimulated emission wavelength, as evidenced in the case of the ZnO random laser [97].

The threshold of a random laser can be influenced by the concentration of scattering particles, with the threshold being inversely proportional to the square root of the concentration ($N^{-1/2}$). Experimental evidence has shown that increasing the concentration of scattering particles can lower the threshold by more than two orders of magnitude [97].Additionally, the threshold is dependent on the refractive index (RI) of the scattering particles compared to that of the surrounding media. Lowering the RI of the surrounding media or increasing the RI of the scattering particles leads to a reduction in the threshold [98]. In recent developments, metal nanoparticles have been employed as scattering particles to further lower the lasing threshold. These metal nanoparticles can induce surface plasmon resonance (SPR) and spatially confine light near the surface, resulting in high gain. With their large scattering cross-section, optimizing the SPR wavelength to match the lasing emission wavelength maximizes plasmonic scattering and minimizes the random laser's threshold [99].

2.4.3 Scattering mean free path

The scattering mean free path l_s is defined as the average distance that light travels between two consecutive scattering events, and is given by: [100]

$$l_s = 1/\rho\sigma_s \quad \text{..... (2.6)}$$

Where, ρ and σ_s are the number density and the scattering cross-section of scattering particles respectively [100].

The transport mean free path l_t is defined as the average distance over which the scattered light is randomized. The relationship between the transport and the scattering mean free path is given by:

$$l_t = l_s/(1 - \cos\theta) \quad \text{.....(2. 7)}$$

where $\cos\theta$ is the average cosine of the scattering angle, when

$\cos\theta = 0 = l_t = l_t$ for isotropic medium Rayley scattering

$\cos\theta = 0.5 = l_t = 2\ l_t$ for Mic scattering

There are three regimes for light scattering in random media [100]:

A- Localization regime ($l_s \leq \lambda$),

B- Diffusive scattering regime ($\lambda < l_s < L$)

C- Ballistic scattering regime ($l_s \geq L$)

Where, λ is the wavelength and L is the sample length.

Therefore, the most appropriate approach for calculating the scattering cross-section (σ_s) is the Rayleigh model, according to the following equation [100] :

$$\sigma_s = \frac{128\,\pi^5\,r^6}{3\,\lambda^4}\left(\frac{n^2-1}{n^2+2}\right)^2 \quad \text{.....(2. 8)}$$

where *r* is the radius of the scattering particle, and *n* is the refractive index. In the past two decades, lasing in random nanostructures has been extensively investigated using both theoretical and experimental studies. Based on the different feedback and gain mechanism provided by random nanostructures, many types of random lasers have been proposed and demonstrated.

2.5 Transition from Incoherent to Coherent Random Laser

In random laser, it is crucial to distinguish between the amplified spontaneous emission ASE (incoherent random laser) and lasing emission (coherent random laser), but the most important of all is the possibility of the transition from a non-coherent random laser to a coherent random laser [101]. To explain this transition, it is useful to use Fig.(2-3) where the scattering centers density increases from left to right while the bottom-to-top represents the pump power increasing [102]. When the scattering centers are weak, as shown in the first image at the bottom of the first column, which represents an incoherent laser state, the photon travels within a random medium of little density in terms of the scattering centers. Therefore it is difficult to form a closed path for not meeting the Ioffe-Regel criterion ($kl_s \leq 1$) which means the scattering mean free path (l_s) is much larger than the emission wavelength ($l_s \gg \lambda$) and thus what happens is an amplification of spontaneous emission or lasing with non-resonant feedback [88]. Therefore; at low scattering concentration and weak excitation, the emission spectrum is broad and low [103]. When pumping rates increase from low to higher values, it is noted that the emission spectrum begins to narrow and its intensity increases as it is observed in

the first column from bottom to the top. However, the possibility of the photon returning and forming a closed-loop which is still weak [74].

Now, with increasing the concentration of the scattering centers, as shown in the Figure (2-3), from left to right, and in order. It is observed that the width of the emission spectrum becomes very narrow and its intensity increases significantly more than the previous state above the pump threshold [104]. With increasing the concentration of nanoparticles, the scattering mean free path becomes close and close to the emission wavelength ($l_s \approx \lambda$) which increases the possibility that the photon will return to its first point of scattering, forming a closed path [105]. More sharp peaks appear when the pump intensity increases further and these discrete peaks result due to light returning to the first scattering position.

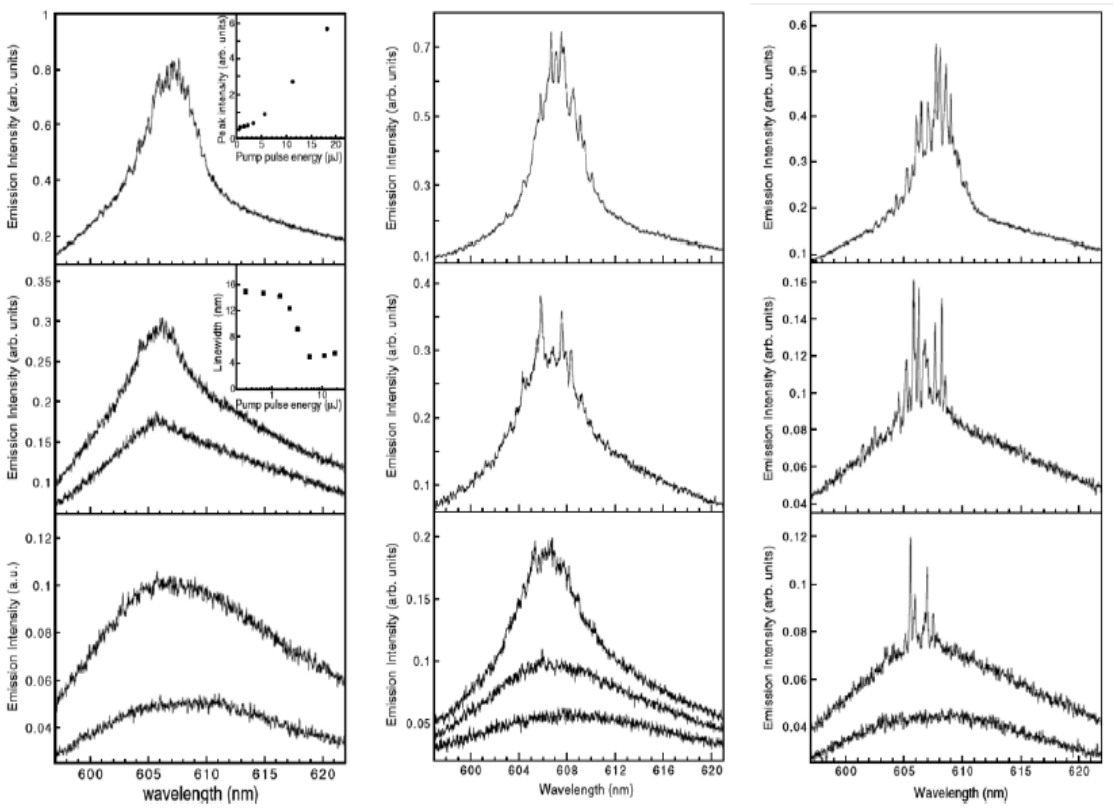

Fig. (2- 3) Evolution of random laser with increasing scattering centers from (left to right) and increasing the pumping power from (bottom to top) [102].

Laser oscillation can occur in these loops which serve as a resonator [106]. The discrete lasing modes correspond to the number of closed loops that formed in the gain medium. Also, one can note the number of modes in the second column is less than those in the third column under the same pumping power. This is due to that the concentration of scattering centers in the third column more than that in the second [88].

Finally, it can be reported that the transition from an incoherent laser state to a coherent laser depends mainly on the concentration of scattering centers and to a lesser degree on pumping sources and that the transformation process is done gradually [101].

2.6 Surface Plasmon Resonance (SPR)

This property appears on the surfaces of some metals and it is a result of the collective movement of free electrons in the nanoparticle when light falls on them [107]. It is a periodic movement in which the direction of electrons' motion changes with a time at the same oscillation of the incident electromagnetic wave [108]. This feature is clearly demonstrated in noble metals such as gold, silver, and copper in the visible light region and is responsible for changing their colors when these elements reach the nano-size [109].

The researches in plasmonics have led to extensive applications in the field of optoelectronics such as light-emitting diodes, waveguides, and nanoscale lasers, as a result of the surface plasmon resonance property of some metallic nanostructures [110]. In a random laser, the gain strongly depends on the strength of the scattering medium where the light interacts with these disturbed amplification media in such systems [111]. The

scattering is mainly occurred due to dielectric or metallic scattered nanoparticles. Metallic nanoparticles (MNPs) play an effective role in spectral narrowing more than dielectric NPs, as we mentioned in a previous section that MNPs have a much larger scattered cross-section than that of the dielectric NPs at the same dimensional. MNPs, especially the noble ones, are rich in the surface plasmon resonance property, which enables the trapping of light near the surface of those particles, which in turn leads to a high gain for random laser [112]. The SPR position is strongly influenced by the material type, size, shape as well as environment of the NPs [113]. These parameters give spectral tuning facilitates overlapping the wavelength of the SPR with the emission wavelength of the desired active medium [72]. Plasmon-enhanced metallic nanoparticles which are implanted in a random laser medium lead to a collective optimization in both the strength of scattering and the gain volume of the random laser. Besides, the confinement of photons near the particle's surface enhances the strength of the local field and thus increases the gain [114]. Whereas, these nanoparticles have the ability to adjust the radiative and non-radiative transition rates of nearby dye molecules [115]. In general, laser dyes have significant Stokes shifts between their absorption and emissions, which can reduce self-absorption and achieve a lower lasing threshold [116]. The emission intensity of the random laser can be enhanced with the assistance of a plasmon by coupling between the dye and a localized SPR of nanoparticle [117] provided that there is a clear overlap between the surface plasmon resonance spectrum of the nanoparticles and emission spectrum of the dye.

2-7 Scattering

Scattering refers to the phenomenon where the original direction of incident light changes upon collision with an obstacle [118]When incident light interacts with particles, such as atoms or molecules, responsible for scattering, the charges within these particles respond to the light. As a result, the electric vector of the incident light shifts, causing the charges to reorient and form microscopic dipoles. These dipoles emit light of the same frequency in various directions, except for the direction aligned with the polarization axes [119].The energy of the incident light is higher than that of the scattered light in all directions. The intensity of the scattered field relies on the scattering angle and the frequency of the incident light.

When the size of the particles responsible for scattering, denoted as x, is much smaller than the wavelength of the incident light ($x << \lambda$), the scattering phenomenon is referred to as Rayleigh scattering [120].In this case, the scattering occurs equally in both backward and forward directions, and the scattering cross-section depends on the wavelength of the light and the size of the scatterer. On the other hand, Mie scattering occurs when the particle size is comparable to the wavelength of the light. In Mie scattering, the intensity of scattering is higher in the forward direction, and the scattering cross-section is larger [121]. Therefore, the particle size relative to the incident light determines whether Rayleigh or Mie scattering takes place, and this distinction can be observed in the figure (2-4).

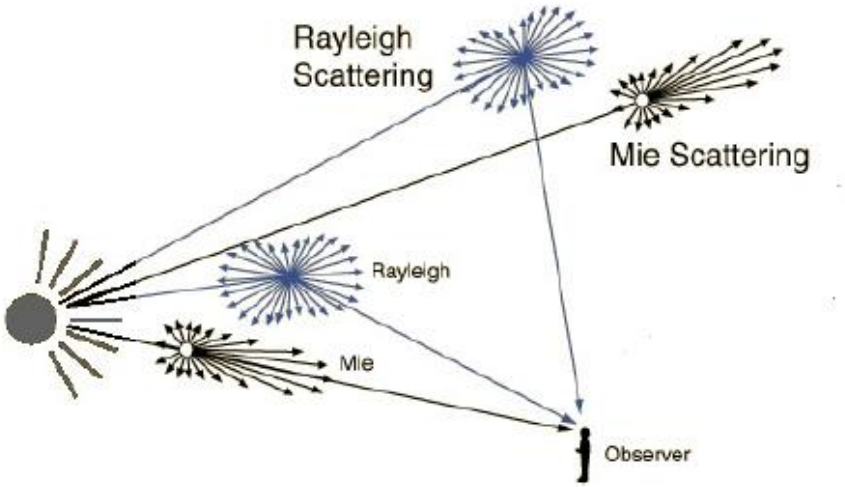

Fig. (2-4) the difference between the Rayleigh and Mie scattering [122]

There is single or multiple scattering of light and the difference between them is, Single scattering refers to the phenomenon where light is scattered by individual atoms or molecules. In this type of scattering, the medium appears random to an observer because there is no discernible relationship between the direction of the incident light and the scattered light [123] Each particle scatters light independently, and there is no consistent phase relationship between the scattered waves. When the concentration of scatterers is low, this type of scattering occurs more frequently in the medium [124].Consequently, the average distance that a photon travels before being scattered, known as the photon mean free path, is long in such a medium. By increasing the concentration of scatterers within the medium, the photon mean free path can be reduced, resulting in increased scattering. This can be utilized to create a coherence random laser.

Multiple scattering of light is influenced by various factors, including the average radius of the particles, the incident wavelength, the density of scatterers, and the refractive index [125]]. When the size of the particles is smaller than the incident wavelength, scattering occurs in all directions. In

this case, the light undergoes multiple scattering as it propagates through the scatterers [126]. The path of the scattered light inside the medium becomes random, and the distance traveled by the light in this type of scattering is longer than the direct path of the waves [127, 128] .

The occurrence of random laser action relies on the presence of multiple scattering and the introduction of a disturbance within a gain medium specifically designed for random lasers. The medium should possess certain characteristics such as homogeneity, small particle size, high refractive index, and low absorption at the excitation wavelength [129].Multiple scattering plays a crucial role by providing the optical feedback mechanism. The density of scattering promotes a strong interaction between the active material's gain and the multiple scattered waves, enabling significant light amplification. Interference effects are particularly pronounced in multiple scattering compared to single scattering due to the large number of scattered arrays originating from different scatterers [130].

2.8.Thin Film Deposition Techniques

This section deals with different methods of synthesis of (Au , FeB ,and AgNw) nanostructures. This section also briefs about the importance of various parameters in controlling the nanostructures diameter, length, growth site and formation density. Low dimensional (thickness ~nanometer to micrometer) material formed by depositing one after the other molecular/ionic/atomic species of the matter is known as a thin film. The dimensions of structures on thin films may be in the nanometer dimension, called nanostructured thin films. There are different techniques available to develop nanostructure thin film for using in the applications like optoelectronic devices. Every method has its advantages and

disadvantages; no method is ideal in all the desired facets (cost of apparatus, nature of the substrate and deposition parameters, etc.). The nanostructured thin film production techniques are generally classified into two classes, (i) physical technique (the evaporation or sputtering of the material from source and deposition on substrate) [131]and (ii) chemical technique (chemical reaction between volatile/non-volatile compound of the material and deposition on the various substrate) [132]The tree table of different nanostructured thin film fabrication techniques is presented in Table-2.1.

in our work, methods of deposition and coating of thin-film will be discussed, namely, the Physical vapor deposition (PVD) ,dip-coating [133] [134], spin-coating [135],

Table -2.1: Different techniques for thin film fabrication [131]

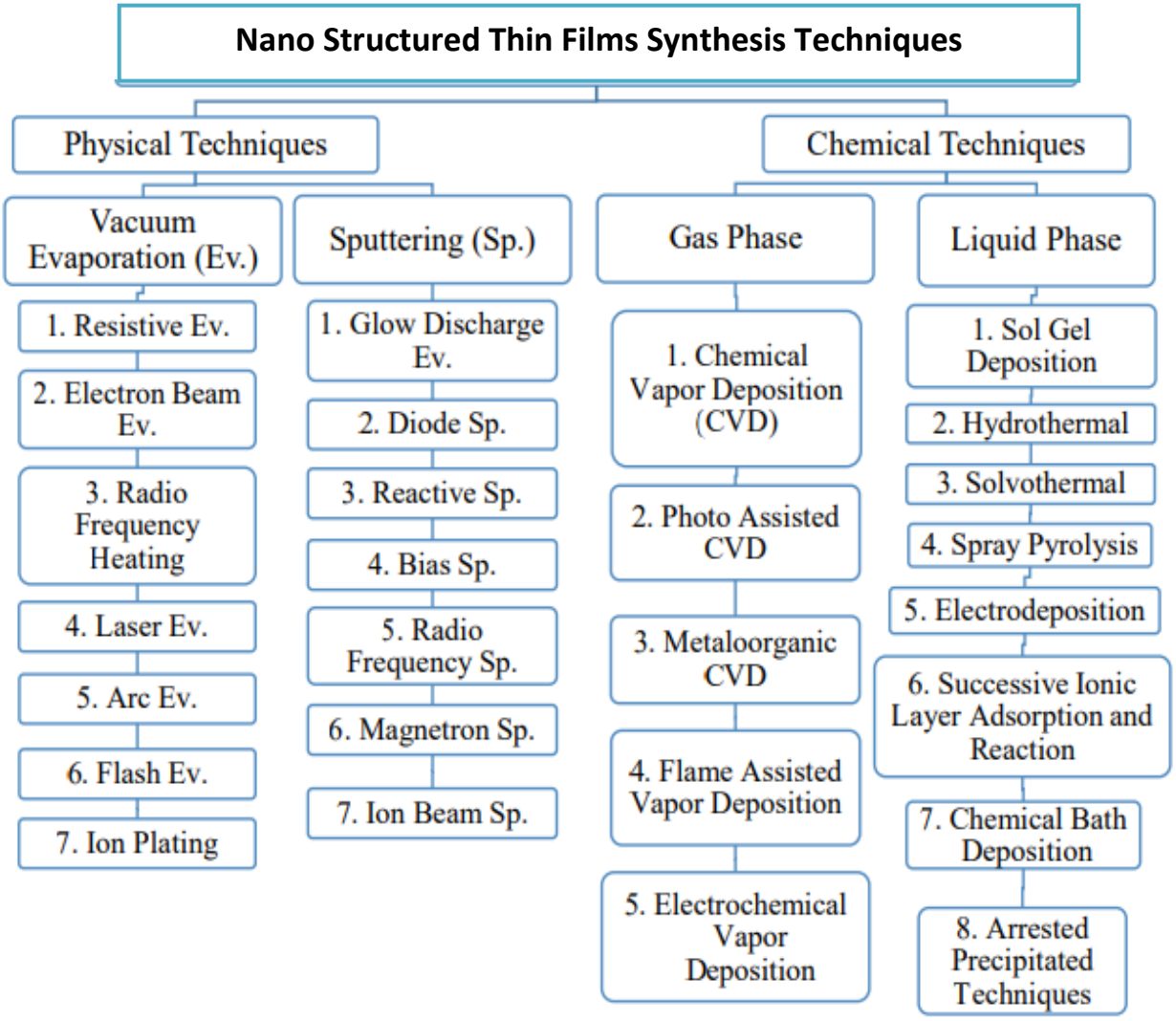

2.8.1 Physical vapor deposition (PVD)

In the Physical vapor deposition (PVD) techniques, the material transforms into its vapor state, deposited on a substrate and formed the thin film. The solid state material heated up until evaporation (in case of vacuum evaporation techniques) or sputtered from the target by high energetic ions (sputtering) [136,137] The process can be described according to the following sequence of steps. (1) The material to be deposited is converted into a vapor by physical means (high-temperature vacuum or gaseous

plasma), (2) the vapor is transported to a region of low pressure from its source to the substrate, and (3) the vapor undergoes condensation on the substrate to form a thin film.There are lots of advantages in physical methods, such as economical and straightforward, top qualities, cleanliness, dry processing, compatible with semiconductor integrated circuit (IC) processing. Still, there are some limitations, such as stoichiometry control is difficult, it requires high process temperature, and the deposition rate is lower. Also, evaporation of dielectric materials is impossible. For crystallization and high capital expenditure, post-annealing treatment may be required [138]. A typical PVD process is shown in Fig. (2.5.)

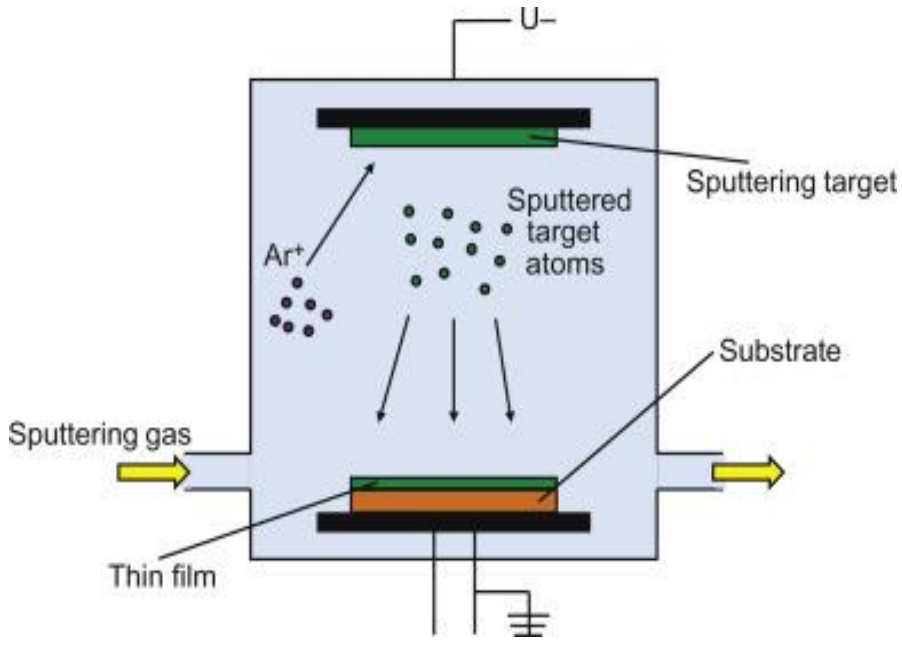

Figure 2.5. Schematic illustration of the physical vapor deposition process[136]

2.8.2 Spin coating

Spin coating is a rapid and cost-effective technique used to create thin and uniform organic films from solutions . In this method, a measured volume of the material solution to be deposited is placed onto the substrate, which is then spun at a controlled speed. The centrifugal force causes the solution to spread evenly across the substrate surface. As the solvent evaporates, a film of the material forms. The thickness of the spin-coated film depends on factors such as the concentration of the solution and the rate of solvent evaporation, which, in turn, is influenced by variables such as solvent viscosity, vapor pressure, temperature, and local humidity. A higher concentration of the solution results in a thicker film. During the spin coating process, the interactions between the substrate and the solution layer are stronger compared to the interactions between the solution surface and the air. One of the key advantages of spin coating is its ability to produce thin films ranging from a few nanometers to a few microns in thickness, offering a quick, easy, and cost-effective approach to film formation. [139]

2.8.3 Drop casting

Drop casting is an alternative method used to deposit a thin film of material onto a solid substrate from a liquid phase. In drop casting, small droplets of the liquid containing the desired material are placed onto the substrate surface, and then the solvent is allowed to evaporate. The outcome of drop casting can vary, ranging from well-formed and homogeneous organic films to poor-quality films that exhibit precipitation effects during the drying process. While drop casting enables the creation of thick organic films, a significant drawback of this technique is the limited control over film thickness and the resulting non-uniformity [140].

2.8.4 Dip Coating

The sol-gel method is widely regarded as one of the simplest and most popular techniques for producing thin films using a diverse range of inorganic, hybrid, and nanocomposite materials. It offers several advantages, including the ability to coat various substrates with complex geometries, including those with holes or intricate patterns. The sol-gel method also allows for a high degree of control over crucial parameters and provides flexibility that surpasses what can be achieved with other conventional processes. [141, 142]

The dip-coating method involves submerging the substrate to be coated into an initial solution and gradually withdrawing it at a consistent speed. This process takes place under controlled temperature and air conditions. By precisely adjusting the withdrawal rate and evaporation conditions, it becomes possible to finely tune the properties of the resulting film, such as its thickness, optical constants, and internal structure. The solution spreads uniformly across the substrate surface due to the combined effects of viscous drag and capillary action. As the process reaches its final stage, evaporation occurs, leading to the gelation of the film. To further modify the film properties, the coated substrates often undergo a post-heat treatment. This heat treatment has an impact on the final characteristics of the films [143]Figure (2.6) illustrates the dip-coating process.

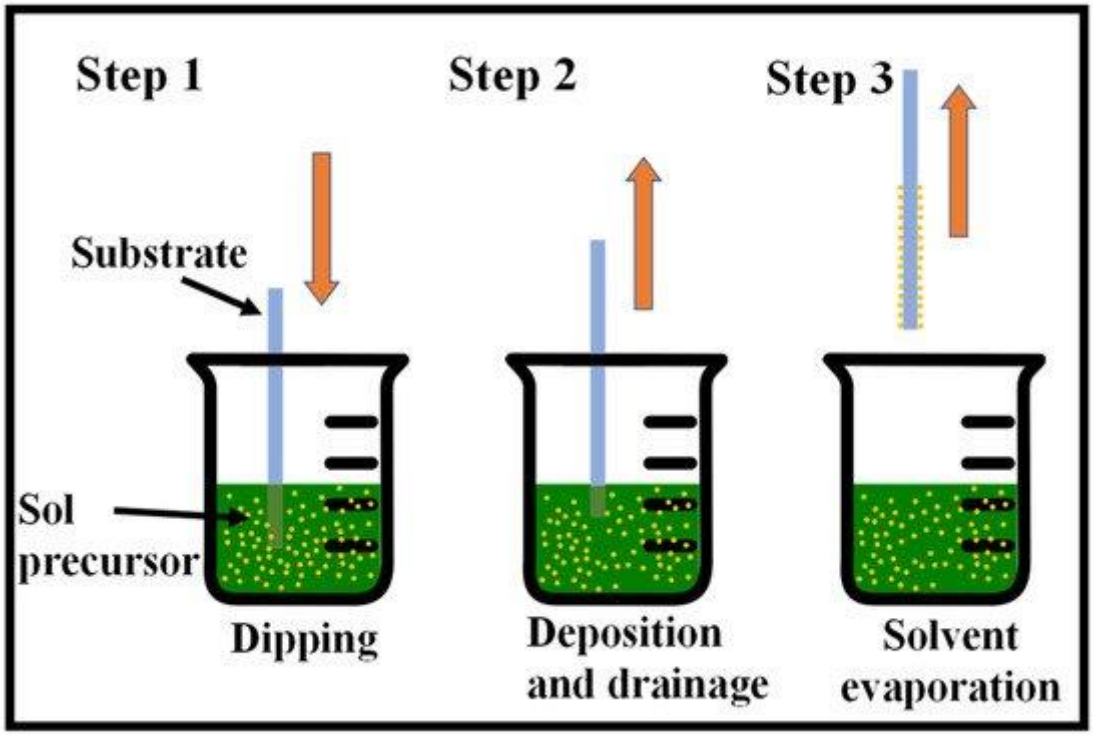

Figure (2.6) Sequential stages of the sol–gel dip-coating method for thin film deposition: Stage 1—the substrate is dipped and immersed in the sol precursor, Stage 2—the substrate is withdrawn at a steady rate, Stage 3—solvent evaporation produces the gelation of the layer[133]

2.9 Organic Lasers Resonators

In this review, we focus on the primary resonators employed in organic solid-state lasers, with particular attention given to thin-film-based configurations like planar waveguides and vertical external surface-emitting cavities. We examine the impact of different resonator types on laser properties such as threshold, efficiency slope, output power, and beam quality. Additionally, we provide a specific emphasis on composite cavities and their influence on these laser characteristics.

2.9.1Cavities Made with Bulk Rods

Laser resonators can adopt diverse shapes and architectures that extend beyond the conventional linear Fabry-Perot cavity or ring cavity, which are typically used with bulk laser gain media. In the early studies of organic

lasers, liquid dyes were often employed within these macroscopic cavities [144, 145] Such resonators consist of two mirrors positioned around the polymer block or the cuvette containing the organic solution. These mirrors play a crucial role in confining and amplifying the laser light within the resonator**.**

In 1993, Hermes et al. conducted an experiment that showcased a pulsed, organic external resonator device. The device exhibited a remarkable slope efficiency of 85% and an output energy of 128 mJ, with a lasing threshold of 12 mJ/cm^2 [146]. The gain medium employed in this experiment was a cylindrical rod made of bulk plastic, specifically hydroxypropyl acrylate/methyl methacrylate, doped with Pyrromethene 570. The rod was positioned inside a cavity equipped with flat dichroic mirrors, which were spaced 7.2 cm apart. The system was end-pumped using a frequency-doubled Nd: YAG laser

Furthermore, the authors achieved the ability to tune the emission wavelength of their device by incorporating a prism within the cavity, resulting in an extended tuning range spanning tens of nanometers. The laser exhibited exceptional photostability and demonstrated an excellent lifetime of hundreds of thousands of pulses when excited at a repetition rate of 20 Hz with a pump energy of 1 mJ per pulse. Notably, in oxygen-free Pyrromethene-doped samples, the lifetime could be further enhanced to millions of pulses.

In the area of solid-state dye lasers, a notable example is the impressive work presented by Bornemann et al. involving a continuous-wave laser system [147]. Their experimental setup consisted of a folded cavity configuration, which included two concave mirrors, an output coupler, and a 50-100 µm thick film of Rhodamine 6G-doped polymer positioned

between two commercially available DVD substrates serving as the gain medium. Additionally, a birefringent filter was incorporated into the setup to enable wavelength tuning. The gain medium was prepared using the drop casting technique.. The disk-shape gain medium ,and pumped with a solid-state laser. The strategy adopted in this work to can be considered as a milestone in the development of Random laser.

2.9. 2 Cavities Based on Thin-Films

As previously mentioned, one significant benefit of incorporating organic semiconductors and dyes into polymeric matrices is their capacity to be readily processed into thin films with micrometer-scale thicknesses or even thinner. This can be achieved using cost-effective, scalable, and precise fabrication techniques. In the case of small-molecule organic semiconductors, thermal evaporation is an additional method that allows for exceptional control over both film thickness and optical quality. Consequently, the most suitable resonator geometry for thin-film organic lasers is the two-dimensional planar waveguide, given its inherent compatibility with these materials.We will focus in this work on composite cavities (solid "thin films" and layers) and (liquid thermal cavities).

2.9. 2.1 Waveguide Lasers

In a planar waveguide laser configuration, the resonator axis runs parallel to the film plane, allowing photons to traverse a considerable distance (several millimeters) through the active medium during each roundtrip. This extended path results in a high overall optical gain. In this geometry, light is guided as a wave within the organic layer, which possesses a higher refractive index, while being sandwiched between a low-index substrate (such as glass or silica) and the surrounding air. Due to the typical thickness of the organic layer being around 1μm, the formation of

waveguides is easily achievable. Optical feedback necessary for laser operation can be achieved through various methods. A waveguide, by its nature, confines and guides light within a medium through total internal reflection at the interfaces with the surrounding media. Thus, for light to be effectively trapped and guided within the waveguide, specific conditions need to be met[148] .

2.9. 2.2 Fabry-Perot Waveguides

In the case of inorganic semiconductor diode lasers, a convenient and cost-effective approach for creating the cavity mirrors involves cleaving the semiconductor to obtain flat facets, resulting in a plano-plano Fabry-Perot waveguide cavity. In this configuration, light is confined and guided within a medium that is sandwiched between two claddings located on the top and bottom. These claddings possess lower refractive indices compared to the medium itself. This arrangement is depicted in Figures (2.7). When guided light emerges from a cleaved facet, it undergoes a sudden change in refractive index, typically transitioning to the surrounding air, resulting in outcoupling of the light

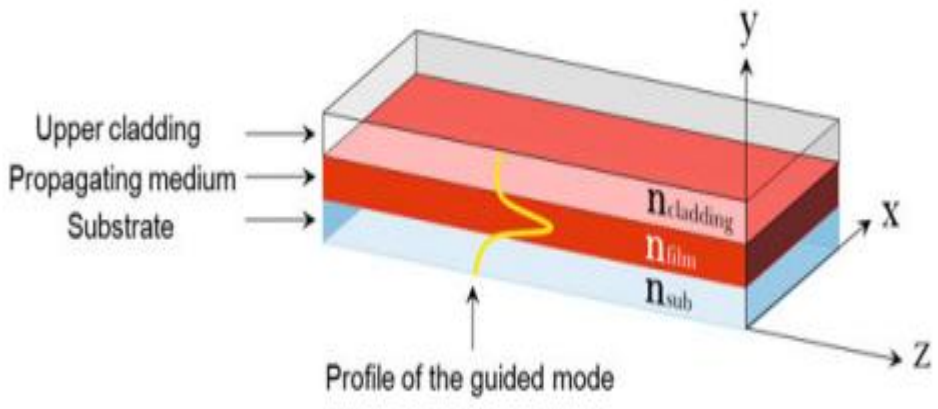

fig.2.7 Three dimensional representation of planar waveguide geometry. For light to be guided one should have $n_{film} > n_{sub}$ and $n_{film} > n_{cladding}$[148]

2.9. 2.3 Distributed Feedback Structures

The process of cleaving thin film facets to achieve laser effects presents two challenges: low reflectivity and difficulties in controlling optical quality. However, an elegant solution involves the use of diffractive grating engraved onto the film surface to serve as cavity mirrors. In this approach, a periodic diffractive grating is utilized to provide efficient feedback within a specific wavelength range. These structures combine the high reflection coefficient offered by the periodic grating with an extended interaction between the laser wave and the gain medium, resulting in low-threshold lasing. The periodic surface corrugation can be classified into two categories: Distributed Bragg Resonators (DBR) and Distributed Feedback (DFB) structures. A DFB laser comprises a thin active layer deposited onto a corrugated substrate.

When light propagates within the waveguide, it encounters the periodic corrugation, which scatters the light. If the scattered waves combine coherently, they form a Bragg wave that propagates in a new direction. The detailed explanation of this mechanism requires the application of coupled mode theory, as described by Kogelnik et al. . [149] For a specific modulation period, only certain wavelengths will experience constructive interference in the opposite direction to the incident wave. This constructive interference provides the necessary feedback for laser operation, as illustrated in (Figure 2.8). The bandwidth, or the width of the "stopband" surrounding the central Bragg wavelength, is influenced by the modulation depth. The central Bragg wavelength is determined by satisfying the Bragg condition.

$$m\,\lambda_{Bragg} = 2n_{eff} \setminus \Lambda \ldots\ldots\ldots\ldots\ldots\ldots\ldots\ldots\ldots\ldots (2\text{-}9)$$

In this context, λ_{Bragg} refers to the wavelength of the laser light, Λ represents the period of the corrugation, and m is an integer that signifies the order of the diffraction process. The term n_{eff} denotes the effective refractive index of the waveguide. Specifically, for the first-order diffraction process (m = 1), the relationship is given by $\Lambda = \lambda_{Bragg} / (2 * neff)$ [149].

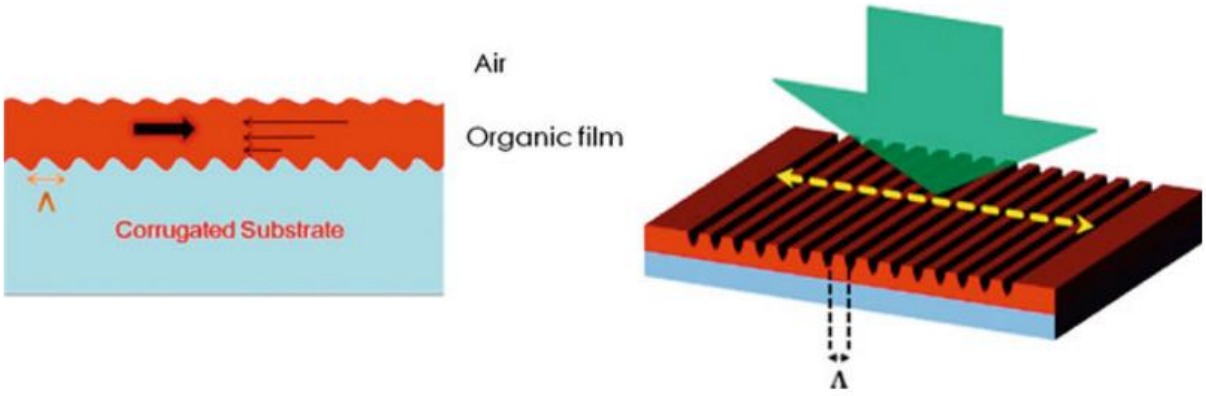

fag (2.8) Possible structure of a DFB laser where the organic film is deposited on a precorrugated substrate with a modulation period equal to $\Lambda = m\lambda / (2n_{eff})$. The light propagating from the left is scattered by the corrugation, and the diffracted waves interfere constructively in the opposite direction, creating a counterpropagating wave[149]

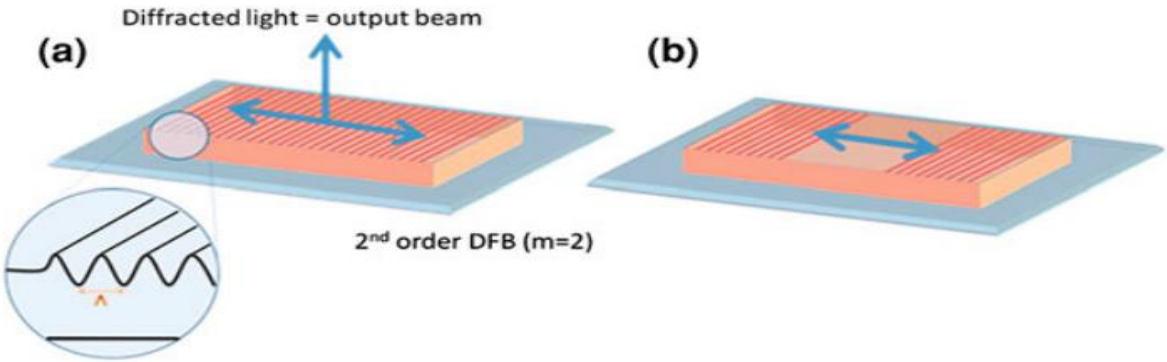

Fig.(2.9 a) DFB structure directly engraved onto a polymeric film. If $\Lambda = \lambda / n_{eff}$. (2nd order grating, m = 2) then a diffracted beam (first diffraction order) is emitted in the direction perpendicular to the film plane, b) DBR structure with no corrugation between two Bragg mirrors[149]

2-10 laser dyes

Laser dyes are commonly employed as gain media in various practical systems. These dyes consist of fluorescence molecules dissolved in organic or water-based solvents. Due to their high fluorescence quantum efficiency and wide emission and absorption cross-sections, dyes can be efficiently pumped and exhibit significant gain. Consequently, they are well-suited for use as gain media. The broad bandwidth of gain provided by dyes enables a wide tuning range in random lasers [150.151]

2.10.1 kiton red Laser Dye

Extensive research has been conducted on Kiton Red, investigating its electrical and optical properties in both liquid and solid dye forms. Kiton Red has proven to be a successful active medium for laser applications. This laser dye is characterized by its dark red color and has a molecular formula of $C_{27}H_{29}N_2NaO_7S_2$, with a molecular weight of 580.65 gm/mol. The laser emission from Kiton Red is tunable at approximately 610 nm [152]. Fig (2-10) illustrates the chemical structure of Kiton Red dye.

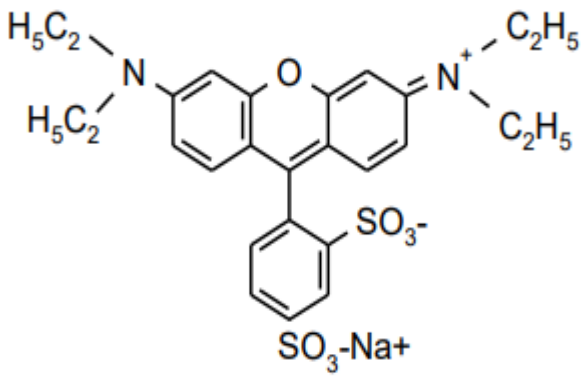

Fig. (2-10) the molecular structure of kiton red laser dye[152]

2-10-2 Rhodamine B Laser Dye

Many studies had been achieved on the Rhodamine B, exploring its electrical and optical characteristics in both liquid and solid dye forms [153]. It has been effectively utilized as an active medium for lasing[154] Rhodamine B, a laser dye, exhibits a color ranging from red to violet. Its molecular formula is $C_{28}H_{31}CIN_2O_3$ with a molecular weight of 479.02 g/mol. The laser emission from Rhodamine B is tunable at approximately 610 nm, and it demonstrates a quantum yield in the range of (0.49 to 1.0) depending on the temperature. Notably, when excited by a Q-switched Nd:YAG laser using second harmonic generation, the absolute fluorescence quantum yield becomes evident [155 , 156] Figure(2-11) illustrates the chemical structure of Rhodamine B dye.

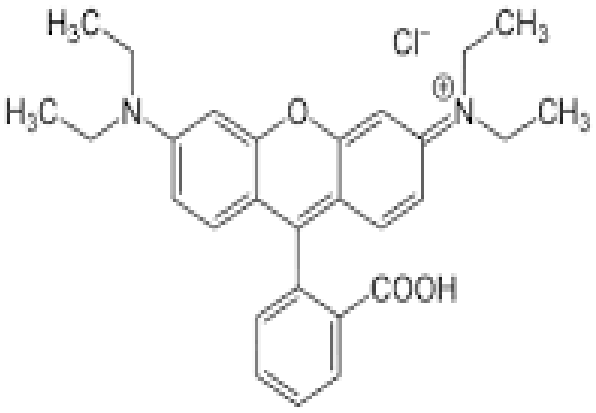

Fig. (2-11) the molecular structure of Rhodamine B laser dye[154]

2-10-3 Rhodamine 6G Laser Dye

Rhodamine 6G exhibits a wide range of frequencies, including orange light at a frequency of 590 nm. It is pumped using a green laser source at 532 nm. The molecular formula of this dye is $C_{28}H_{31}N_2O_3\,CI$, with a molecular

weight of 479.02 g/mol. Rhodamine 6G is known for its high efficiency, capable of converting 20% of the incident energy into lasing output[157]. The quantum efficiency plays a crucial role in determining the random lasing properties, making it a significant parameter to consider[158].

Rhodamine 6Gcan be used in applications as pigments and fluorescent probes for describing the surfaces of polymer nanoparticles, studying molecular structures, and serving as an active medium in random lasers. Its high fluorescence quantum yield makes it particularly suitable for this purpose [159] [160] Additionally, Rhodamine 6G has various other uses [161]. Figure (2-12) illustrates the chemical structure of Rhodamine 6G dye.

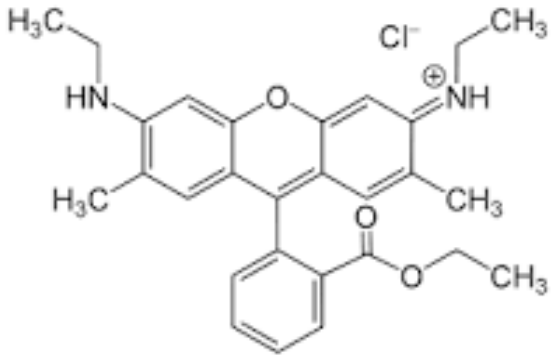

Fig. (2-12) the molecular structure of Rhodamine 6G laser dye[157]

2.11 Optical properties of nanomaterials

Optical properties displayed by nanometer-scale metal particles hold immense aesthetic, technological, and intellectual significance. At a fundamental level, the absorption spectra of light provide insights into the electronic structure of these small metallic particles. Colloidal solutions containing noble metals such as copper, silver, and gold exhibit vibrant colors and demonstrate pronounced absorption bands. Notably, the optical characteristics of these particles differ significantly from both the bulk

material and individual atoms. Also, the significant reduction in the size of nanomaterials affects their optical properties [163].

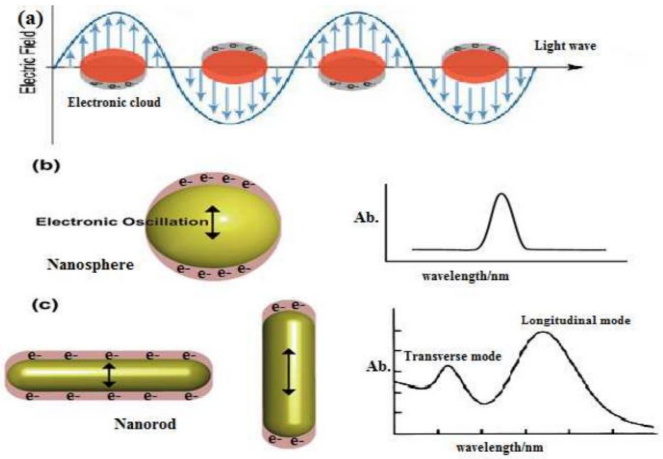

Fig. (2- 13) Schematic representation of (a) localized surface plasmon resonance, (b) electric oscillation of nanoshere, and (c) nanorod with respective extinction spectrum due to LSPR and TSPR [163].

The change in optical properties is caused by two factors, the quantum confinement of electrons within nanoparticles and the surface plasmon resonance.

When the metallic nanoparticles are irradiated by electromagnetic light wave, the free electron in the metals are in driven by the alternating electric field with collectively oscillate in a phase with the incident light Fig. (2-13). When the dimensions of a metal are reduced, boundary and surface effects become very prominent, and for this reason the optical properties of MPs are dominated by collective oscillation of conducting electrons in response to an incident electromagnetic radiation, which is typically known as surface plasmon resonance (SPR). The linear and nonlinear optical properties of such materials can be finely tailored by controlling the crystal dimensions, the chemistry of their surfaces and fabrication technology becomes a key factor for the applications [164].

The free electrons in metal (specially, the 'd' electrons in silver and gold) travel through the material. The mean free path in gold and silver is ~50 nm. In particles smaller than ~50 nm, no scattering is expected from the bulk [165]. This means that the interactions with the surface dominates. When the wavelength of light is much larger than the nanoparticle size it sets up standing resonance conditions as represented in Fig. (2-14).

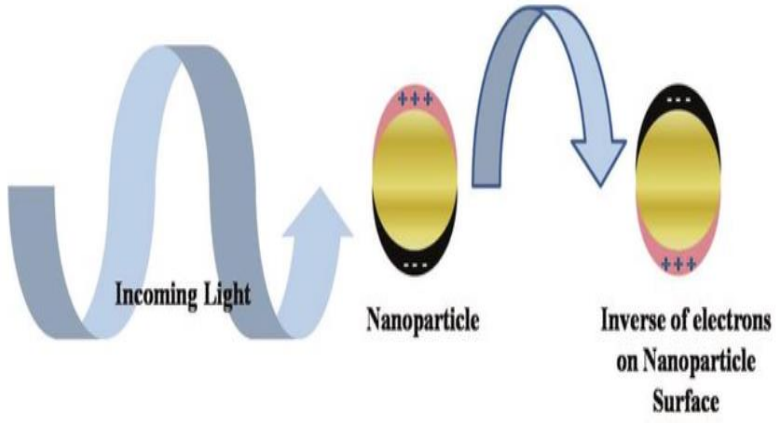

Fig. (2- 14) Origin of surface plasmon resonance due to coherent interaction of the electrons in the conduction band with light [166]**.**

Light in resonance with the surface plasmon oscillation causes the free-electrons in the metal to oscillate. As the wave front of the light passes, the electron density in the particle is polarized to one surface and oscillates in resonance with the light's frequency causing a standing oscillation. The resonance condition is determined from absorption and scattering spectroscopy and is found to depend on the shape, size, and dielectric constants of both the metal and the surrounding material [167]. This is referred to as the surface plasmon resonance (SPR), since it is located at the surface. As the shape or size of the nanoparticle changes, the surface geometry changes, causing a shift in the electric field density on the surface. This causes a change in the oscillation frequency of the electrons

and generates different cross- sections for the optical properties including absorption and scattering.

2.11.1 Gold (Au) Nanoparticles

Gold nanoparticles have unique optical properties because they support surface plasmons. At specific wavelengths of light, the surface plasmons are driven into resonance and strongly absorb or scatter incident light. This effect is so strong that it allows for individual gold nanoparticles as small as 50 nm [168].So the Absorption and scattering of light by gold nanoparticles of sufficiently small size that are comparable to or less than the mean free path of electrons in a spatially extended material should be mentioned especially[169].In this case, it becomes necessary to account for the scattering of free electrons at the boundary of the gold nanoparticle. This is usually interpreted as a limitation of the mean free path of electrons, which leads to an additional pathway of free electron energy dissipation [170].

2.11.2 Silver Nanowire

Ag nanowire is a metallic type of nanostructure in the form of a wire with the diameter of the order of a nanometre. More generally, nanowires can be defined as structures that have a thickness or diameter constrained to tens of nanometers or less and an unconstrained length. Silver NWRs have attracted a lot of attention in the electronics, chemistry, physics, biology, and medicine fields because of their unique properties that depend strongly on the composition, size, shape of metal nanostructure [171]. The ability to control the size and shape of metal nanostructures provides a great opportunity to check the electrical and optical properties of these materials and opens up prospects for use in different applications as random laser systems [172] .

Ag nanostructures contain a set of properties that can be adjusted or improved by controlling their shape. Ag has the highest thermal and electrical conductivity among the metals. It also has unique optical properties, and this is evident in its major role in photography. The nanosilver's advantages over other noble metals in relation to its physical and chemical properties are: stability at ambient conditions, low cost than other noble metals such as gold and platinum, broad absorption band in the visible region of the electromagnetic spectrum, chemical stability, and non-linear optical behaviour [173]

Silver nanowires have been shown to significantly enhance light scattering with different gain materials, because the interactions between the emission centers and the surface plasmons can be controlled in the visible range from 442 to 785 nm [174]. Depending on the size and shape of silver nanomaterials, the peak resonance wavelength may be varied at the range of (380-470) nm [175] .

2.11.3 Fe_2O_3magnetic Nanoparticles

Iron (III) oxide, with the chemical formula Fe_2O_3, is a naturally occurring compound found in nature as the mineral magnetite. It belongs to the family of iron oxides and contains both Fe2+ and Fe3+ ions. Iron oxide manifests as a red-brown substance that displays permanent magnetism, making it ferromagnetic [176]. Its primary application lies in its use as a black pigment. In this context, it is synthesized rather than extracted from the naturally occurring mineral, allowing for control over particle size and shape through the chosen production method

he synthesis method and chemical structure play a significant role in determining the physical and chemical properties of magnetic

nanoparticles. Typically, these nanoparticles have sizes ranging from 1 to 100 nm and can exhibit superparamagnetism in many instances [177].
Magnetic nanobeads, which consist of clusters of individual magnetic nanoparticles, have a diameter ranging from 50 to 200 nanometers [178]. These clusters serve as a foundation for further magnetic assembly, forming magnetic nanochains. Recent research has focused extensively on magnetic nanoparticles due to their appealing properties, holding potential applications in catalysis such as nanomaterial-based catalysts, biomedicine and targeted tissue delivery, magnetically tunable colloidal photonic crystals, microfluidics, magnetic resonance imaging (MRI), [179]

Different chemical synthetic methods are also used to to fabricate magnetite nanoparticles with specific desired physical and chemical characteristics. One common approach involves the coprecipitation of an aqueous solution containing ferrous (Fe^{2+}) and ferric (Fe^{3+}) salts by introducing a base [180].

2.11.4 Fe B nanoparticles

feB is a soft ferromagnetic compound ,be a grey powder that is insoluble in water [181].And iron boride refers to various inorganic compounds with the formula FexBy[182] Two main iron borides are FeB and Fe_2B. Some iron borides possess useful properties such as magnetism, electrical conductivity, . Some iron borides have found use as hardening coatings for iron. Iron borides have properties of such as thermal conductivity and electrical conductivity, and properties of metal properties, Boride coatings on iron are superior mechanical, Amorphous iron-boron film is well known as a magnetostrictive material[182]

Chapter Three

Experimental Part

Materials Preparation

Preparation Experiments

3.1 Introduction

In this chapter, the characteristics of materials used in our experiments to generate random laser with specific outputs will be presented. The ways and methods used in preparing the research active medium, scattering center and compounded cavity will also be covered. The experimental setups which employed whether to test the performance of the random laser or to calculate some of its related parameters will also be demonstrated.

3.2 Outline of the Experimental Part

The block diagram in Fig.(3.1) illustrates the flow chart that will be focused on in our experimental work to improve the performance of the random lasers. It includes the elements that make up the random medium (gain medium, scattering centers, host medium, and supporting materials). Then, the optical and structural properties of these components are measured and examined. And in a proactive step, some factors that have a clear impact on random laser action will be discussed. After, different random media will be formed in terms of type, shape, and concentration of the nanomaterial to test the performance of the random laser under the influence of these parameters associated with the dispersion centers

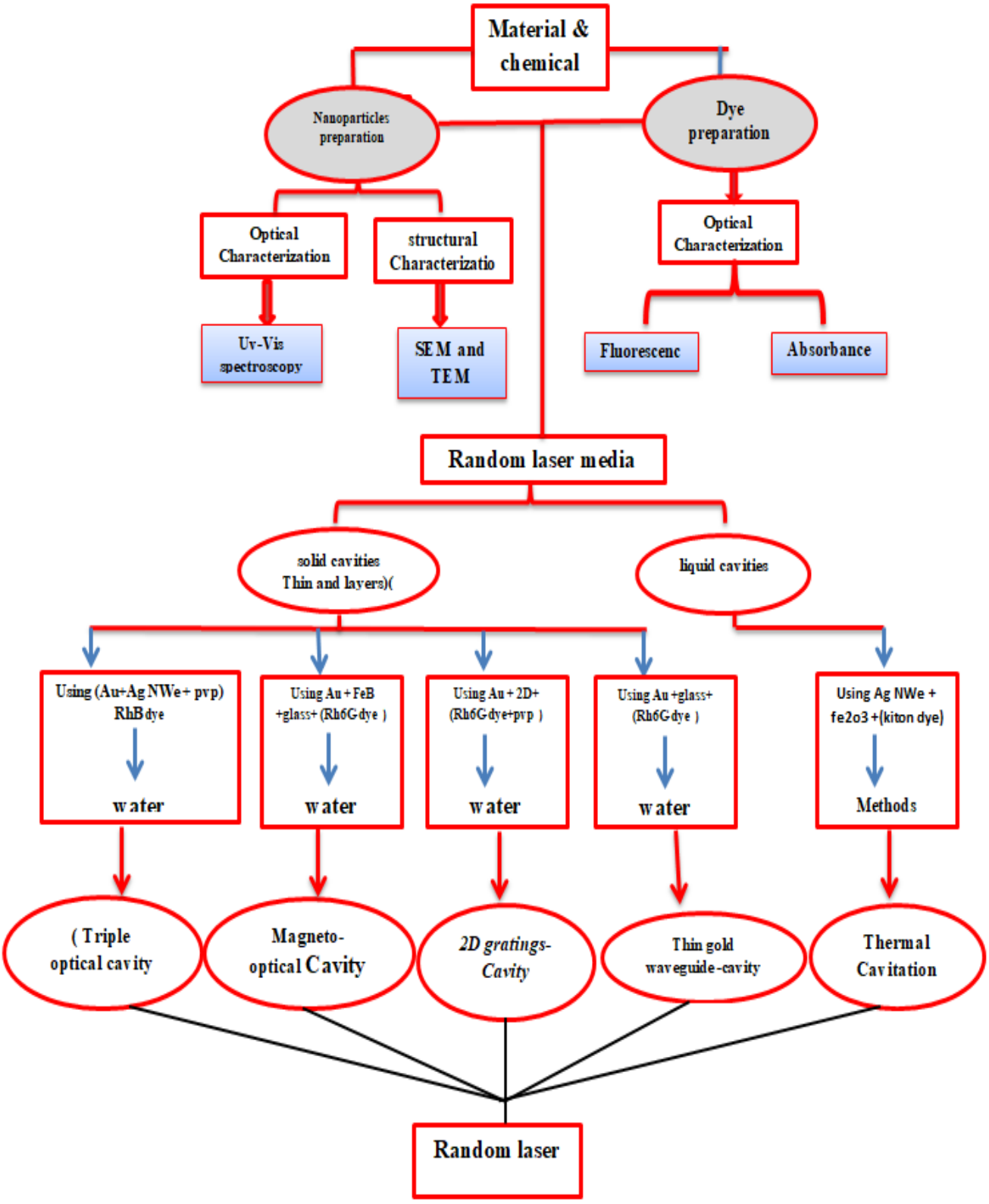

Fig. (3-1) Flow chart of the experimental part in this project.

3.3 Chemical materials

Table (3-1) It includes the characteristics of chemical materials whose used in the experimental part.

Raw material	Chemical Formula	Vendor	Purity
Kiton red	: $C_{27}H_{29}N_2O_7S_2Na$	USA , Sigma – Aldrich	Without further purification
Rhodamine 6G (Rh6G)	$C_{28}H_{31}N_2O_3Cl$ 479.02 g/mol	USA , Sigma – Aldrich	Without further purification
Rhodamine B (RhB)	$C_{28}H_{31}ClN_2O_3$ 479.02 g/mol	USA , Sigma – Aldrich	Without further purification
Silver nanowire	Ag New	Plasma Chem	99.9%
Iron oxide	Fe_2o_3	Plasma Chem	99.9%
Gold	Au	Germany , Sigma –Aldrich	99.9%
Methanol	CH_3OH 32.04 g/mol	Germany , Sigma –Aldrich	99%
Distilled water	H_2O 18 g/mol	---	---
polyvinylpyrrolidone (PVP)	$(C6H9NO)_n$	USA , Sigma – Aldrich	99%

3.4 The Preparation of(Kiton ,Rh6G and RhB) dyes

Organic laser dye solutions have been prepared by dissolving the required amount of RhB and Rh6G dye in water solution ,kiton dye in methanol. This amount of dye was weighed by a digital accurate balance, with a sensitivity of 10^{-4} ((Matter company). The concentration of solution was calculated depending on the following formula [183]

$$m = \frac{M_w \cdot C \cdot V}{1000} \quad \text{..... (3-1).}$$

Where C represents the concentration of dye solution reported in M (mol/L), m is the mass of dye in grams (g), V describes the volume of solvent in a liter (L), and M_w refers to the molecular weight of the dye in grams/mole (g/mol). The high required concentration of kiton ,Rh6G and RhB dye solution was $5*10^{-3}$ M has been prepared and to maintain the same amount of dye, the other concentrations were obtained by changing the amount of the solvent by using the dilution law [184]

$$C_1V_1 = C_2V_2 \quad \text{..... (3-2)}$$

where C_1 and C_2 represent the available and required concentration respectively, V_1 is the amount of solvent for the first concentration, and V_2 is the amount of solvent assumed to be used to obtain the desired concentration. Then the process has been repeated to get the rest concentrations.

According to the aforementioned, the following concentrations kiton ,Rh6G and RhB dye solution were obtained (1×10^{-3} M, 5×10^{-4} M, 1×10^{-4} M, 5×10^{-5} M, 1×10^{-5} M, 5×10^{-6} M and 1×10^{-6} M) . As example the Kiton solution shown in Fig.(3.2). These different concentrations of dye have been kept in a dark place to avoid the optical decay of the dyes.

Fig.(3.2) The real image for different concentrations of kiton red dye solution

3.5**: Nanoparticles Preparation**

It is known that random laser output is affected by the type, shape, size, and characteristics of nanoparticles. Therefore; groups of nanoparticles were prepared: (AuNPs, AgNWe ,Fe_2O_3MNPS, FeBNPs) . These will be discussed in details as follows:

3.5.1 The Preparation of Au Nanoparticles

The Au nanoparticles have been prepared by laser ablation of Au metal plate in an aqueous solution (deionized water). Pure 99.95% Au plate was washed using alcohol to remove bacteria and other contamination. The Au metal plate was placed on the bottom of a glass vessel filled with 5 ml deionized water. The target has been securely fixed inside the glass container. The Q-switched Nd:YAG laser operating at a wavelength (1064 nm), the pulse width of (5 ns), and repetition rate of (10 Hz) was focused on the surface of the target and shot for 30 mins. to produce AuNPs nanosphere colloids. A reflective mirror has been placed tilted at 45^0 in relation to the vertical plane to change the direction of the laser beams that were directed at the target by a lens (focal length of 25 cm). During the

process, the vessel containing Au samples is moved slowly and continuously to obtain evenly distributed nanosphere colloids by the motor. To prevent water splashing and protect the laser lens, the container was covered at the top with a microscopic glass slide which has hole in the middle that allows the passage of the laser beam. Fig.(3.3) represents the experimental setup of the preparation Au NPs by laser ablation

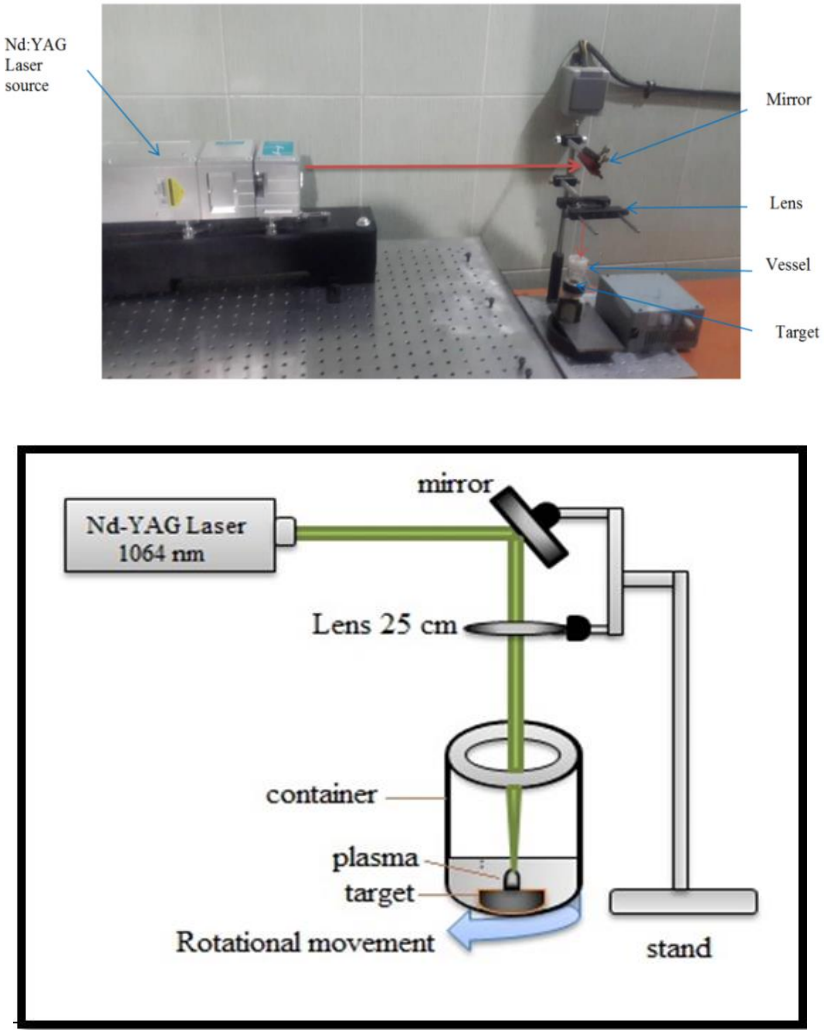

Fig.(3.3) The experimental setup of the preparation Au nanospheres by laser ablation

The size of the gold nanomaterial that had been produced by the laser ablation were verified using transmission electron microscopy (TEM). UV–VIS absorption spectra of the samples were recorded.

3.5.2 Ag NWs

In this type, two kinds of Ag nanowires (diameter 50, 100, nm, length ≤ 50 microns) have been used which were purchased from the German Plasma Chem company.,in this work, (0.2mg/mL) were prepared in (deionized water) and again in (ethanol)and placed in an ultrasound machine for (5 minutes), and studied the absorption spectrum

3.5.3 Fe_2O_3 Magnetic Nanoparticles

It is about nano-iron oxide, which was purchased from (Plasma Chem) company. After that, converted into nanoparticles of specific concentration in ethanol by mixing a certain weight with a certain volume of ethanol. In this work, (0.2mg/mL) nanoparticles were prepared and placed in an ultrasound machine for (5 minutes).

3.6 Preparation Gain Mediums

After the dyes have been prepared with different concentrations (10^{-3}, 10^{-4}, $5x10^{-5}$, 10^{-5}, $5x10^{-6}$ and 10^{-6} M) and also nanoparticles with different types, sizes, and concentrations, the best concentration was selected from each kind of dye and mixed with different types and concentrations of nanoparticles to form various gain medium of random laser , then these media were compared to get the best results.

3.6.1 Gain Medium (kiton dye: Fe_2O_3:Ag Nw)

the gain medium was prepared that includes, Ag nanowires (0.2mg/mL) was prepared .(diameter 50 nm, length ≤ 50 microns) and Fe_2O_3 (0.2mg/mL) in ethanol and the dye solutions have been prepared by dissolving the required amount of kiton dye in ethanol .After that.the

dissolving the required amount of kiton dye in ethanol .After that.the concentration of kiton dye was fixed (1×10^{-5} M). Accordingly, five different random media have been prepared : the first random medium containing (Fe_2O_3 25% +kiton dye 75%), the second medium consisted of (Fe_2O_3 50% +kiton dye 50%), and the third one formed from (AgNw25% +kiton dye 75%). and the fourth (AgNw 50% +kiton dye 50%) and fifth random mediumcomposed of (AgNw 25% +Fe_2O_3 25% +kiton dye 50%,)

3.6.2: Gain Medium (Rh6G dye: PVP polymer : Au thin film)

Here of Au NPs have been prepared by the laser ablation technique. and The dye solutions have been prepared by dissolving the required amount of Rh6G dye in deionized water mixed with 0.03 mg/ml PVP polymer to obtain three different concentrations (1×10^{-3} ,1×10^{-4}, and 1×10^{-5} M). After that, these three different dye concentrations were Spin-coated on a glass substrate at 2,500 rpm. To form three samples of gold thin films.

3.6.3: Gain Medium (RhB dye: Ag Nw)

In this type, the Ag nanowires (diameter 100 nm, length ≤ 50 microns) have been used which were purchased from the German PlasmaChem company. ,in this work, (0.2mg/mL) were prepared . in (deionized water) . The concentration of RhB dye was fixed (1×10^{-5} M). mixed with 0.03 mg/ml PVP polymer) Accordingly, five different random media have been prepared: the first random medium containing (RhB dye + PVP), the second medium consisted (RhB dye + PVP+Ag nanowires10%), and the third one formed from (RhB dye + PVP+Ag nanowires20%). For the fourth random medum, (RhB dye + PVP+Ag nanowires30%) while the fifth random medium composed of (RhB dye + PVP+Ag nanowires40%)

3.7 Fabrication Cavities

3.7.1 Thermal Cavitation

To prepper our samples, we used Kiton red dye dissolved in ethanol at a concentration of $1*10^{-5}$, purchased from Sigma Aldrich Company. The USA Sigma Aldrich Company was the source of the other materials, which included Ag nanowires (length 50 microns, diameter 100 nm), and Fe_2O_3NPS (spherical shape, grain size 50 nm each was prepared with concentration (0.25 gm / 10 ml). After that, the mixture of Kiton dye solution with nanoparticles by ultrasonic bath at 15 min to prepare five samples with different concentration

3.7. 2Thin gold Waveguide -cavity

To get multi wavelength random lasing, this report used the diffused gold NPs in our proposed solid-state random laser substance into the glass. For this purpose, thermally annealed plasmonic glass based on Au NPs was fabricated using the thermal treatment of the thin gold film and investigated for random laser applications. Fig. (3.4) shows the schematic of the manufacturing process of plasmonic glasses based on gold NPs using the thermal annealing method. First, a thin layer of gold with a thickness of 7 nm was deposited on the glass substrate using the physical vapor deposition (PVD) technique. Afterward, the gold-coated glass was placed in the central part of a tubular furnace (AZAR FURNACES, TF5/25 1250) at 550 °C for 4 hours. The oven temperature was increased at a rate of 2 °C per minute, and the cooling mechanism inside the furnace was carried out at the same rate. The annealing process was carried out at atmospheric pressure. A thin gold layer on the glass substrate shows a light gray color before thermal annealing. While after the annealing process, the sample's color changed to pink, confirming the formation of gold nanoparticles. The continuous gold film was gradually dewetted during the annealing process

and converted to the collection of discrete nano-islands. Heat treatment increases the mobility of gold atoms in the thin gold layer and as a result, a continuous gold film becomes a collection of discontinuous nano-islands. The cavities between the nano-islands expanded as the thermal annealing continued, and the separated gold nanoparticles grew. Then Rh6G dye with PVP in different concentrations was added to the substrate.

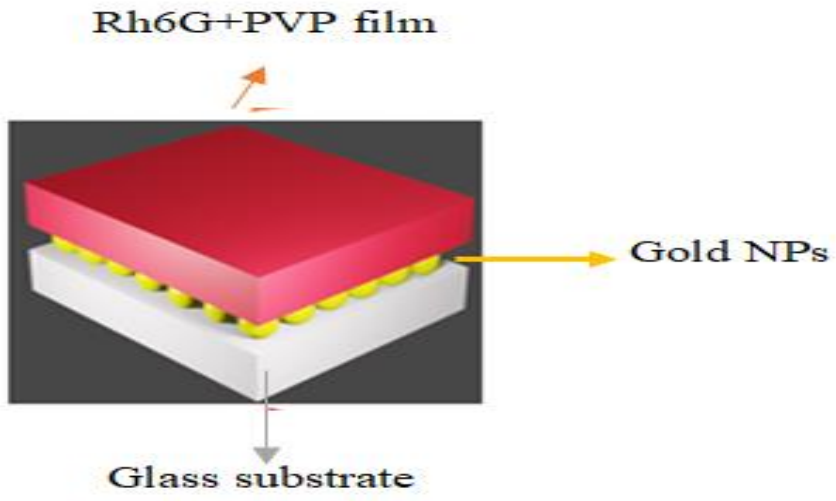

Fig.(3.4) Schematic diagram of the main sample

3.7. 3 (2D gratings-Cavity)

The current research has proposed and carried out the microstructure pattern transferring using a novel, simple-design, and cost-efficient method based on the soft lithography technique, with random lasing properties of the proposed structure investigated. The charge-coupled device (CCD) of a camera was utilized as a stamp, which has a two-dimensional periodic square pattern with a periodicity of about 2.6 μm. First, a CCD was gently extracted from a camera without scratching its surface, and then a layer of Kapton tape was stuck on the CCD stamp by applying pressure Fig.(3.5) (a). Thereafter, the sample was placed on a heater for 1 h at 75 ℃ to

achieve a high-quality pattern transfer. The sample was pressurized at room temperature for one day to stabilize the two-dimensional pattern onto the Kapton film. After 24 h, the Kapton tape was carefully peeled off of the CCD stamp, where a 2D perforated Kapton film was obtained as shown colorful in Fig.(3.5) (a).

Subsequently, the patterned Kapton and curved glass substrate (watch glass) were placed under a vacuum plasma treatment for 10 min to enhance the adhesion and activation of their surfaces. The schematic of the surface modification by plasma technology employed argon gas plasma in a vacuumed chamber is displayed in Fig.(3.5) (b). The experimental setup consists of a high voltage DC power supply, vacuum chamber with high voltage and grounded sample holder electrode (for glass substrate), plus gas feeding and the measurement systems. The perforated Kapton film and glass substrate were placed on the grounded electrode in the plasma treatment chamber. Afterward, the grade 5 argon gas was injected into the chamber, which elevated the pressure to 13.3 Pa so that the plasma can be initiated. After the formation of plasma, the pressure was reduced to ~0.53 Pa, in which the surface modification would show the best quality. The plasma treatment was continued for 10 min to enhance the surface activation and adhesion properties. The DC power supply output was set to a voltage of 340 V and a current of 40 mA . After the plasma treatment process, the patterned Kapton film was stuck on the glass substrate, and the sample was kept at room temperature for 1 h. After 1 hour, the Kapton film was gently removed from the glass substrate, and the 2D periodic square array was successfully transferred onto the glass substrate.

Finally, a thin layer of gold (35 nm thick) was deposited on the 2D glass substrate using the physical vapor deposition (PVD) method. In this way, a two-dimensional gold square array on a glass substrate was successfully

produced using a novel, simple-design, and cost-efficient method based on the soft lithography technique and plasma technology. A mixture of polyvinyl pyrolidone (PVP) polymer and Rh6G dye solutions was coated onto the fabricated 2D gold square array using the spin coating method at 2000 rpm to achieve the structure as Glass/ 2D perforated gold structure/ PVP+Rh6G.

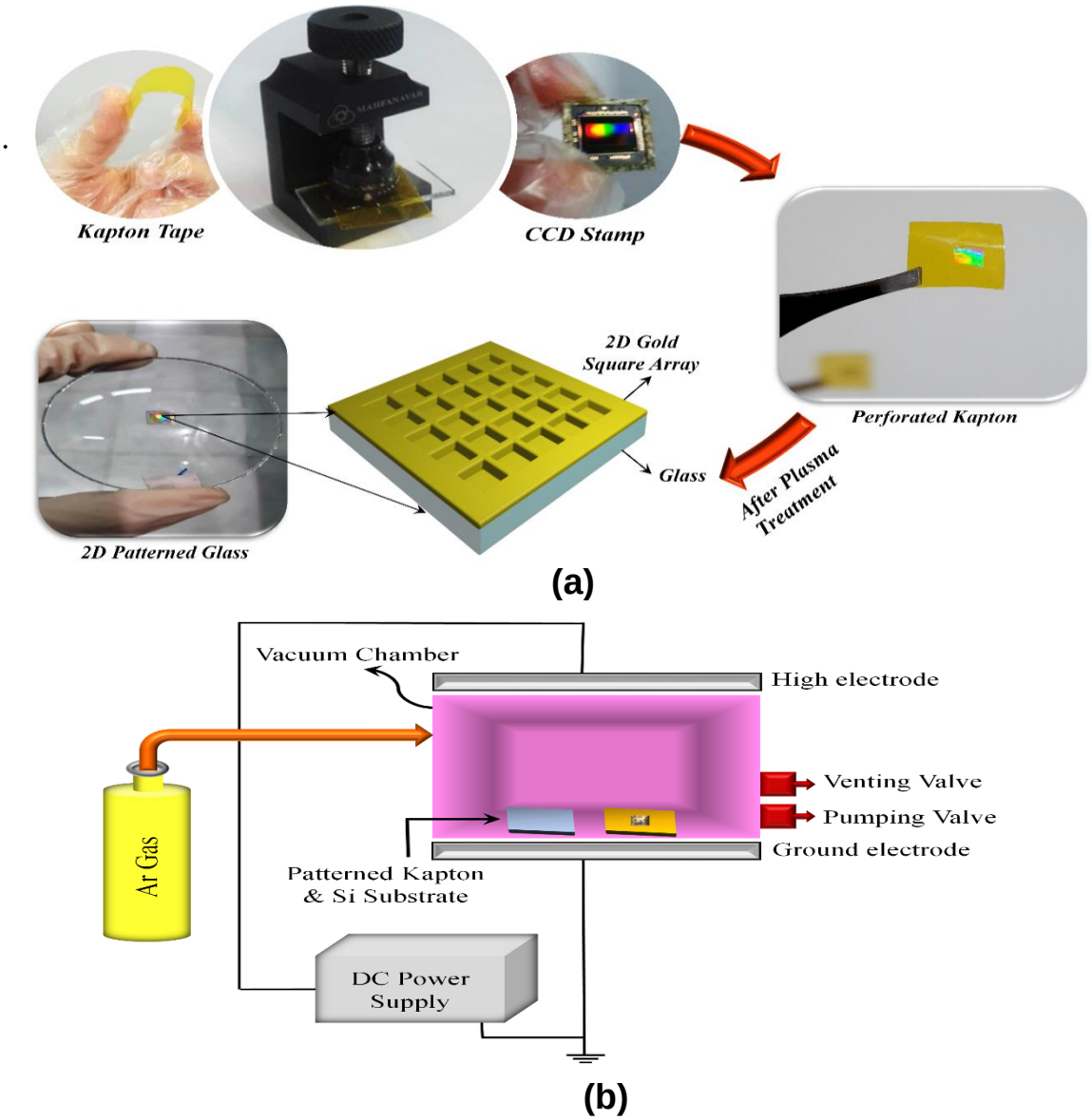

Figure (3.5) (a) A process flow diagram of the sample preparation process using the real images of the perforated Kapton and 2D patterned glass, and (b) a schematic array of the plasma treatment process.

3.7.4 Magneto-optical Cavity

Two dimensional structure were fabricated by soft lithography method onto the Polydimethylsiloxane (PDMS) substrate as explain in detail in ref [20]. When two dimensional structure get ready, it was deposited by gold thin layer by thickness of 35 nm via sputtering machine and it covers by FeB thin layer by radio frequency (RF) sputtering machine method.

It should be mentioned that the sputtering deposition of FeB thin film, 45 nm, was performed under the process conditions as follows: RF power of 70 W, chamber pressure of 0.004 mbar and substrate rotation speed of 28 rpm. Also, DC sputtering deposition of FeB thin film was performed under the conditions of DC voltage of 340 V, plasma current of 0.03 mA, chamber pressure of 0.004 mbar and substrate rotation speed of 28 rpm. As well as, DC sputtering deposition of gold thin film was carried out under the conditions of DC voltage of 365 V, plasma current of 0.01 mA, chamber pressure of 0.005 mbar and substrate rotation speed of 28 rpm. Finally, the sample coat by Rhodamine 6G dye and after drying process, Fig.(3.6) ,it pumped by Nd: YAG laser to get the random lasing under external magnetic field set to 50 mT.

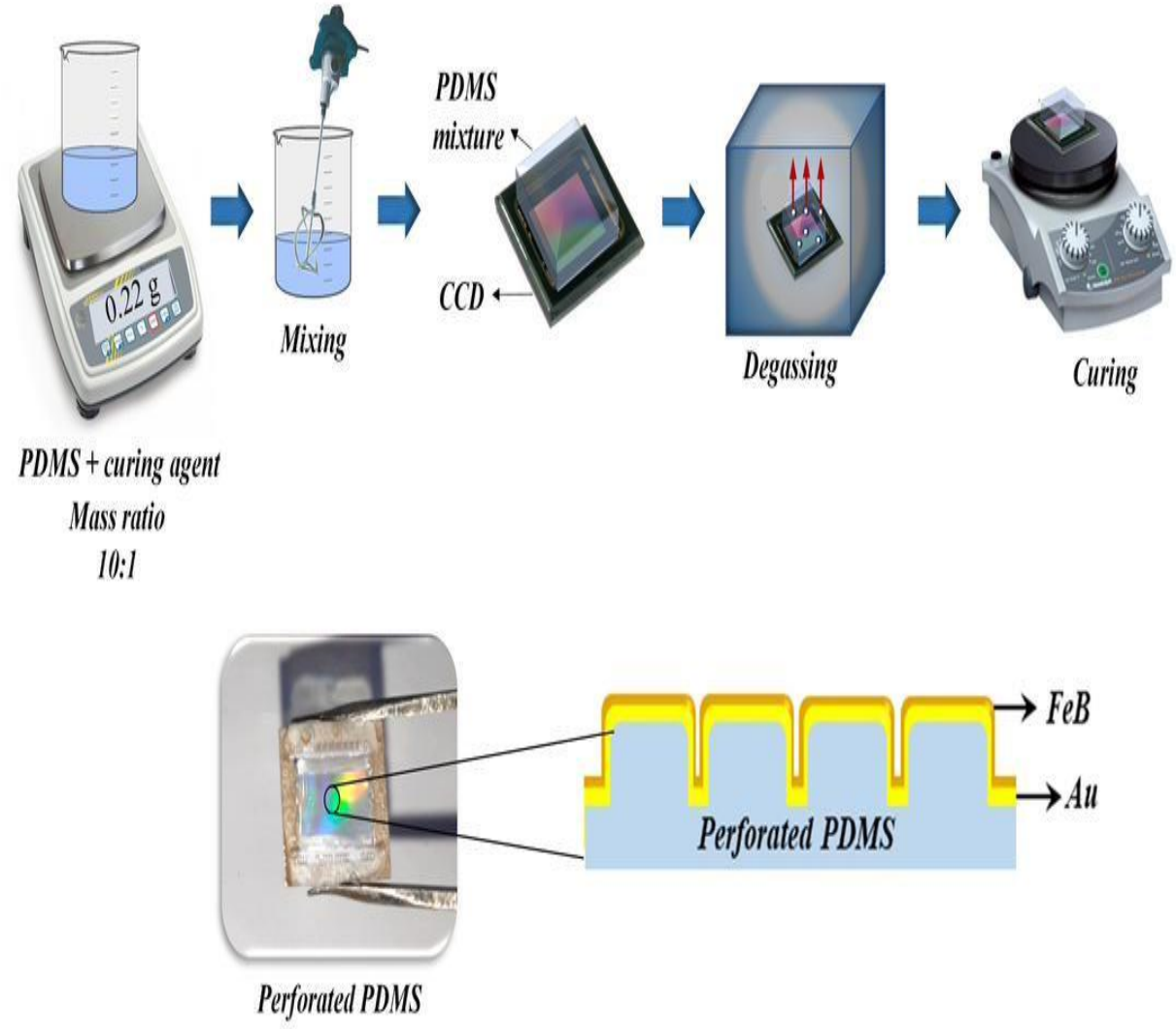

Fig.(3.6) A process diagram of the sample preparation process the and real images 2D

3.7. 5 Triple optical cavity

In this work, to form a ring resonator, a silica glass material with a thickness of (2 mm) was used, and a circular hole was drilled with a diameter of (9 mm) and a depth of (2 mm) and care was taken that the edges be irregular to provide the scattered reflection of both the pumping beam and the radiation generated by the dye this ring resonator was then placed on glass substrates to form a cavity. Then, this annular cavity was coated with gold using the (dip coating) method. Where this annular cavity

was immersed from the inside with a nano solution formed (water + gold) with (10) times, and each time it was completely immersed in a time of 2 minutes. Then it is withdrawn at a very slow speed .Thereafter, the sample was placed on a heater for 5 min at 75 ℃ to achieve a high-quality pattern transfer. . until it is coated from the inside (sides and bottom) until the thickness of the film becomes approximately (7µm). Then this ring cavity is filled with (RhB dye dissolved in pure water with a polymer (PVP) with Nw Ag at different concentrations. Thus, the laser chamber was formed to form an annular resonator plus an external reflective surface in addition to the main resonator of the random laser consisting of (dye + nanomaterial + polymer). Fig.(3.7)

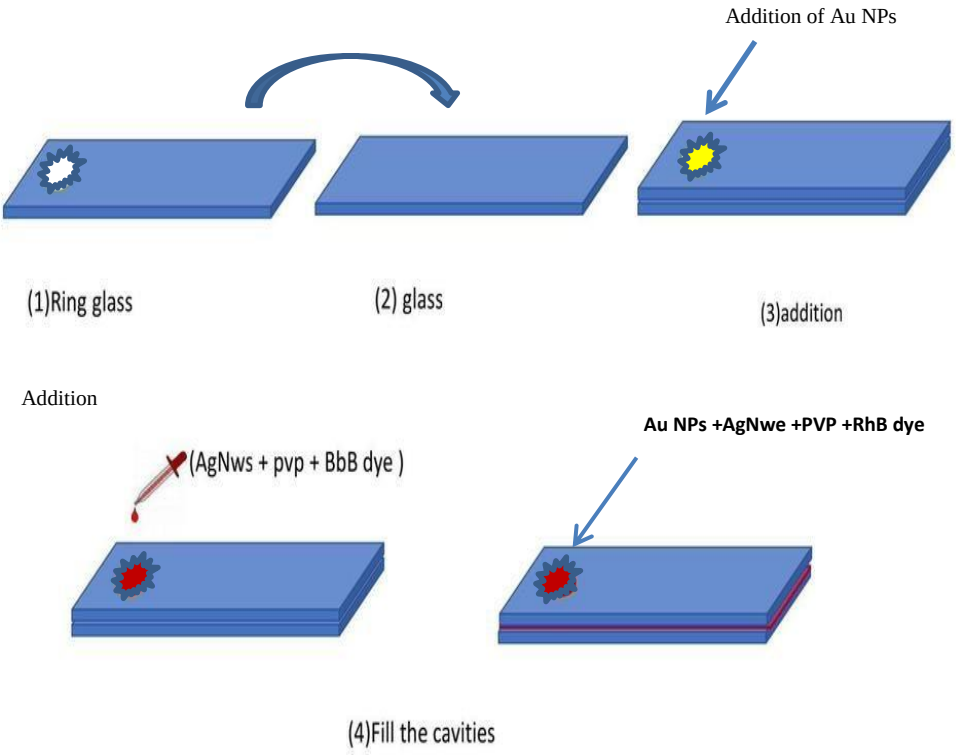

Fig.(3.7) Schematic diagram of the sample preparation

3.8 Random laser measurements

Two experimental setups were used in this section, the first one for liquid samples, and the second for thin-film and layers samples

3.8.1 Experimental setup for thermocavitation generation and random laser parameter analysis

The schematic of the experimental set-up for thermocavitation formation via microbubbles is shown in Fig.(3.8). A CW laser beam with a 405 nm wavelength and 100 mW of power was used as the pump beam. The laser beam was attenuated with an iris, blocking a large part of the beam reduction. The low power ensured that the laser beam produced a slight increase in the temperature of the dye solution and it was focused (by lens at f = 8 cm) inside a liquid cuvette (dimension is 1 × 1 × 4.5 cm) filled with Kiton red dye solution and NPs to increase the temperature and generate bubbles. The pumping beam, after passing through a cuvette, falls onto the screen to record far-field patterns are recorded by a video camera that is indicative of the conversion from SPM to TB and beyond TB. Also, the scattered light from the cuvette from the pump beam is measured at an angle θ = 60° from the forward direction using a video camera. To record the bubble effect with a CCD camera, a probe beam He-Ne laser (= 632.8 nm, 75 mW) is aligned with two mirrors perpendicular to the direction of a cuvette and crossed with a pump beam laser inside the cuvette.

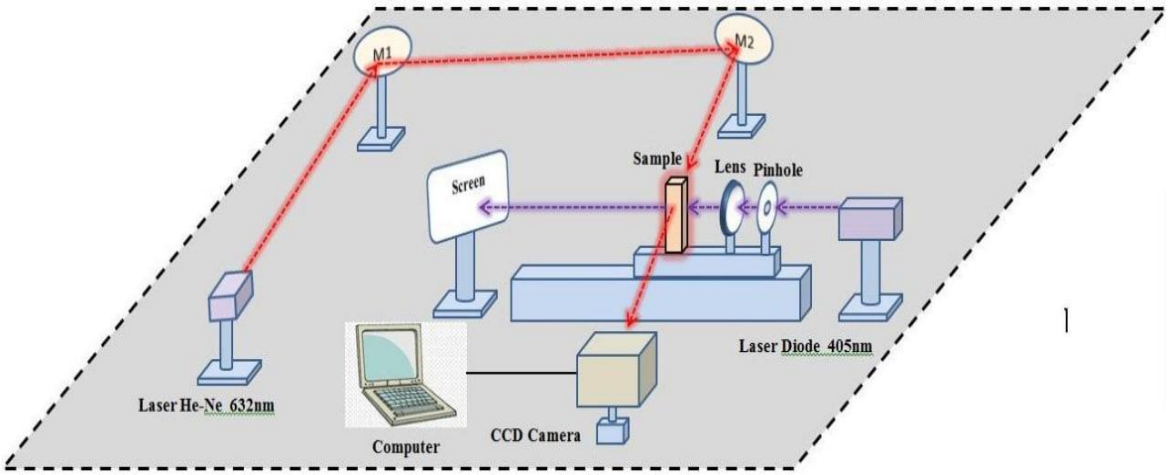

Fig.(3.8). Experimental setup used to generate and analyze thermal cavittation.

3.9 Experimental setup for Random Laser Parameter Analysis in Liquid and Solid Phases

3.9.1 Experimental setup for thermal cavitation in liquid samples

To get random lasing, second harmonic generation (532 nm) of Nd:YAG pulsed laser was used a pumping sourse with a different pumping energy, repetition rate of 10 Hz and a pulse width of 5 ns. with and without laser (407 nm) 90^{o} degrees relative to the direction second harmonic generation (532 nm) of Nd:YAG intersected inside the cuvette . By this source we pumped our samples and collected the lasing by avantes spectrometer in 45^{o} degrees relative to the pumping beam direction as shown schematically in Fig.(3.9)

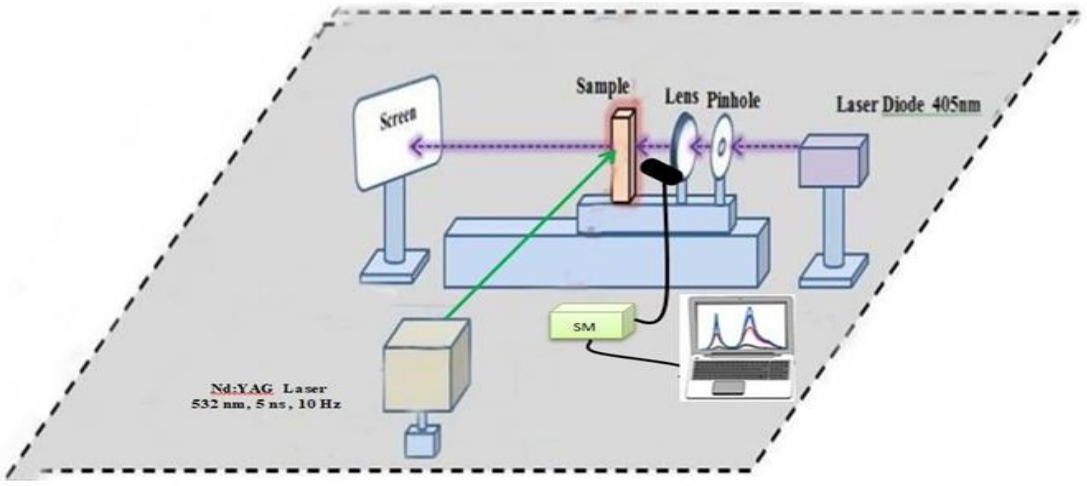

Fig.(3.9) Experimental setup used to generate thermo cavittation.and analyze random laser parameters

3.9.2 Experimental setup (2D gratings-Cavity)

The experimental arrangement for the RL based on of the proposed 2D plasmonic square array on a glass substrate is shown in Fig. (3-10). During the experiment, A second harmonic generation (SHG) at 532 nm . The emissions from the samples were collected by using a fiber-coupled spectrometer (Ocean Optics USB2000+UV-VS-ES with 0.3 nm spectral resolution) and the fiber probe was placed at a fixed distance (typically 2 cm) at angle 45 from the center axis of the cell by the rotatable arm. The Pump laser power incident on the sample was controlled using appropriate neutral density filter (NDF)

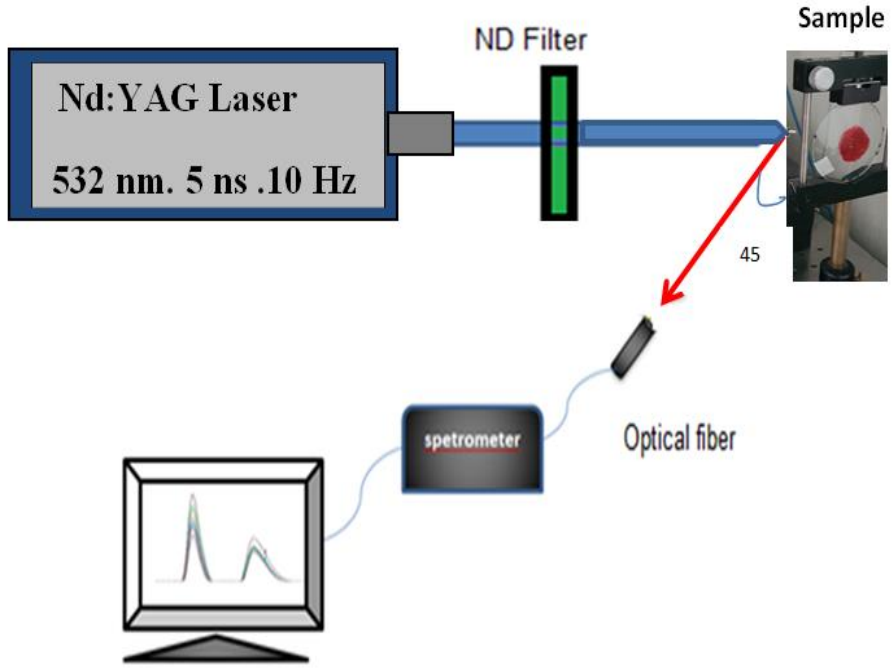

Fig.(3-10) Experimental setup of PVP+Rh6G of the 2D for Random Lasing performance

3.9.3 Experimental setup (Magneto-optical Cavity)

Figure (3.11) shows the experimental setup used to magnetically control the random laser The sample (1cm x 1cm) was placed under the external magnetic field. the Q-switched frequency was orientated to double Nd: YAG (532 nm, pulse width 5 nm, pulse repetition rate 10 Hz) with respect to the normal shape of the sample face. Laser emission from the front face of the enclosure was collected using a plain spectrophotometer to a fiber-coupled spectrometer (Ocean Optics USB2000 + UV-VS-ES with a spectral resolution of 0.3 nm) at an angle of 45°. Direction of the magnetic field was perpendicular to the light propagation on the sample with a distance of 10 cm.

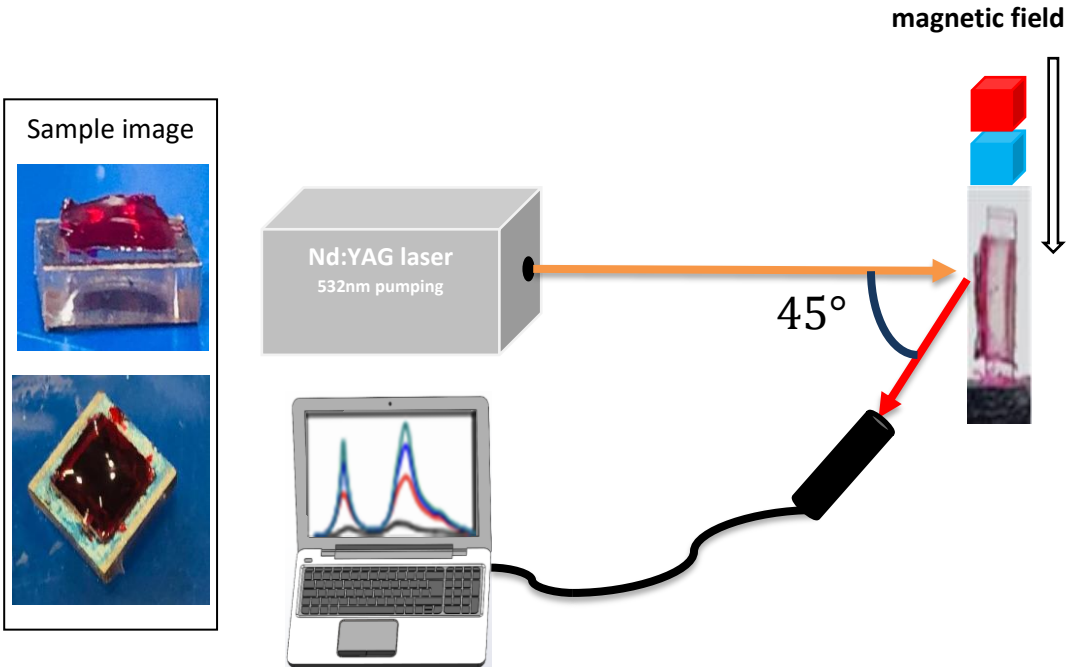

Figure (3.11): Real picture of the sample and the schematic diagram of experimental setup.

Chapter Four
Results
And
Discussions

Chapter Four Results and Discussions

4.1 Introduction

In this chapter, the structure characterizations of the prepared samples were investigated by TEM. With regard to optical characteristics, the absorption spectrum for each of the noble metal group and not noble(AgNWe, fe2o3@AgNWe , and Au nanoparticles) were studied. And also the absorption samples by using UV-VIS spectrometer, and fluorescence spectrum of (RhB, Rh6G, and kiton dyes) with and without mixing with nanoparticles were studied, it was determined the appropriate concentrations for our work. The result of the spectral study also includes plasmonic multi-wavelength random laser emission tests for different concentrations and gain media (liquid and film)to form composite cavities. In these tests, different pump energies were used, to achieve the coherent random lasing, and also to determine the laser threshold for each samples Then to compare between our results for each concentration, and output peak intensity, and FWHM. , the sample was exposed to pulsed laser With and without an external magnetic field

4.2 (Thermal Cavitation) Random Laser

In this part, the most important composite cavities affecting the random laser properties will be reviewed and the consequent determination of the appropriate value for this or that factor based on the improvement it brings to the random laser output. The impact results of these composite cavities will be discussed in some detail.

4.2.1 Optical Characterizations

4.2.1.1Absorption Spectrum of Kiton red Dye

Eight different concentrations of the kiton red dye (1×10^{-6}, 5×10^{-6}, 1×10^{-5}, 5×10^{-5}, $1\times^{10-4}$, 5×10^{-4}, 1×10^{-3} and 5×10^{-3}) M which dissolved in ethanol have been studied. Only three of the eight concentrations obtained an absorption spectrum within the acceptable limit as shown in Fig. (4.1).

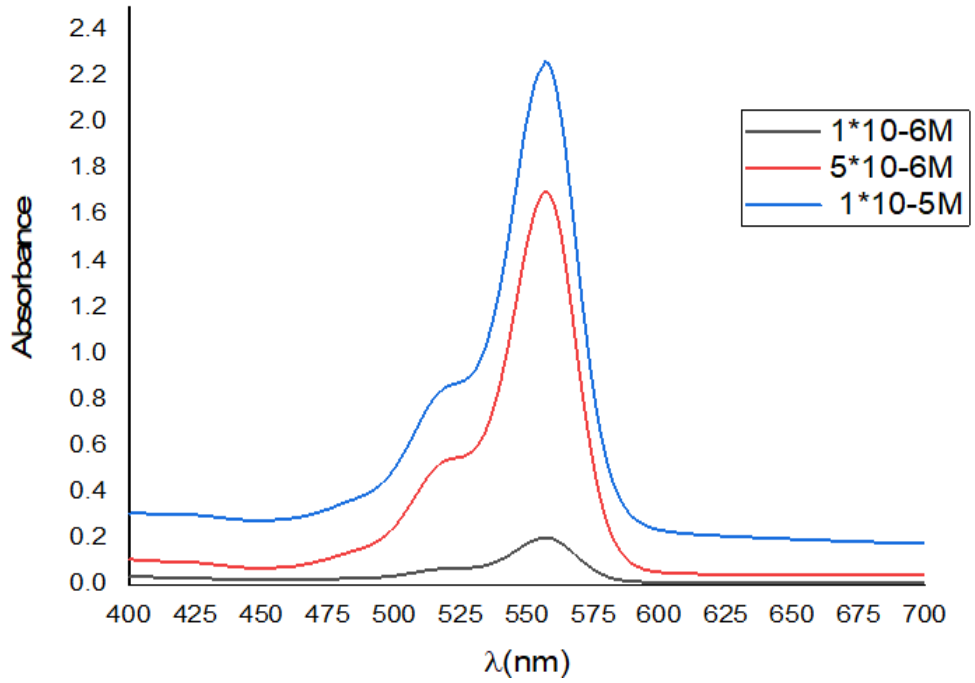

Fig.(4.1) Absorption spectra of kiton red dye dissolved in ethanol with different concentrations

It is very clearly and as it appears from the Fig.(4.1) that with increasing the concentration of the dye in the solution, the absorption spectrum increases and regularly in a certain range of wavelengths around 470-600 nm with its maximum peak wave length at 560 nm Whereas, it is known

that the dye solution has a lower absorption spectrum at wavelengths less than 470 nm, and for the region of wavelengths greater than 600 nm, the absorbance minimizes to the lowest, regardless of the dye concentration.

Therefore, the best absorption spectrum of kiton red dye was obtained at concentration 1×10-5 M at 559.3 nm. Thus, this concentration will be adopted for the remainder of our random laser action. Also, used of methanol as a host for the kiton red dye in part of the work in line with the host medium of the nanomaterials used are Ag NW, Fe_2O_3Nps.

4.2.1.2 Fluorescence Spectrum of Kiton Red Dye

After preparing solutions of kiton red dye (in ethanol) and studying the absorption spectrum of this dye with different concentrations in the previous section, the fluorescence spectra curves for the different concentrations of kiton red dye were illustrated in Fig.(4.2) using a green source (532 nm).

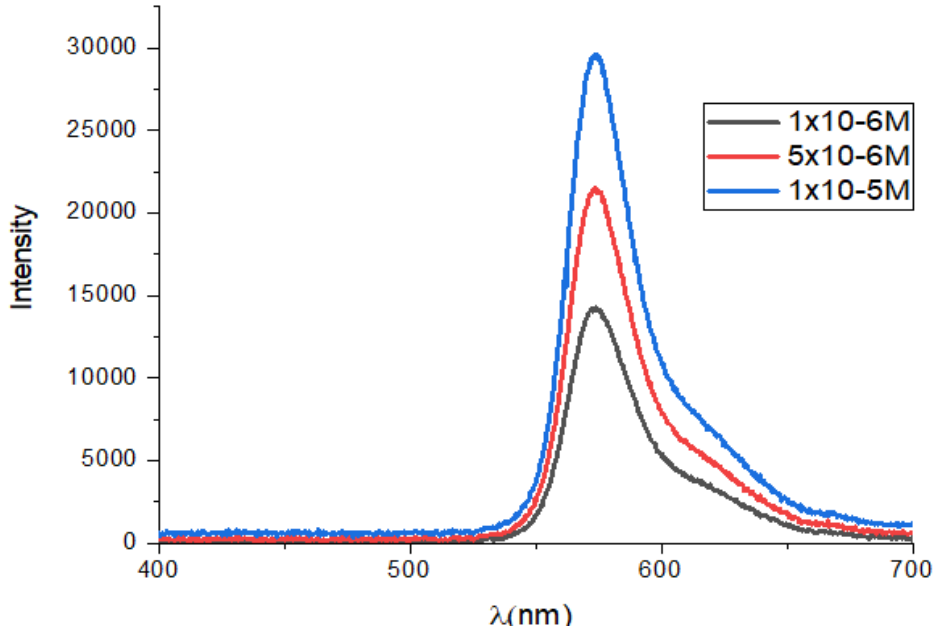

Fig. (4.2) Fluorescence spectrum of kiton red dye in ethanol at different concentrations

For the intensity of the fluorescence spectrum, it is common, and as literature shows, that it increases with increasing dye concentration, and this is evident in the above figure when moving from a lower concentration 1×10^{-6} M to a higher concentration 1×10^{-5} M, where the intensity of the fluorescence spectrum is clearly increased but the verse is reflected in relation to the rest of the concentrations where a decrease in intensity fluorescence is observed with an increase in the concentration of the dye, and this can be attributed to the appearance of dimers as supported by [185]. Dye concentration 1×10^{-5} M showed the best fluorescence spectrum and therefore strengthened our selection as the best suitable concentration for random laser action based on the absorption spectrum.

Moreover, increasing the dye concentration causes the fluorescence spectrum to shift towards longer wavelengths (redshift). It is shifted from 587 nm at concentration of 5×10^{-6} M to 603 nm at concentration of 1×10^{-4} M. Thus, the displacement amount towards the longer wavelengths (red

shift) is about 16 nm. Which means that the fluorescence of laser dye has moved to another wavelength. The redshift in the fluorescence spectrum of the kiton red dye due to its increased concentration can be attributed to the fact that the dipole moment of the excited state is higher than that of the ground state and these results got supported by [186].

4.2.1.3 Absorption spectrum of Kiton red dye mix with NPs

Fig.(4.3) shows the absorption spectra of a pure red kiton dye at a concentration of 1 x 10-^{5} M and a kiton dye solution mixed with two different types of nanoparticles (AgNW and Fe2O3 NPs) at different concentrations of each one. The pure red dye's absorption spectrum, which has a peak at 560 nm, is shown by the blue curve. The dye's absorption spectrum has a full width at half-maximum (FWHM) value greater than 80 nm. This figure also shows that the dye's absorption peak shifted from 560 to 570 nm and broadens when it is combined with Ag NWs at various concentrations, It was also noticed that adding Fe_2O_3 with and without Ag NWS nanoparticles to pure dye has the same effect, causing the wavelength to shift from 560 nm to 585 nm and 560 to 580 nm, respectively, with the broadening of the bandwidth, the results agree with [187].

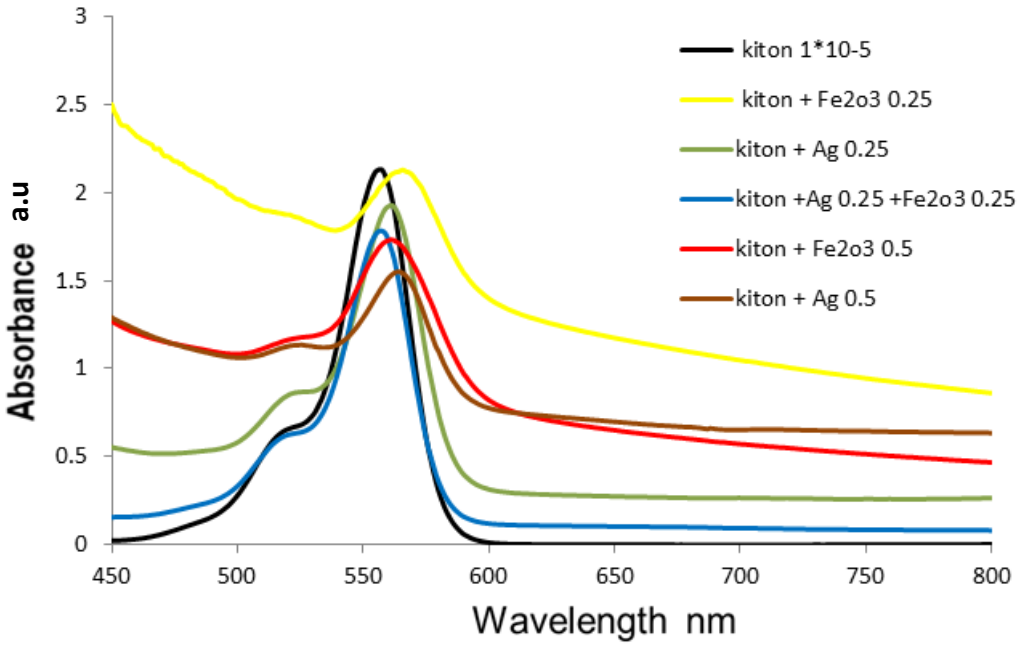

Fig.(4.3). Absorption spectrum of Pure Kiton red dye (black blue curve) , mix (Kition red dye + Ag NWs 0.25 gm/10ml) (brown curve) , mix (Kition red dye + Ag NWs 0.5 gm/10ml) (pureple curve), mix (Kition red dye + Fe_2O_3 NPs 0.25 gm/10ml) (red curve) , mix (Kition red dye + Fe2O3 NPs 0.25 gm/10ml) (green curve) and mix (Kition red dye + Fe2O3 NPs 0.25 gm/10ml + Ag NWs 0.5 gm/10ml) (blue curve)

4.2.2 Structure Characterization

In this type of random laser,Fe2O3 NPs and Ag nanowires have been used as thermal cavities , as scattering centers in a random medium containing (kiton red dey) as the gain medium. which included $Fe_2O_3NP_S$ (spherical shape, grain size 50 nm) and the Ag nanowires with an average particle size (50 nm) and lengths less than 50 microns were purchased from the German PlasmaChem company. Fig.(4.4) displays the transmission electron microscopy (TEM)was conducted using a specific instrument, the (CM10 PW6020 model) from Philips-Germany. and Field Emission Scanning Electron Microscopes (FE-SEM) type (Model: LEO 1450 VP, voltage: 20 kv) (made in Germany) .For both materials (Fe_2O3 NPs and Ag nanowires) , as well as the real images of the boxe as received from the supplier company..

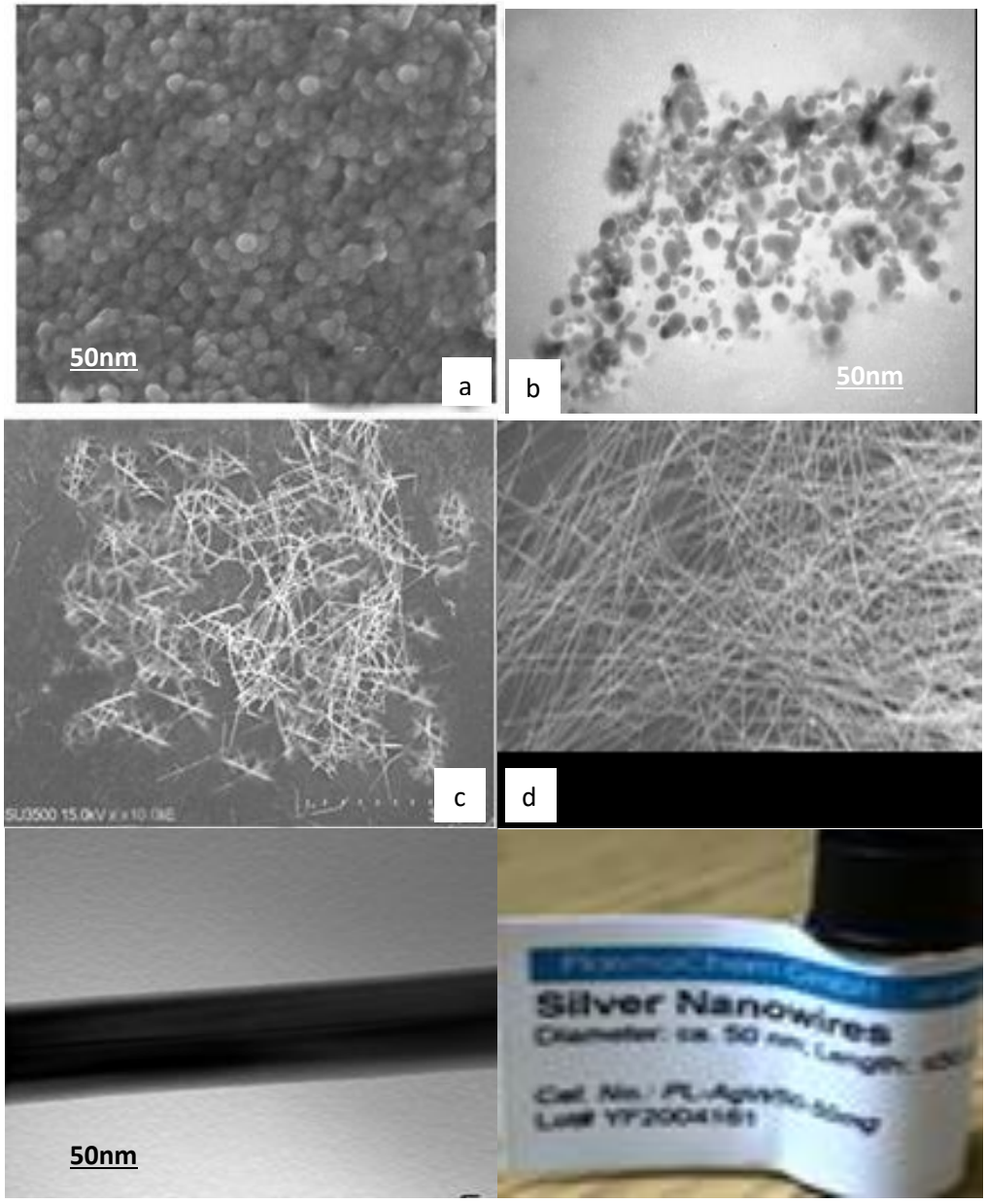

Fig.(4.4) (a) FE-SEM image Fe2O3 NPs(b) TEM images of Fe2O3 (c) FE-SEM image of Ag nanowires (d)TEM images of Ag nanowires,in addition to real images of boxe as received from the supplier company.

4.2.3 Thermal Cavitation

4.2.3.1 Thermal Cavitation Generating Process

The most common method of generating the thermal cavity includes the constant wave concentration (CW) of the laser beam on a liquid medium. In this work, we have studied the phenomenon of the composition of the thermal cavity using the CW laser with a wave length of 405 nm and a 100 mwatt optical power that focuses on the quartz cavity that contains a dye solution with different types of nanoparticles. The heat caused by NP_S and the heat lost in the surrounding dye solution bubbles, we have noticed the effect (Ag Nwe, Fe_2O_3NPs and (Ag Nwe: Fe_2O_3NPS) on the speed of the bubble formation and its number. The scattered light from the Covet pump package was measured at an angle $\theta = 60$ degrees from the front trend using a video camera. (105 frames per second), CCD camera, a probe beams He-Ne laser (632.8 nm, 75mW) is aligned with two mirrors perpendicular to the direction of a cuvette and crossed with a pump beam laser inside the cuvette. The efficiency for the absorbance of laser beam can be enhanced by adding light-absorbing nanomaterials . The Fe_2O_3 and Silver (AgNWS) is one of the preferred and popular nanoparticles for bubble generation. In this work, we will focus on the cavity generated by a continuous wavelength rather than pulsed laser, as it results from the absorption of a beam laser by liquid (ketone dye in ethanol solution) with the addition of nanomaterial, and the formation of hot bubbles, In thermal media, the absorbed optical power heats the material causing a temperature change, and thereby a change in the refractive index. This study also discusses the fundamental theory of self-phase modulation (SPM) in thermal media and its effects. Investigations are also being conducted into thermal blooming (TB), which happens beyond SPM.

As mentioned earlier, as the pump power increases, the SPM due to the thermal lens turns into TB. Fig.(4.5) shows the far-field diffraction patterns of the pump beams generated by the thermal lens and switching from SPM to TB, causing bubbles to form in a 3D optical cuvette with different densities and sizes. After the laser is pointed at the cuvette holding a ketone dye solution ($1x10^{-5}$ M), the ring pattern is symmetric, and the number of rings depends on the power of incident beam, absorption medium, dye concentration, and cuvette length.as demonstrated by [188]. After a while of incident, the laser beams on the mixture, we notice that the bubbles start to form, but in a limited number and are unstable. We observed that the bubble reconstructs over time (120 secs after initial bubble formation). The number and size of bubbles formed depends on the type and concentration of nanoparticles added to the mix solution, the break-down region is also not limited to the focal point but extends up to the Rayleigh length of the laser source, which results in the formation of many bubbles of different diameters. Due to the has a silver to the resonance plasmonic at the wavelength of the incident laser beam, which improved the interaction between the laser beam and the dye, the mixture (75% Ag + 25% kiton) depicted in the figure (5-c), produced the best results for bubble production and quantity. The same results were also obtained using the mixture (75% Fe2O3NPs + 25% kiton) shown in figure (6-e,), but the results were improved here because the Fe_2O_3 has high nonlinearity properties, which agrees with [189].

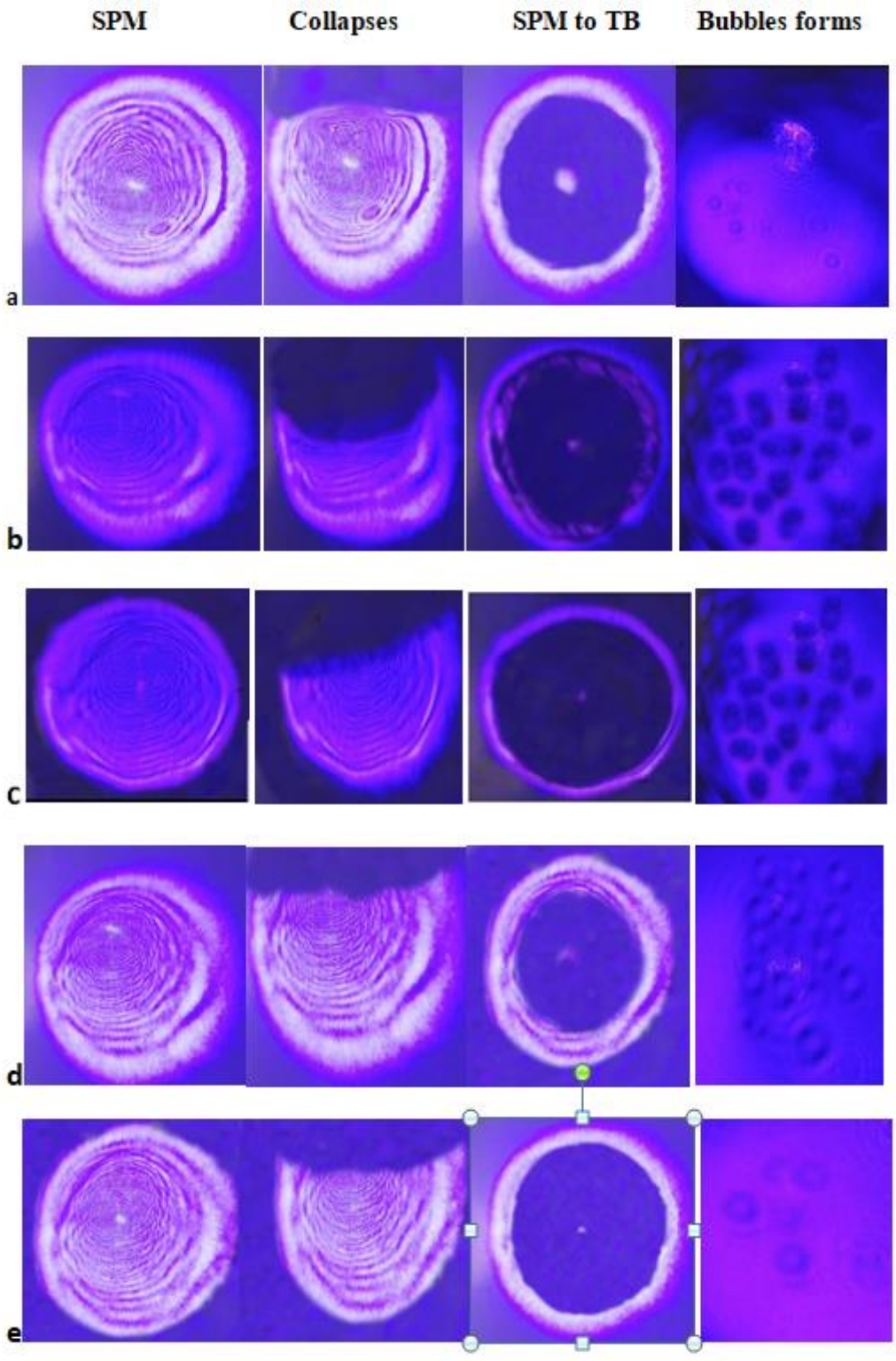

Fig.(4.5) Experimental far-field diffraction patterns of pump beams for a-Kiton dye solution (1×10^{-5}) , b-mix solution (50% AgNW + 50% kiton), and c-mix solution 25% Ag + 75% kiton) d-mix solution (50% Fe_2O_3NPs + 50% kiton), e-mix solution (25% Fe_2O_3NPs + 75% kiton)

4.2.3.2 Bubbles created by Lasers and NPs effect on Scattering Light

After the generation of bubbles by the focused laser beam (100 mW) and scattering the laser radiation, pictured with the camera shown in Figure Fig (4-7 a to f) on the side of the cuvette, at different causes. The direction of scattering is due to the proximity of the bubbles to the focus point of the laser beam, the number of bubbles and the type and concentration of nanomaterials. Fig (4-6)a- no scattering was observed on the pump laser beam when there was only a pure kiton dye solution in the cuvette. This indicates that the laser creates no small bubbles even after 2 minutes of beam presence. However, on other figures, it has been found that when the nanomaterial (AgNWs + Fe_2O_3 NPs) is added to a pure Kiten dye solution in various ratios of incorporation, light scattering is still present but has varied values. The type of scattering caused by this dispersion in the laser radiation of beam was (Rayleigh scattering) due to the grain size of the nanomaterials used is less than the wavelength of the laser beam. The microbubble generation interaction between the incident pump beam and mixture (dye solution + NPS) leads to the heat generated from NPs transferring to the dye solution and generating micro bubbles. The micro bubbles have a diameter approximately equal to the wavelength of the incident pump beam, which causes the Mie scattering. The best results have been observed in Fig.(4.6) (e and f). This has another meaning and the concentration and type of nanomaterials have a great effect on the formation of bubbles and thus affecting the amount of scattered beam.

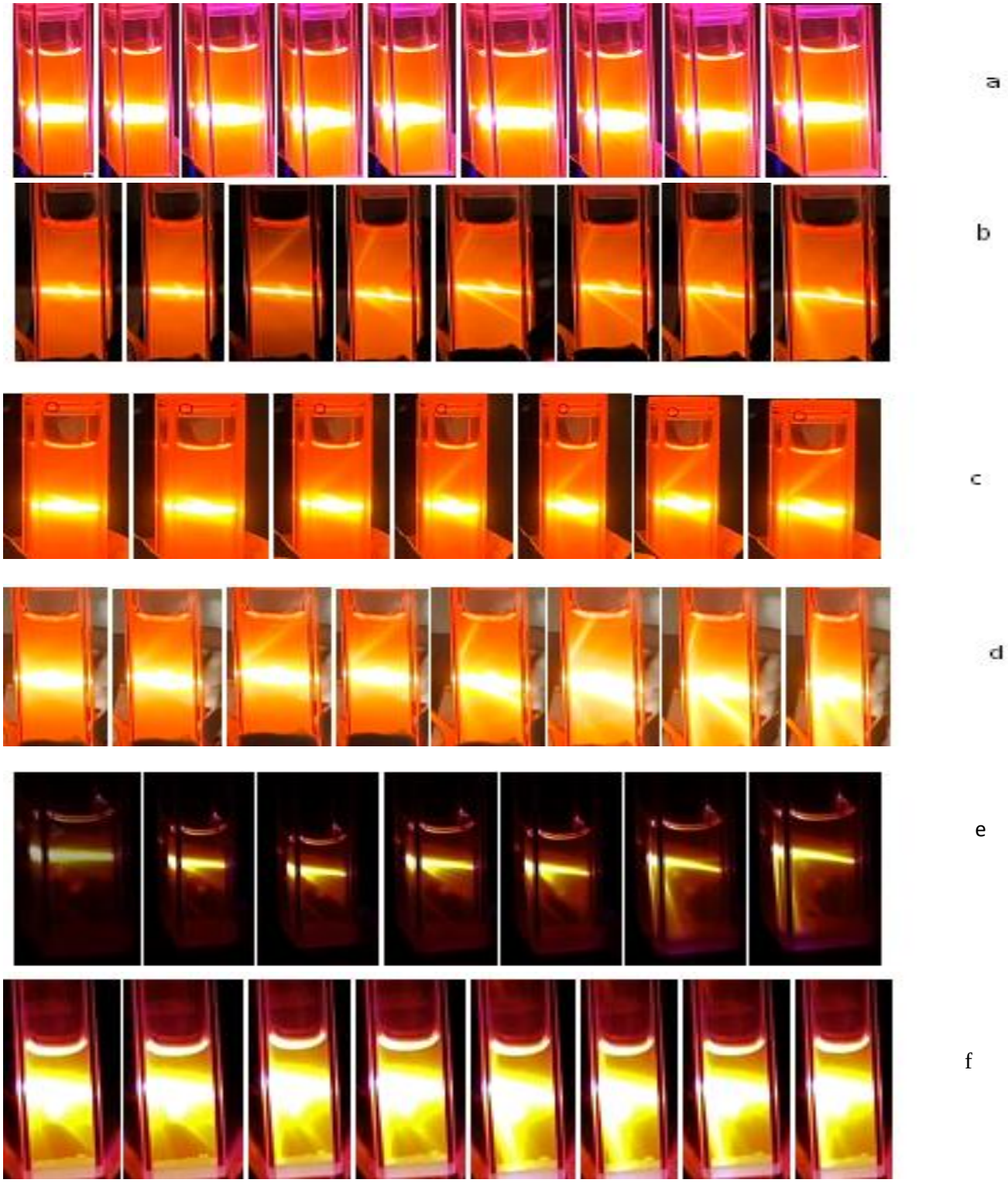

Fig.(4.6) Left to right : a number of pictures taken at increasing time sequence , showing microbubble scattering of the incident pump laser radiation on a- pure kiton red dye solution at a concentration of 10-5 b- the mixture (75% Kiton red + 25 %Fe_2O_3 NPs). C- the mixture (50% Kiton + 50 %Fe_2O_3 NPs). d- the mixture (75% Kiton + 25 % Ag nanowire). e- the mixture (50% Kiton red + 50 % Ag nanowire). f- the mixture (50% Kiton red +25 % Ag nanowire +25 %Fe_2O_3 NPs)

4.2.3.3 Effect the bubbles on Probe Beam of laser propagates through it is.

The Fig.(4.7)shows the radial profiles of the Gaussian beam propagation through one of the best samples (a mixture of 50% Kiton red +25 % Ag nanowire +25 %Fe_2O_3 NPs)) during which it easily generate bubbles of different densities, sizes, and locationse in the temperature area which were recorded with a CCD camera on a time sequence of about 14 s. The maxima distributed over the complete area of the spot has been observed at after time (12s) from initial intensity distribution Gaussian at time = (0s); this distortion in the pump beam profile may have arisen due to thermal blooming, microbubble nucleation centered around beam and turbulences.

A low power focused 632 nm laser beam (probe) is introduced into our samples and the transmitted powers are tested for the following six cases with and without the power-pumping beam: 405 nm. The data measurements are displayed in Table(1)

(a) Laser probe only at t=0s (b) laser probe+ laser pump at time 4s

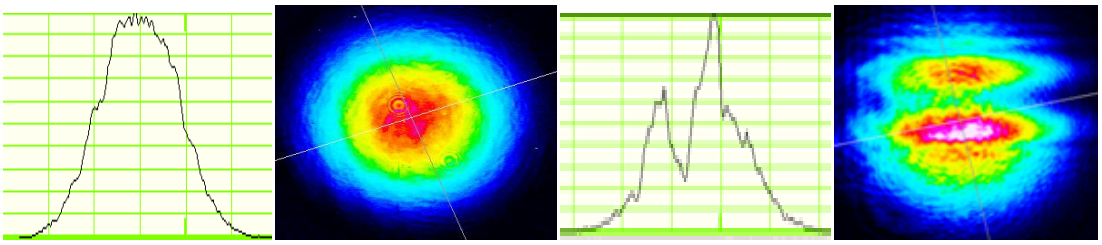

(c) laser probe+ laser pump at time 8 s (d) laser probe+ laser pump at time 12s

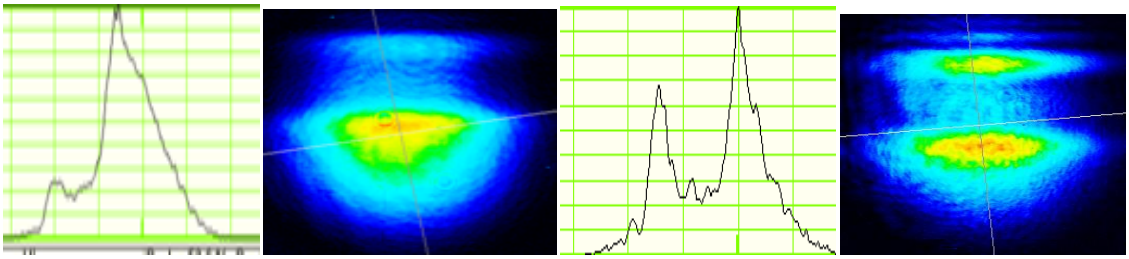

(e) laser probe+ laser pump at time 14s

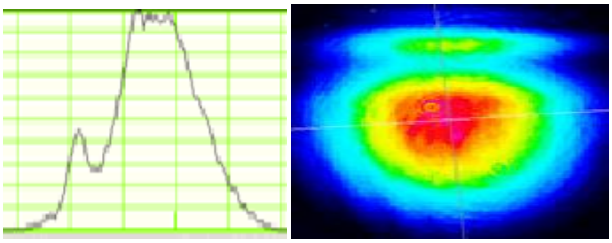

Fig (4.7): Probe Beam profile distortion (a) without pump laser and thus bubbles (t=0) and with bubbles after (b) 4s, (c) 8s, (d) 12s and (e) 14s on sample (mixture of 50% Kiton red +25 % Ag nanowire +25 %Fe_2O_3 NPs)

A possibility of generating bubbles and affecting laser beam transition can be observed by examining the ratios between incident power and transmission power from samples with and without the power pumping beam: 405nm. The first ratio (without pumping beam) illustrates the absorption effect of dye solution and nanoparticles with a absence of a bubbles. And the second ratio (with pumping beam) illustrates the absorption effect of dye solution and nanoparticles with a present of a bubbles . It is clear that there is increased absorption from the samples in the presence of the bubbles and decreased the transmittance

Table(4.1): Measured transmitted power of 632 nm laser for six trials each for without and with pump beam 405nm.

Samples	Transmittance	
	Transmittance without pump beam (%) (first ratio)	Transmittance with pump beam (%), (second ratio)
Pure kiton red dye solution at concentration of 10^{-5} M	0.84	0.80
Mixture (75% Kiton red + 25 %Fe2O3 NPs)	0.73	034
Mixture (50% Kiton + 50 %Fe2O3 NPs)	0.65	0.29
Mixture (70% Kiton red + 25 % Ag nanowire)	0.7	0.31
Mixture (50% Kiton red + 50 % Ag nanowire)	0.6	0.28
Mixture (50% Kiton red +25 % Ag nanowire +25 %Fe2O3 NPs)	0.58	0.25

We demonstrated that cavitation bubbles can be generated using a CW laser focused on a Kiton red dye solution containing nanoparticles, with the added benefit of easy bubble formation and controllable density and size, which in turn is a function of the laser power and concentration of nanomaterials. In addition, with the addition of the Kiton red dye nanomaterial and an increase in its concentration, the total time elapsed between the SPM and TB is reduced. The findings demonstrate that thermal bloom causes a change in the intensity and distribution of the beam's image as it passes through the bubbles, and that the bubbles' effect on beam scattering is not a nonlinear optical phenomenon. They can also be employed as scattering centers in the random laser due to the quantity of scattering in the laser beam created by bubbles.

4.2.4 Effect of Thermal Cavitation on Random Laser parameters

Effect of thermal cavity on the laser modulus of a ketone dye solution with five different concentrations dissolved in ethanol and two nanomaterials (AgNws, Fe_2O_3NPs and Ag Nws: Fe_2O_3NPs) with and without a thermal cavity Fig. (4.9). Evolution of the emission spectra without the thermal cavity using a 532 nm laser, which consisted of 70% ketone red dye with a concentration of (1×10^{-5} M) 30% Fe_2O_3 and the same concentration with at different pumping energies (ranging from 0.17–1.19 mJ).The insets show the highest intensity and FWHM of the final peak as a function of pump power and the larger emitted view at higher pump intensity

As inferred from Figure (4.8) (c) sample-1, there is a significant change in intensity with increasing pumping energy from (0.17-1.19 mJ) up to (15023A.U). Energy was seen as tending to improve to overcome loss and thus achieve RL emission. Therefore, the remarkable threshold activity can be observed at (0.68mJ) the FWHM values changed between 24-21.5 nm with increasing pumping energy from (0.17-1.19 mJ) and the emission spectrum can be seen narrowing more than the previous one and its intensity rapidly increasing. Later, when the pumping energy exceeds the threshold, that is, the rate of photon generation becomes higher than its loss in the case of using Fe2o3, and using Ag, we notice an increase in intensity with increasing pumping capacity from (0.17-1.19 mJ) up to (21154A.U) as It is shown in Figure (4.8) (d) sample-2. There is a significant change in the FWHM values with increasing pumping energy from (0.17–1.19 mJ), resulting in a decrease in the FWHM from 15.5 to 13 nm. Accordingly, instead, the type of nanomaterial and the pumping energy affect both the FWHM and the peak intensity of the emission spectra and the energy threshold.

70% kiton red Dye + 30 % Fe2O3 SNPs

70% kiton red Dye + 30 % AgNws

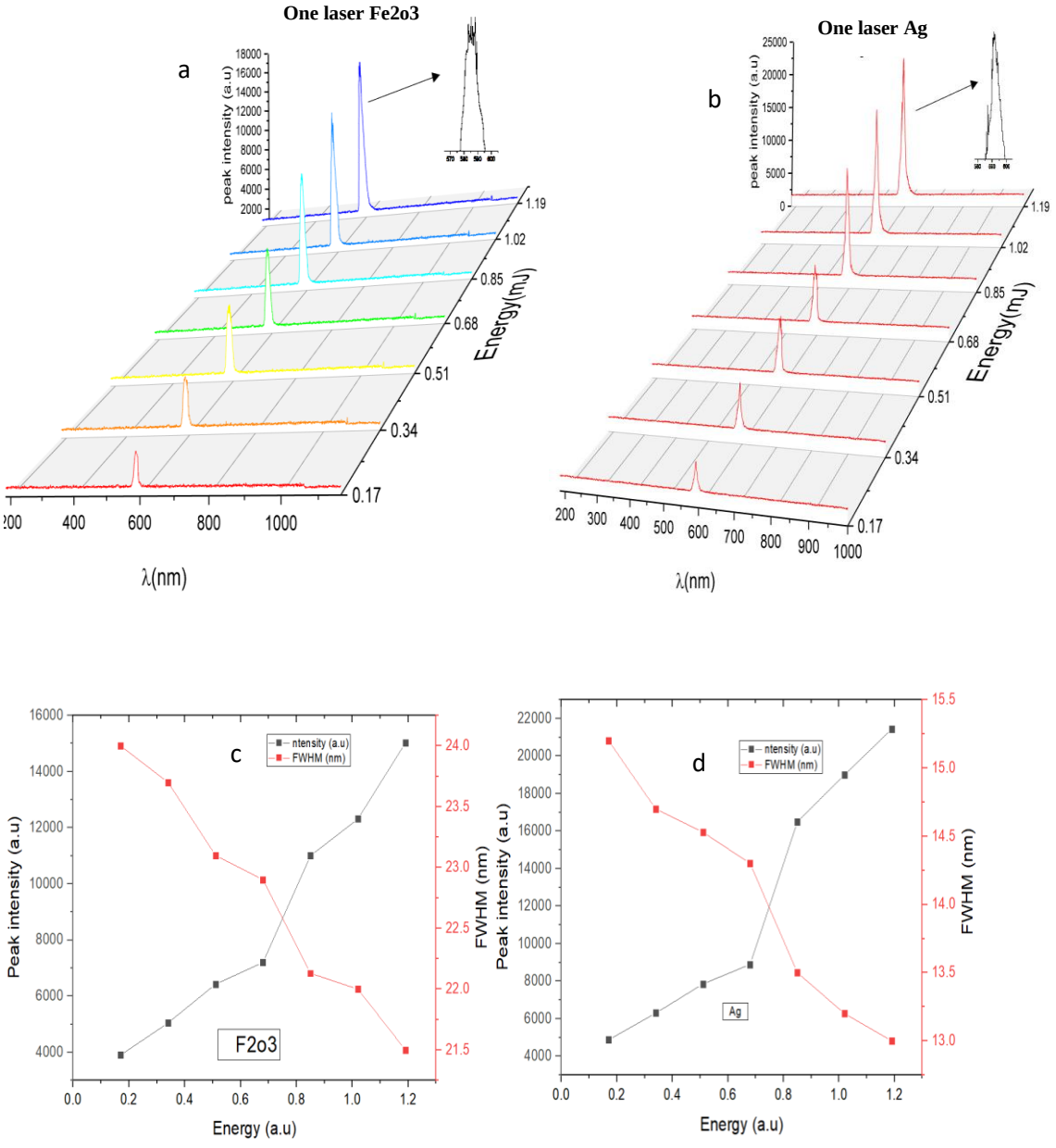

Fig. (4.8) Emission spectra of a mixture of kiton red dye with ethanol at different pumping energies (a) 70% kiton red dye -30% Fe2O3 SNP (b) 70% kiton red dye -30Ag SNP differences in peak intensities and FWHM as a function of pumping power at: (c) 70% kiton red dye -30% Fe2O3 SNP (d) 70% kion red dye -30% Ag SNP

figure (4.9) shows, the evolution of the emission spectra of a ketone dye solution with three concentrations (AgNws, Fe_2O_3NPs, and AgNws:

NPsFe_2O_3), dissolved in ethanol in the presence of the thermal cavity using 532 nm and 405 nm lasers, And an angle of 90^o between the two lasers inside the cavity .and this concentration consists of 70% ketone red dye with a concentration of (1×10^{-5} M) (30% Fe_2O_3 SNPs and the same concentration with AgNws and the third concentration was a mixture of 50% ketone (at a concentration of (1×10^{-5} M) 25% Fe_2O_3SNPs and 25% AgNws at different pumping energies (ranging from 0.17–1.19 mJ).

Figure (4.9) (c) sample-3, with an increase in pumping energy from (0.17-1.19 mJ), we notice here an increase in intensity until it reaches (37065). , the remarkable threshold activity can be observed at (0.51mJ), and the emission spectrum can be seen narrowing more than the previous one and its intensity increased rapidly and the FWHM values changed between 18.7–17.1 nm with the increase of pumping energy. When the pumping energy exceeds the threshold, that is, the photon generation rate becomes higher than its loss in the case of using the Fe_2O_3 nanomaterial, and by using Ag, we notice an increase in intensity with the pumping energy until it reaches (40972 a.u) as shown in Figure (4.9) (d) sample-4. And as there is a significant change in the FWHM values with increasing pumping power,

As the energy of the incident photons increases, the emission spectrum becomes narrower, showing a small bandwidth of about 6.55 nm at 0.17 mJ. However, more pumping energy, the spectrum reaches its threshold where the gain balances with the loss, and it can be seen that this spectrum narrows further until the FWHM reaches 6.2 nm at 0.34 mJ and its intensity rapidly increases. Later, when the pumping energy exceeds the threshold, i.e. the rate of photon generation becomes higher than its loss, the emission spectrum narrows more than its predecessor and reaches the lowest value

for this sample around 4.8 nm. The type of nanomaterial and the pumping energy affect both the FWHM and the peak intensities of the emission spectra and the threshold energy.

70% kiton red Dye + 30 % Fe2O3 NPs

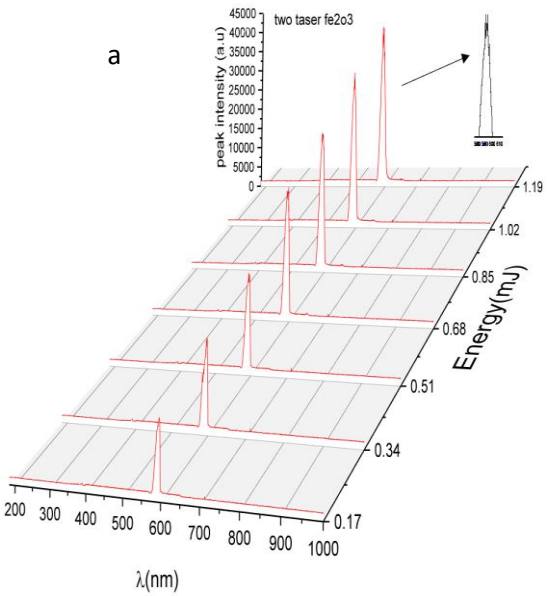

70% kiton red Dye + 30 % AgNw

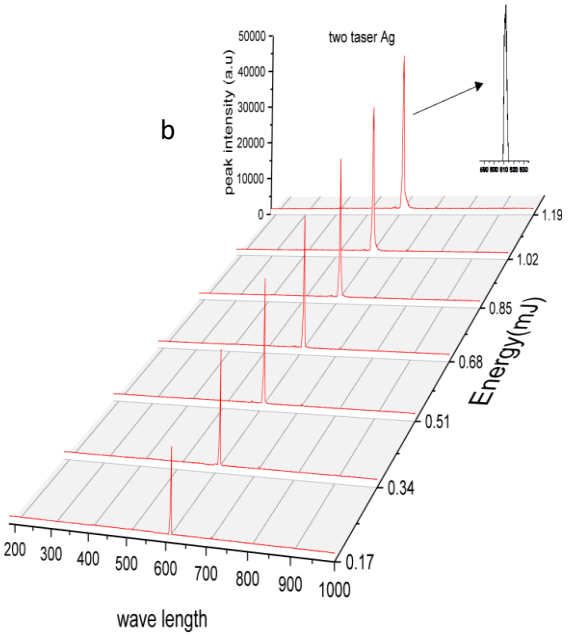

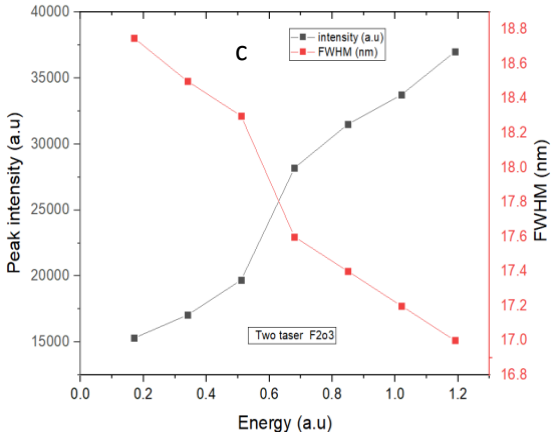

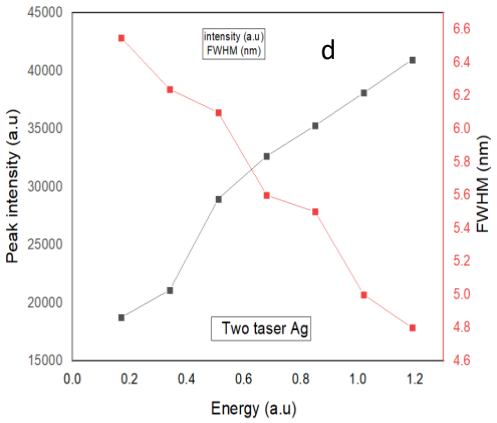

50% kiton red Dye + 25 % Fe2O3 NPs+ 25 % AgNws

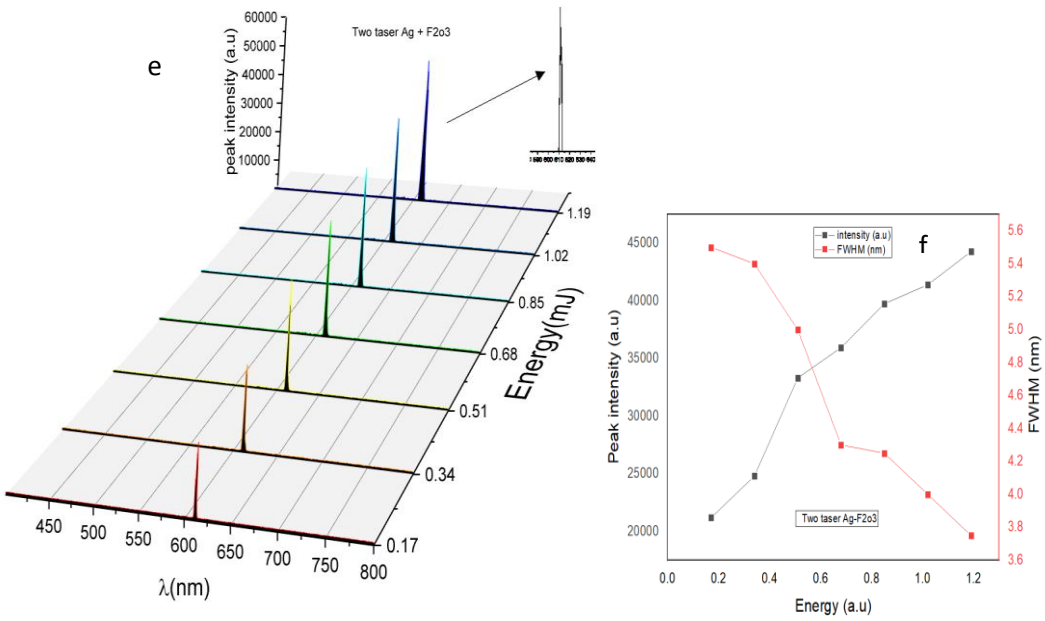

Figure (4.9) Emission spectra of a mixture of kitone red dye with ethanol at different pumping energies with thermal cavity (a) 70% kitone red dye -30% Fe2O3 SNP (b) 70% kitone red dye -30Ag (c)kiton red Dye + 25% Fe2O3 SNPs + 25% AgNws peak intensities and FWHM as a function of pumping energy in: (d) 70% keton red dye-30% Fe2O3 SNP (e) 70% kiton red dye-30% Ag SNP(f) 50% kiton red dye + 25% Fe2O3 SNPs + 25% AgNw

Figure (4.10) (f) Sample-5, which consists of red dye 50% ketone + 25% Fe2O3 SNPs + 25% AgNws. We note with increasing pumping energy from (0.17-1.19 mJ) the emission spectrum becomes narrower, and the width of A small band of about 5.5 nm at 0.17 mJ. However, as the pumping energy continues to increase, the spectrum reaches its threshold where the gain balances the loss, and it can be seen that this spectrum narrows further until the FWHM reaches 5.1 nm at 0.34 mJ with rapidly

increasing intensity. Later, when the pumping energy exceeds the threshold, the rate of photon generation becomes higher than its loss, the emission spectrum narrows more than its predecessor and reaches the lowest value for this sample around 3.7 nm. The intensity reaches (44279 a.u) at the energy (1.19 mJ).

By comparing these five samples that were prepared above to study the effect of thermal cavity and bubble formation on the random laser action and by adding the nanomaterial. Also observed is a clear improvement in random laser emission properties (emission intensity, FWHM, and laser threshold) after thermal cavity formation. As shown in Table (2-4), it shows the extent of the increase in the emission intensity with and without the thermal cavity. By comparing the results, the emission peak increases and the emission spectrum narrows, as the FWHM decreases from 21.1 nm without a thermal cavity to 13 nm with a thermal cavity (Fe_2O_3). While from 17.1 nm without a thermal cavity to .84 nm with a thermal cavity for Ag. Also, the decrease in the laser threshold is shown in Figure (4.10), so the laser threshold decreases from 0.68 nm without a thermal cavity to 0.51 nm with a thermal cavity Fe_2O_3) while from 0.68 nm without thermal cavity to 0.34 nm for Ag. The best results are observed for sample 5 which is a mixture of Fe_2O_3+ Ag. This has another meaning is the type of nanomaterials have a significant effect on the formation of bubbles and thus affect the amount of scattered beam. This in turn increases the contrast between the refractive index of the nanomaterial and its surroundings and the formed bubbles, and this difference leads to an increase in the refractive index. This increase in refractive index increases the scattering cross-section (σ_s) and decreases the value of each scattering mean free path mean (l_s) and mean free transport (l_t) according to Eqs. (2.6), (2.7), and (2.8), respectively. A decrease in the value of l_s and l_t means a higher

scattering efficiency and thus an improvement in the random laser properties. These results were reinforced by [49].

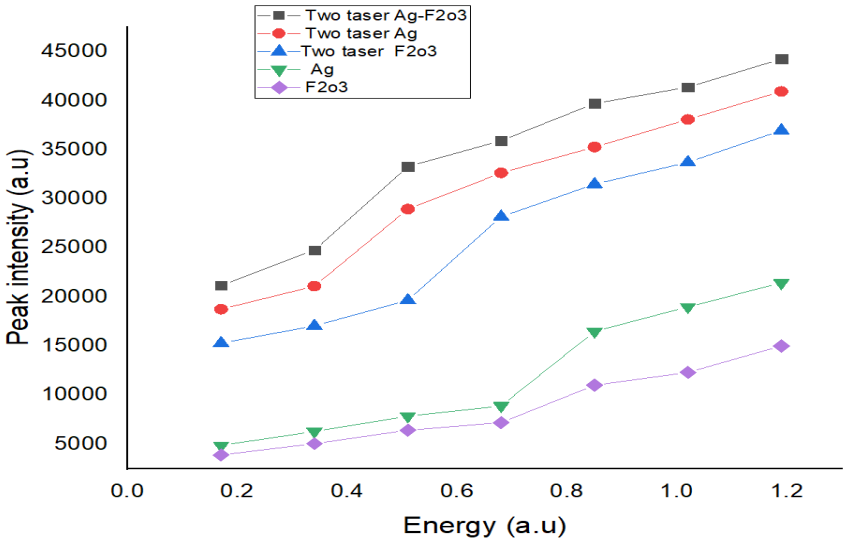

Figure (4.10) Peak emission intensity as a function of pumping energy with and without thermal cavity for the five samples

Table (4-2). Random laser parameters with and without thermal cavity for the five samples

Nanomaterials (scattering centers)		Peak intensity (a.u)	Threshold pumping(mJ)	FWHM(nm)
Without thermal cavity	Fe_2O_3	15023	0.68	21.5
	Ag	21154	0.68	17.1
With thermal cavity	Fe_2O_3	37065	0.51	13
	Ag	40972	0.34	4.8
	Fe_2O_3+Ag	44279	0.34	3.75

4.3 (Thin gold waveguide -cavity) random laser

Thermally annealed plasmonic glass based on Au NPs was fabricated using the thermal treatment of the thin gold film and investigated for random laser applications.

4.3.1 Absorption spectrum of Rh6G dye dye mix with NPs

In this type of random laser, The dye solutions have been prepared by dissolving the required amount of Rh6G dye in deionized water mixed with 0.03 mg/ml PVP polymer to obtain three different concentrations (1×10-3,

1×10^{-4}, and 1×10^{-5} M) Figure (4-11-a) . After that, these three different dye concentrations were spin-coated onto gold thin film at 2500 rpm.The absorption spectra of the samples were measured using Ultraviolet-visible spectrophotometry (UV–Vis) in the wavelength range of 220–1100 nm. Fig (4-12-b) shows the effect of dye concentration on the emission spectrum. It offers a broad absorption spectrum (430-575 nm) with the maximum absorption peak at the wavelength (550 nm). Figure (4-11-c) shows the UV-Vis spectrum of the dispersed gold nanoparticles shifting to higher energy (blue shift), indicating the maximum absorption in the visible region at 500-600 nm. Furthermore, the absorption decreases in the wavelength range between 350–1000 nm

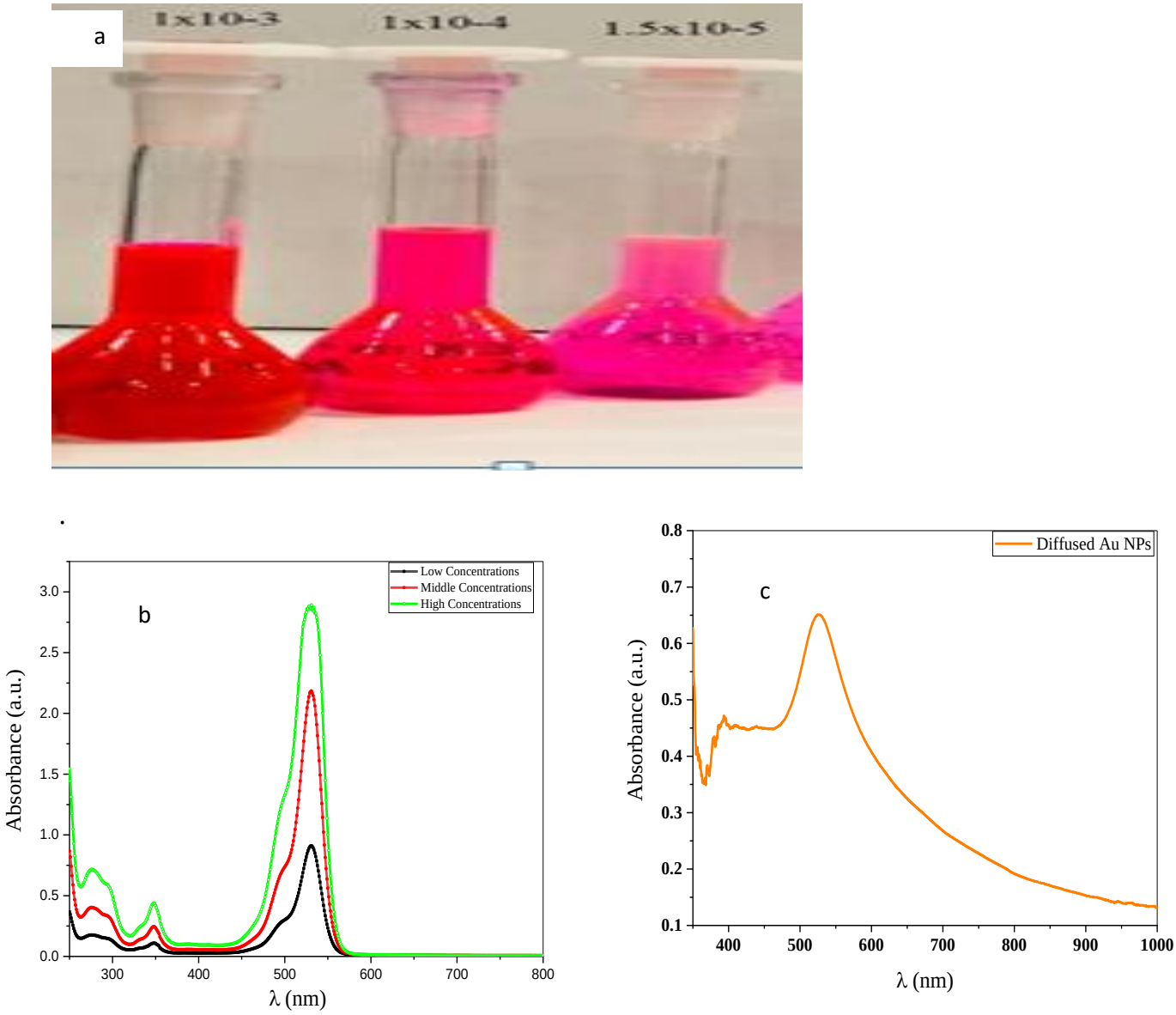

Fig (4-11)(a) Rh6G dye solution prepared at different concentrations. (b) Absorption spectrum of the mixture consisting of Rh6G dye and nanomaterials for the three samples with different concentrations with the PVP polymer (c) Spectra of the glass with diffused gold NPs

4.3.2 Structure Characterization

The (Field Emission Scanning Electron Micrscopes) (FE-SEM) and also transmission electron microscopy (TEM) image of NPs which dropped onto the glass slide show the formation of Au nanoparticles by size range 30-50 nm, as shown in figure (4-12-a) .As the figure shows (4-12-b) . and shows all the layers with the active medium used in the experiments.

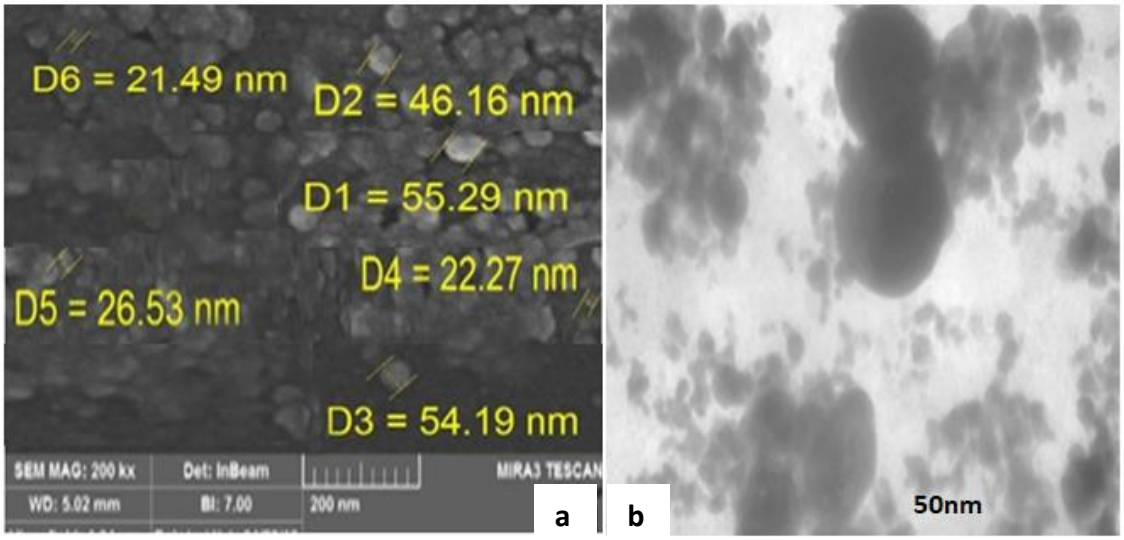

Fig. (4-12) (a) FE-SEM Au NPs. (b) TEM image of Au NPs

4.3.3 Lasing characteristics

Gold nanoparticle bases covered the random laser properties in three different active environments. Then it was studied on the glass substrate using the physical vapor deposition and with spin coating with varying concentrations of Rhodamine 6G dye mixture and PVP polymer..

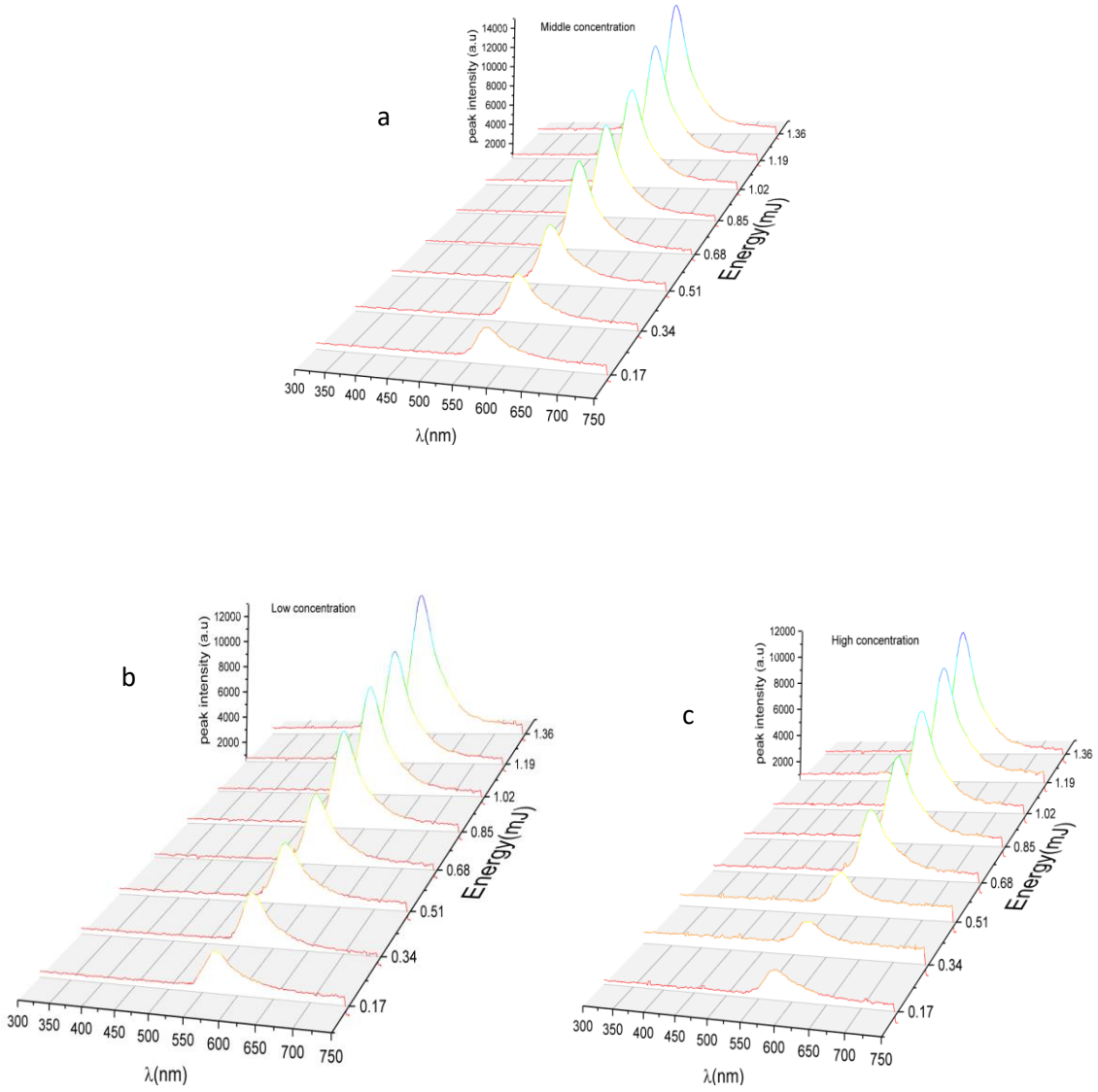

Figure (4.13) the emission peak of random laser as function of the pumping energy for (a) middle, (b) low and (c) high concentrations.

Figure (4.13-a) shows that the profile of the scattering centers of these media shows sufficient optical feedback, and the effect of dye concentration on the emission spectra of these media was also prominent. The middle concentration (1×10^{-4} **M)** was the best; the emission becomes narrower, the bandwidth appears small, the range reaches a threshold where the loss balances the gain, and it can be seen that the spectrum gradually narrows and the intensity increases rapidly. Later, when the pumping power

exceeds the threshold, the photon generation rate becomes higher than its loss, the emission spectrum narrows further than before, reaches its lowest value for this sample, and then stabilizes at this value even if the dye concentration continues to increase. In contrast, its intensity continues in the emission spectrum and rapidly increases. It undergoes a collapsed state in the emission spectrum, announcing the appearance of spikes in the upper part of the spectrum representing the state of closed paths (standing wave) occurring within the random medium, indicating random coherent lasers. Furthermore, in this concentration, we extract the ellipsometric parameters of the sample as shown in Figure (4.14) which indicates the main phase difference for to polarizations and also reflection coefficients at the main green pump laser's wavelength. we record the reflection spectrum of the samples in 45 degree in both p and s polarizations which is elliptically polarized and the parameters of the polarization ellipse are determined by applying the optical constants of both media, using these measured s- and p-polarization components (R_s and R_p), the ellipsometric angles as Ψ and Δ can be extracted as follows [190].

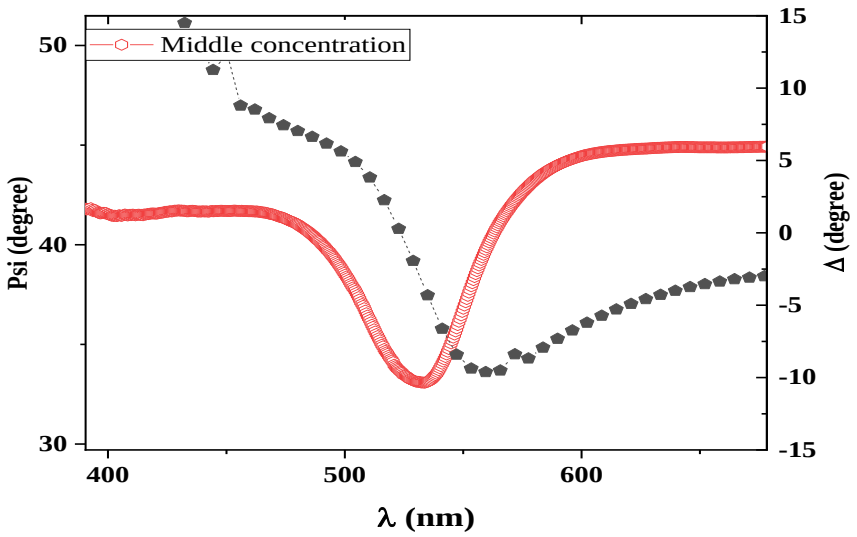

Figure (4.14) ellipsometric parameters of middle sample

$$\rho = \frac{r_p}{r_s} = tan\psi \exp(i\Delta) \tag{4.1}$$

where $r_{s,p}$ is Fresnel's coefficients for s and p polarizations which should be extracted from the measured reflectance ($R_{p,s}$).

So far, Ψ has been calculated easily. To calculate Δ, the following equation was obtained by applying the dependency on the incident light frequency(ω)

Additionally, Δ is defined as the phase difference between p and s polarizations. Thus, we have:

$$\begin{aligned} \Delta &= \theta_p(\omega) - \theta_s(\omega) \\ &= -\frac{2\omega}{\pi}\int_0^{\infty} \frac{ln\sqrt{R_p(\omega')} - ln\sqrt{R_s(\omega')}}{\omega'^2 - \omega^2}\, d\,\omega' + [\theta_{0_p}(\omega) \\ &- \theta_{0_s}(\omega)] = -\frac{2\omega}{\pi}\int_0^{\infty} \frac{\ln\left(\sqrt{\frac{R_p(\omega')}{R_s(\omega')}}\right)}{\omega'^2 - \omega^2}\, d\,\omega' + \Delta\theta_0 \end{aligned} \tag{4.2}$$

Where ($\theta_p(\omega) and\ \theta_s(\omega)$) is the parallel and vertical rotation angle

where,

$$\Delta\theta_0 = -\frac{2\omega}{\pi}\, ln\left(\sqrt{\frac{R_p(\omega')}{R_s(\omega')}}\right)\int_0^{\infty}\frac{1}{\omega'^2-\omega^2}\, d\omega' \qquad (4.3)$$

As described above, ellipsometric parameters can now be extracted from the measured reflection spectrum.

To clarify the effect of dye concentration on the intensity of the spontaneous laser emission Figure (4.15):. By comparing the emission spectrum of the three samples of different concentrations. The most suitable sample among the three models was with medium dye concentration (1×10^{-4} M). which makes it possible to compare the laser threshold of the three pieces. The color sample with medium concentration had the most relevant result compared to low and high concentrations. The reason was the strong coupling of the average concentration, which increased the peak intensity and decreased the laser threshold and FWHM [191].

Figure (4.16): shows that an intermediate dye concentration sample has a lower emission spectrum than the other two samples. The appearance of bumps within the laser random emission spectrum indicates a transition from coherent to coherent randomness. The laser also reflects what is happening inside the laser medium. Thus, the effect of the concentration of nanomaterials on the appearance of these spikes and their number will be discussed—the appearance of these spikes under the influence of the emission spectrum of nanomaterials dye [192]. As for the number of these protrusions, At low concentrations (1×10^{-3} M), they appear to have reached three separate peaks at the top of the emission spectrum, while (1×10^{-4} M), which is the best, exceeded five different heights at the top of

the emission spectrum and one on each side, it was found that these bumps grow and increase in number with the increase of the scattering centers, and the number of separate peaks When the upper part of the emission spectrum reaches exactly five heights and two bulges, the new first approaches these five different peaks. Sometimes it seems to the reader that the number of discrete peaks is less despite the increase in the number of scattering centers, but the truth is the opposite is the number of peaks.

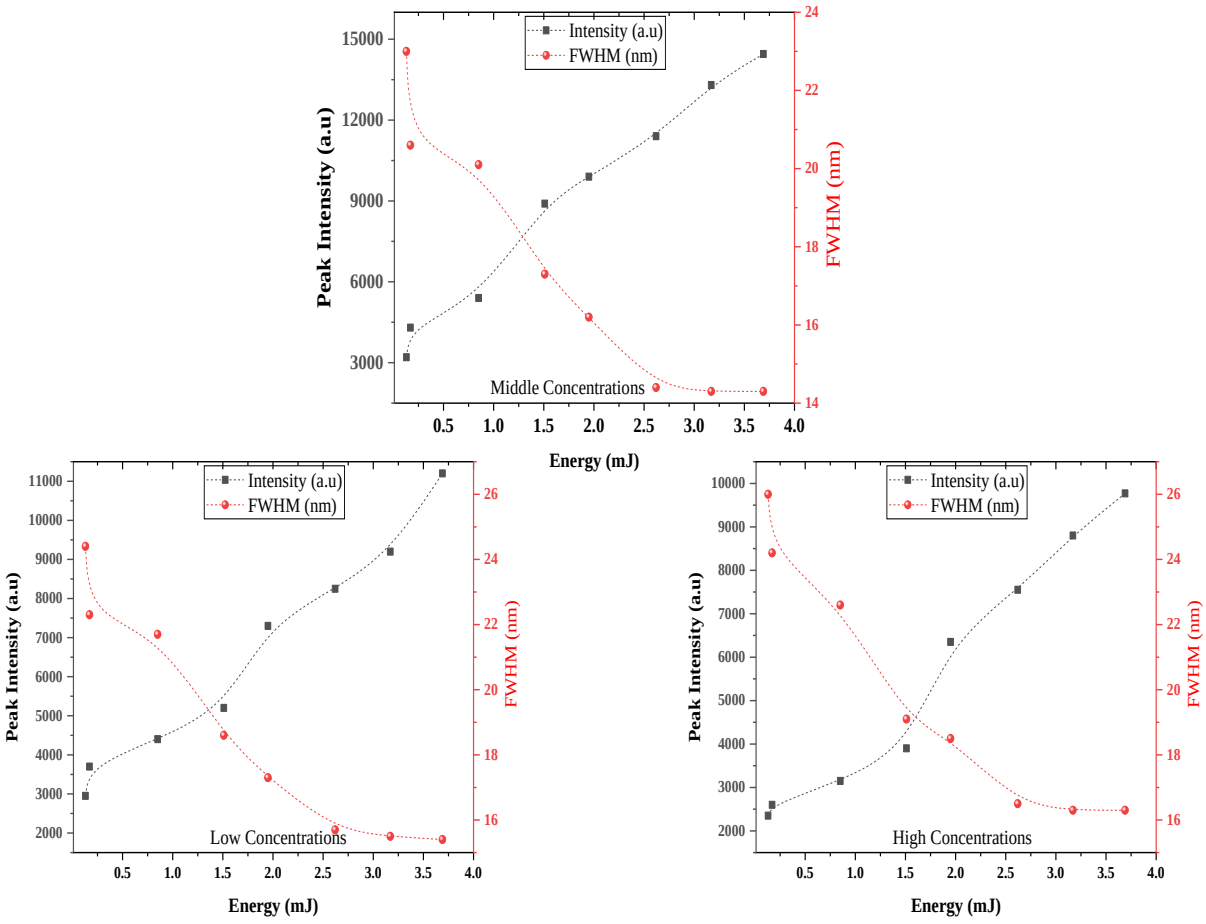

Figure (4.15): the emission peak of random laser as function of pumping energy and The FWHM of the pumping energy for (a) middle, (b) low and (c) high concentrations.

These peaks are constantly increasing and merging due to the increase in their number, so the interval frequency becomes little between vertices and

others. our optical emission spectroscopy could not distinguish between these peaks because the resolution is less than the interval frequency between these peaks [193]. Still, at a concentration (1×10^{-5} **M),** the number of peaks was less.

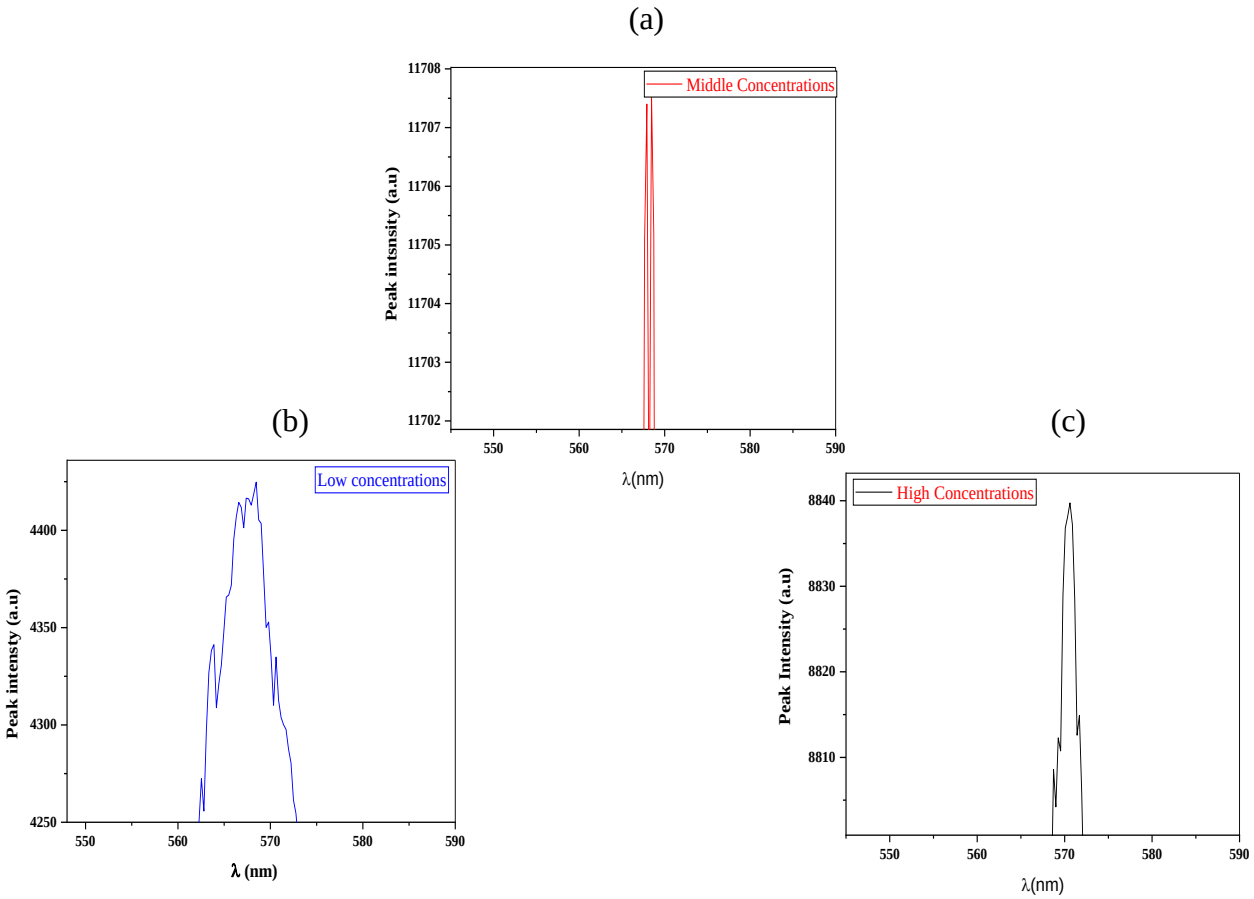

Figure (4.16) Evolution of bumps with different concentrations in (a) middle, (b) Low and (c) high concentrations of dyes.

4.4 (2D gratings-Cavity) Random Laser

in this work, a multi-layered 2D structure was used on a curved glass substrate (clock glass), a charge-coupled camera device (CCD) as a seal, and a gold nanostructure with rhodamine6G dye.

4.4.1. Absorption spectra and Structural characteristics

The absorption spectra of the PVP+Rh6G layer and scanning electron microscopy (SEM) image of the proposed 2D plasmonic square array on a glass substrate are indicated in Figure (4-17) (a) and (b), which confirms that the proposed 2D plasmonic structure has a 2D periodic square pattern with a good resolution.

The main optical modes due to the surface lattice resonance of our proposed 2D plasmonic structure arise from the coupling of localized surface plasmon resonance of each motif corner as shown in Fig. (4.17) (b) and diffraction order of two dimensional arrays. The main nanowires in each motif has the size in the order of 600 nm which yield to two modes before and after 600 nm in the center of visible region.

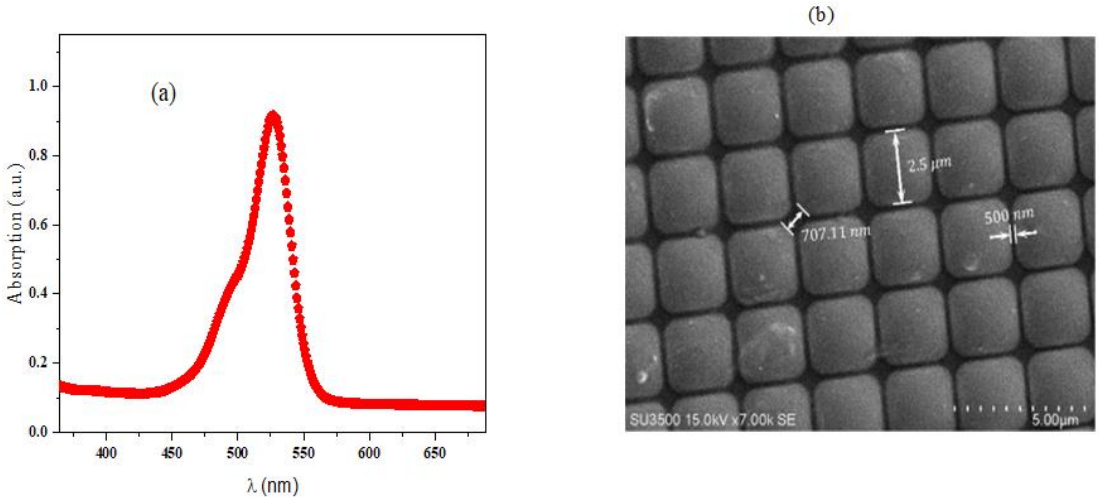

Figure (4-17): (a) Absorption spectrum of the dye solution, (b) SEM image of the base 2D structure

4.4.2 Lasing characteristics

The emission spectra of two different sides of a random plasmonic random laser sample pumped by 532 nm have been investigated, where the laser beam is shed on the sample from the inside, which is concave, and the outer, which is convex as shown schematically in Fig.(4-18). Fig (c) and (d) illustrate sufficient optical feedback where the effect of pumping energies on the emission spectra of these media was also prominent. The emission spectra of the sample can be observed at low pumping energy, usually in the region of 0.13 mJ. There is a broad emission within this sample range (from 550 to 650) nm with two distinct peaks; first at 575 nm and FWHM around 22 nm and the second at 630 nm with a bandwidth of 10 nm. This was the amplified spontaneous emission (ASE) of an (internal) laser random sample which is better. As the energy of the incident photons increases, the emission spectrum becomes narrower, showing a small bandwidth of about 19 nm at 0.35 mJ.

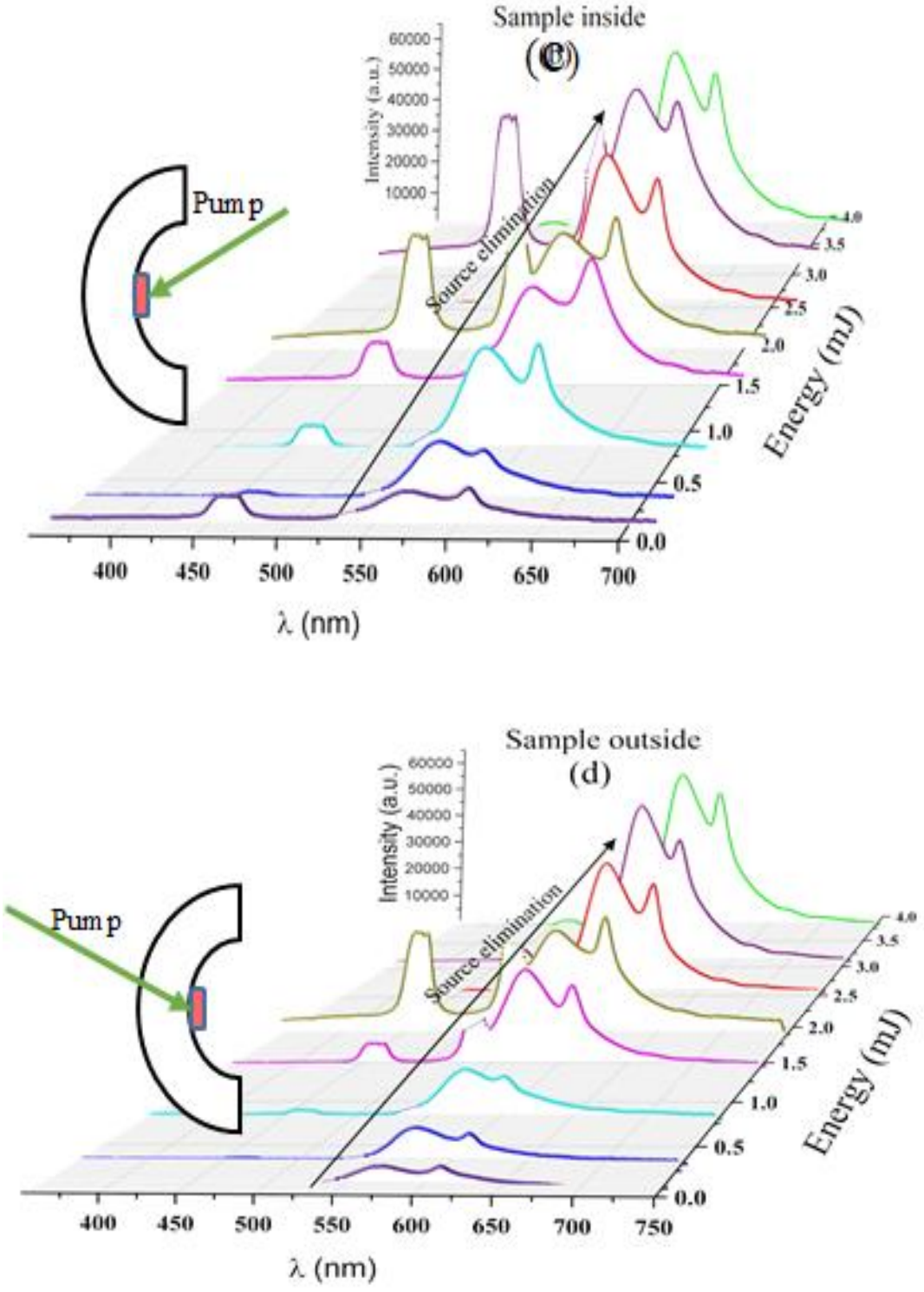

Figure (4-18) Emission spectra broad band plasmonic random laser as a function of pumping energy with two different sides (c) inside and (d) outside respectively with schematic of laser pumping.

spectrum continues to rise very rapidly and undergoes a collapsed state in the emission spectrum mutations appear in the upper part of the spectrum which is closed paths representing a state (standing wave), which occurs within the random medium indicating the emergence of random non-coherent lasers.

To gain further insight into the lasing from the sample, we plot the laser intensity Heatmap of both modes as a function of pumping intensity in Fig. (4-18) (a) and (b). It indicates higher lasing energy in the first mode in green region and lower ones in red ones as two separate main modes.

Furthermore, since the optical losses have an equally important role as that of the optical gain in lasing media, the laser intensities as a function of the pumping power FWHM of output modes from inside and outside of the sample are shown in Fig. (4-20) (c) and (d) respectively.

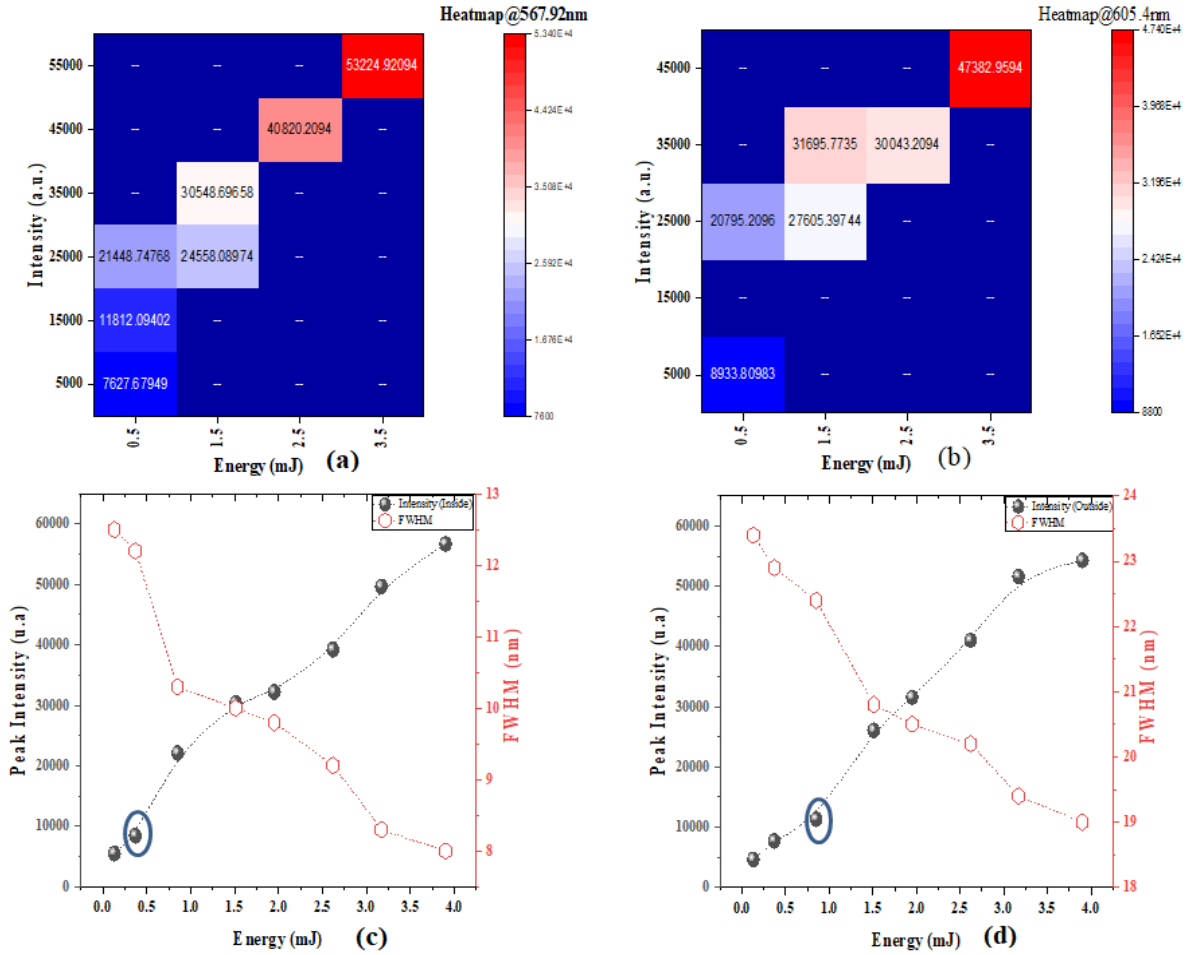

Figure (4.19) Heat map of peak emission intensity in (a) inside and (b) outside and Peak emission and FWHM as a function of pumping energy for (c) inside and (d) outside of the substrate

Figure (4-19) (c) and (d) reveals that the inside threshold is 0.35 mJ less than the external threshold, 0.85 mJ as shown by blue circles in these figures. It also seems clear from my guess that the efficiency of the slope better than that of the other slope respectively. It is observed that the FWHM is lower for the random medium, with an increase in the pumping power, while the random mean FWHM (inside) is narrower. Note that the laser is always accompanied by the non-correlation of the random laser, as for the narrow peaks, the inside is better than the outside, as with the wide peaks.

This indicates that the photons are scattered from the inner surface and this is a clear indication of the increase in the gain in this medium. Further, this improvement in laser output is attributed to a change in the 2D periodic square pattern, causing reduced distance between them, so that photons can stay in the medium as long as possible. This work adds a new twist by adding functionality and investigating the applications of tunable random lasers.

4.5 (Magneto-optical Cavity) Random Laser

study the effect of an external magnetic field on new FeB based two dimensions' magneto-plasmonic structure which cover by gold thin film and Rhodamine 6G from the bottom and top respectively propose as new kind of random laser substance under the external magnetic field.

4.5.1 Absorption spectrum of Rh6G dye dye mix with Au NPs

In general, Fig.(4.20ab) shows the absorption spectrum of Au nanoparticles as measured with UV-visible spectroscopy. It was found that the absorption (SPR) peak of Au nanoparticles obtaining in the visible region (528) nm

Fig.(4.20b)shows the absorption spectrum of R6G dye . The absorption spectrum peaks toward the wavelengths (526) nm

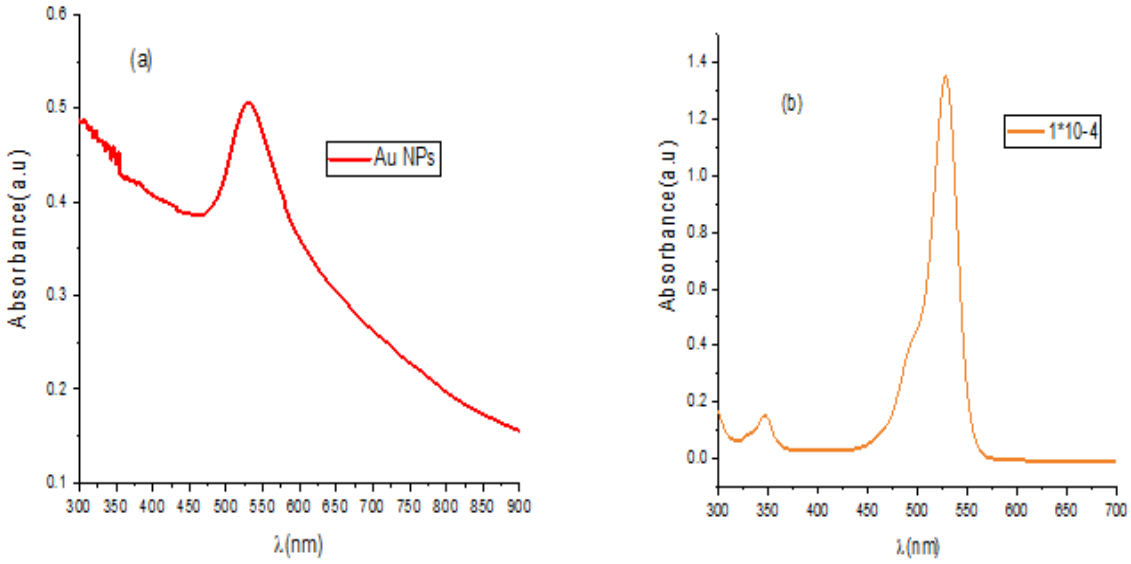

Fig.(4.20)(a) The absorption spectrum of Au nanoparticles (b) Absorption spectrum of R6G dye 1x10^{-4}

4.5.2 Structural characteristics

Fig.(4.21a.d) shows the Real picture of the sample and The SEM image of 2D plasmonic structures top surface fabricated samples that have been prepared , the behavior of gold nanoparticles is arranged in a periodic array for 2D grating samples. It is worth noting that periodic arrays of metallic nanoparticles can exhibit extremely narrow extinction line shaping excitations called surface lattice resonances (SLRs).are a result of the coupling between localized surface plasmon resonances (LSPRs) coming from metallic nanomaterial in the sample associated with individual nanoparticles and diffractive orders (DOs) present in periodic structures. The diffraction coupling occurs when nanostructures are spaced with the optical path length between the neighboring particles equals to an integer multiple of the incident wavelength.

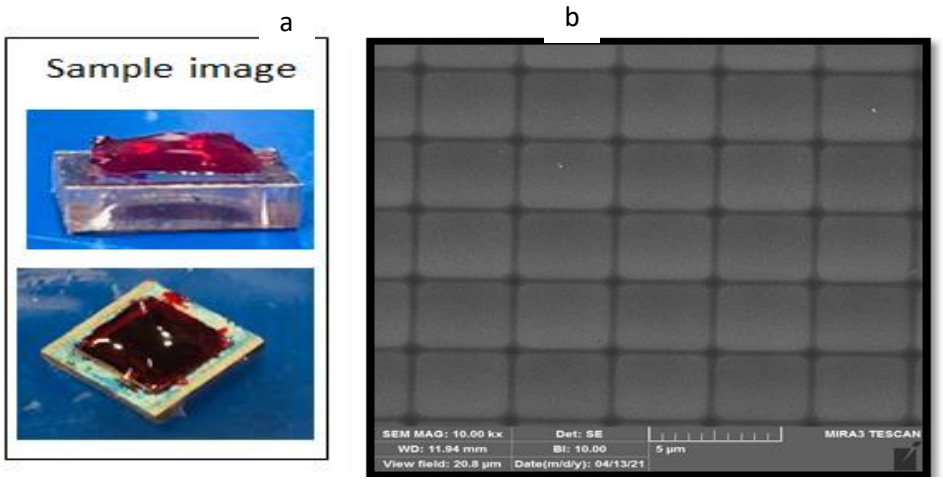

Fig.(4.21)(a): Real picture of the sample (d)The SEM image of 2D plasmonic structures samples.

4.5.3 Lasing characteristics

As explained before in the experimental part, the fabricated sample exposed by Nd:YAG pump laser and the intensity of laser output recorded with and without external magnetic field (MF).

There is an increase in the emission spectrum with the increase of the pumping energy with the presence and without the magnetic field as shown in Figures (4-22) (a) and (b). The magnetic field was placed vertically above the sample with a distance of (10 cm). This remarkable enhancement comes from the effects of the magnetic field on the materials in the sample and from the fact that noble NPs such as Au have a large scattering cross-section due to surface plasmon resonance (SPR) that would trap photons near the surface and scatter with high gain. As well as for the FeB material, which has new magnetic properties, and this would cause an increase in the intensity of the emission spectrum resulting from the effects of the magnetic field.

Moreover, the sample with the presence of the external magnetic field, was the best, as it had the smallest laser threshold 0.35 mJ which is smaller than that of the laser without the magnetic field which shows larger laser

threshold energy 0.66 mJ (Figure (4-23) (c)). We notice an increase in the intensity of the output laser while the FWHM decreased due to the applied magnetic field Figure (4-23) (d).

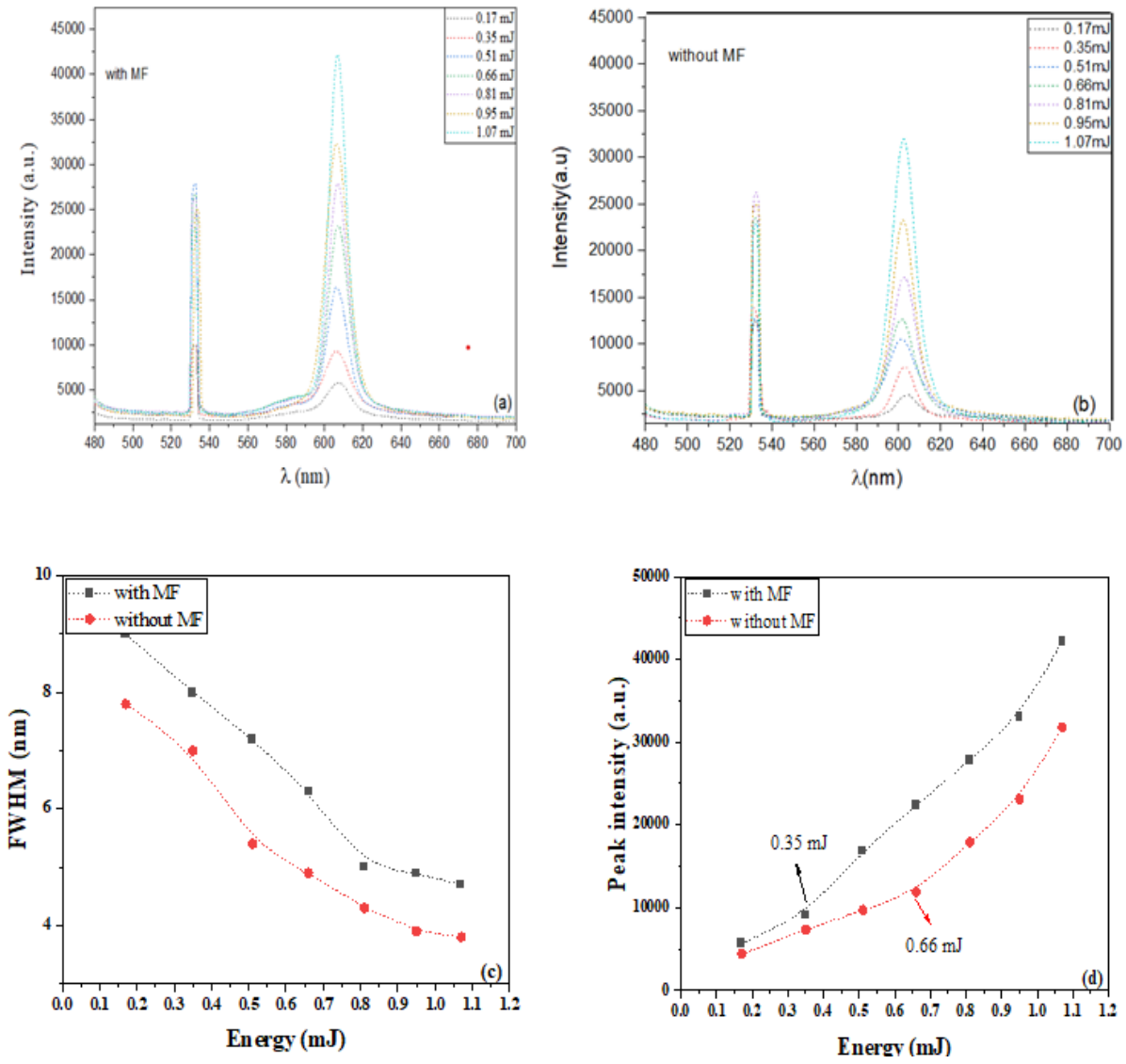

Figure (4-22): Emission spectrum of samples at different pumping energies (a) with the magnetic field (b) without the magnetic field (c) FWHM and (d) Intensity as a function of pumping energy.

The FWHM decreases from 7.8 to 4 nm under the influence of an external magnetic field, the FWHM value decreases to reach 9 and 5 nm with no magnetic field. The same applies to the laser threshold, where it was found that the presence of an external magnetic field leads to a lower laser threshold than it was from 0.66 to 0.35 mJ. Both the laser threshold and the FWHM decrease under the influence of an external magnetic field. It was also observed that an increase in the emission intensity occurred with the increase in the pumping power in both cases, but the increase in intensity was greater with the presence of the external magnetic field.

In addition, as the second glance, we investigate the main effect of external magnetic field onto the main output mode in the order of 600 nm. For this purpose, we define relative intensity between with and without external magnetic field as I_{MF}-I_0, in which I_{MF} means the laser intensity under external MF, while I_0 means the laser intensity in the same pumping energy and without external MF. As shown in Figure (4-23), enhance in the pumping energy yield to more difference in the output laser intensity and also the overall red and blue shift in the relative intensity before and after the main peak respectively.

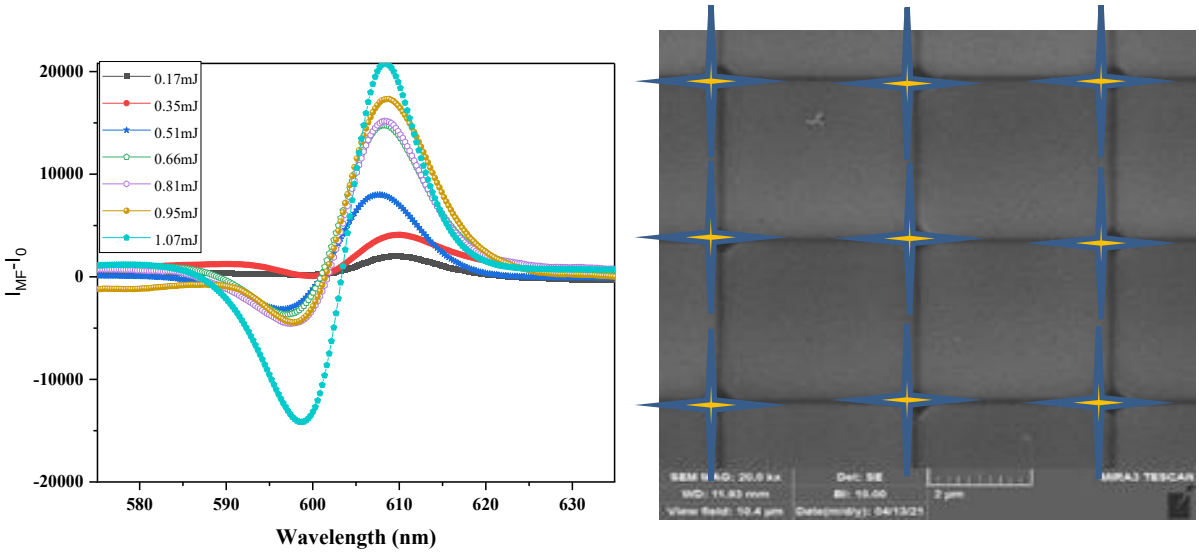

Figure (4-23): Relative Emission spectrum of samples at different pumping energies from 0.17 to 1.07 mJ) and (b) Schematic diagram of the main two dimensional substances before dye coating.

To get more sense about the effect of external MF onto the laser output, we must think about this fact that we have two dimensional structure of FeB onto the palsmonic Gold structure as shown schematically in Fig. (4-23) (b). As shown in this schematic, in each motif corner of the main structure (stars points), we have magnetization localization and thus magnetic dipole which can be more arranges in the external MF direction by enhance in the pumping energy or localized electric field enhancement. It means we have more SPR of the gold cover layer in each star points and more coupling of magnetization of FeB layer, the SPR of metallic gold layer and also the excitons in the top dye layer by enhancement in pumping energy. In addition, due to the coupling between them, when we apply external MF, we have the rotation of magnetization in these star points and thus change in the field localization which can be yield to the output wavelength's shift. The possibility of improvement in random laser parameters in the presence of the magnetic field was evaluated and confirmed up to acceptable values. Emission spectrum resulting from the presence of the applied external

magnetic field compared to the absence of the magnetic field and many scattering centers formed by FeB in the excited region. It was also found that the emission power increases with the growth in the density of the scattering centers in each motif's corner of two dimensional structure.

4.6 (Triple optical cavity) Random Laser

4.6.1 Absorption Spectrum of RhB Dye

Figure (4-24) represents the absorption spectra of RhB dye with different concentrations. It was noted that by increasing the concentrations of the dye, that leads to an increase in the absorbance peak, related wavelength and the bandwidth of the absorption spectra. Where, noted that the absorption of RhB at (553 nm), and the best absorbance at the concentration ($1*10^{-5}$ M). The behavior of the absorption spectra with the increasing of dye concentration can explained as the highest values of the dye molecules in the lower energy level consolidates the absorption probability per time ,so the largest contribution by molecules in absorption appears in the wide absorption band width.

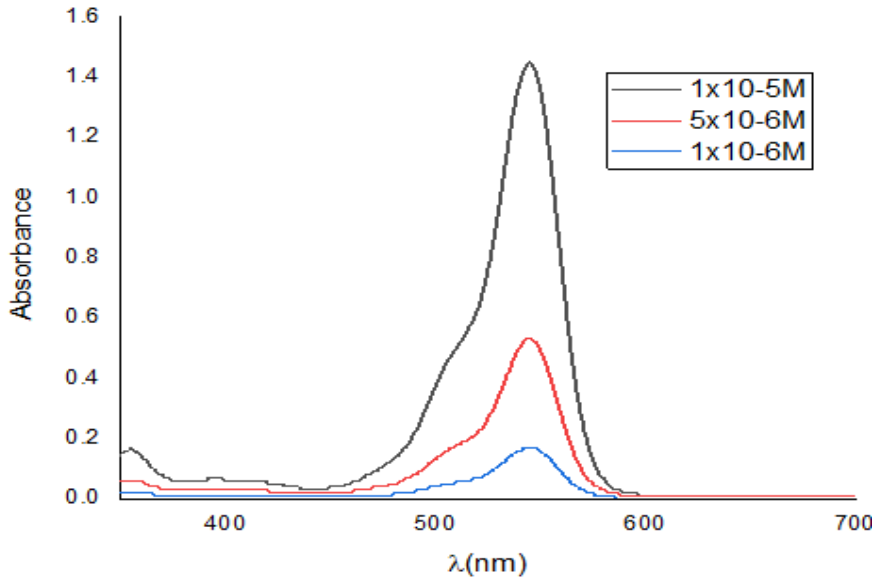

Figure (4-24): Absorption spectra of RhB dye with different concentrations in the water solution.

4.6.2Absorption spectra of RhB mixed with different concentrations of Ag NWs:

The best concentration of RhB dye was mixed with different concentrations of Ag NWs, where, figure (4-25) represents the absorption spectrum of this mixture. It is obvious that by adding the nanowires to the dye, that leads to increase in the absorption spectrum. Noted that the effect of increasing the concentration of NWs on the dye is obvious in the mixture RhB ($1*10^{-5}$ M) + Ag NWs (40%), and the highest absorption of the Ag NWs in this mixture was at the wavelengths of (351 and 372 nm).

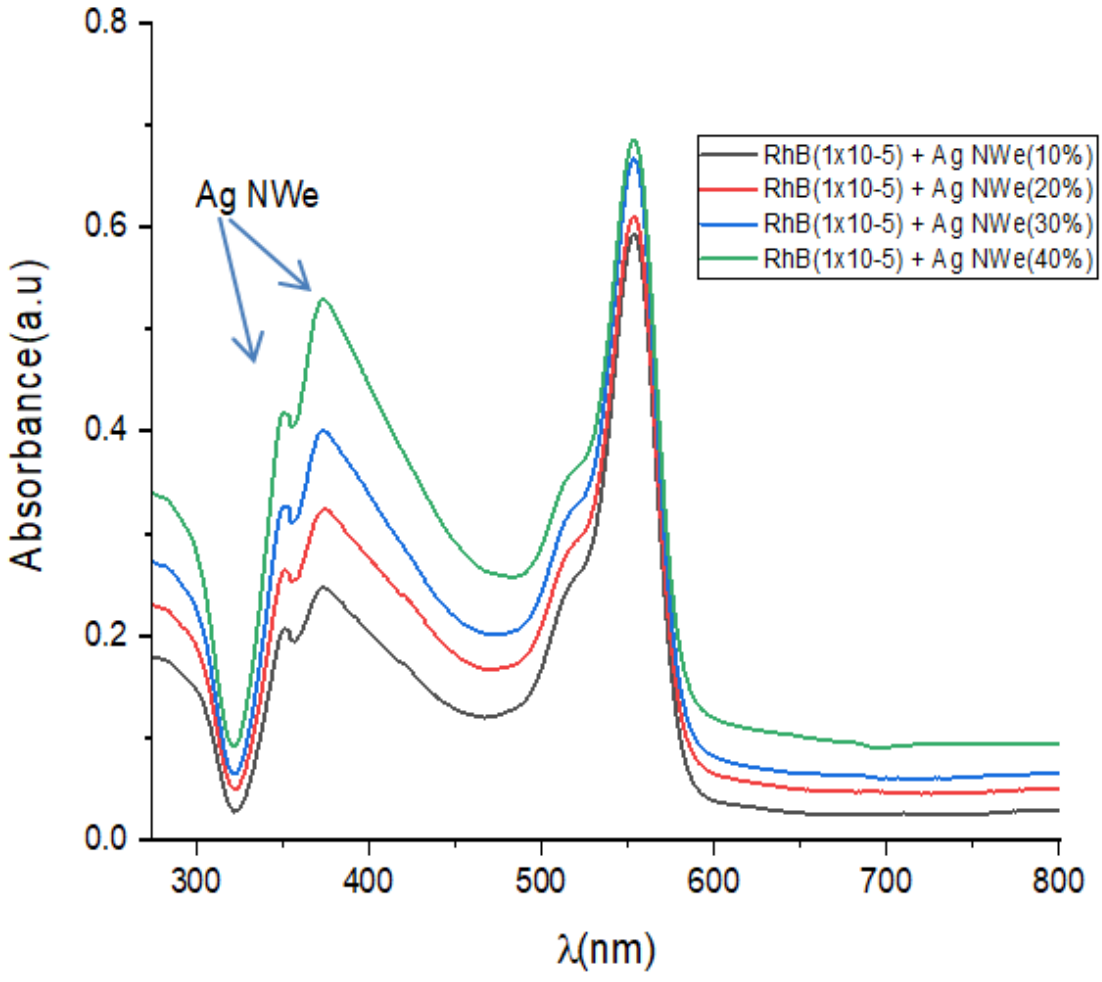

Figure (4-25): Absorption spectra of RhB dye ($1*10^{-5}$ M) mixed with a different concentrations of Ag NWs.

4.6.3 Fluorescence spectra of RhB mixed with different concentrations of Ag NWs:

Figure (4-26) represents the fluorescence spectra of the mixture (RhB $1*10^{-5}$ M + different concentrations of Ag NWs). It is clear that by increasing the Ag NWs that leads to increase the emission spectra, while, the quenching happened at the last spectra (RhB $1*10^{-5}$ M+ Ag NWs (40%)

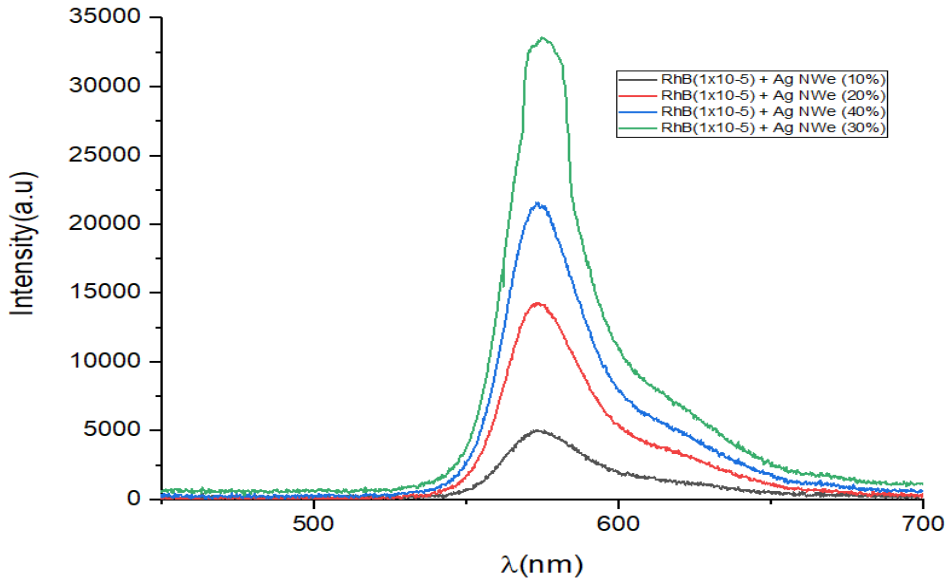

Figure (4-26): Fluorescence spectra of RhB dye ($1*10^{-5}$M) mixed with different concentrations of Ag NWs.

4.6.4 Structure characterizations

In this type of random laser,Au NPs have been used inside a glass cavity ,with Ag nanowires as scattering centers in a random medium containing (RhB + pvp) as the gain medium. The Ag nanowires with an average particle size (200 nm) and lengths less than 50 microns were purchased from the German PlasmaChem company. Fig. (4-27) displays the transmission electron microscopy (TEM) and Field Emission Scanning Electron Microscopes (FE-SEM)of the (Au NPs and Ag nanowires) , as well as the real images of the boxe as received from the supplier company.

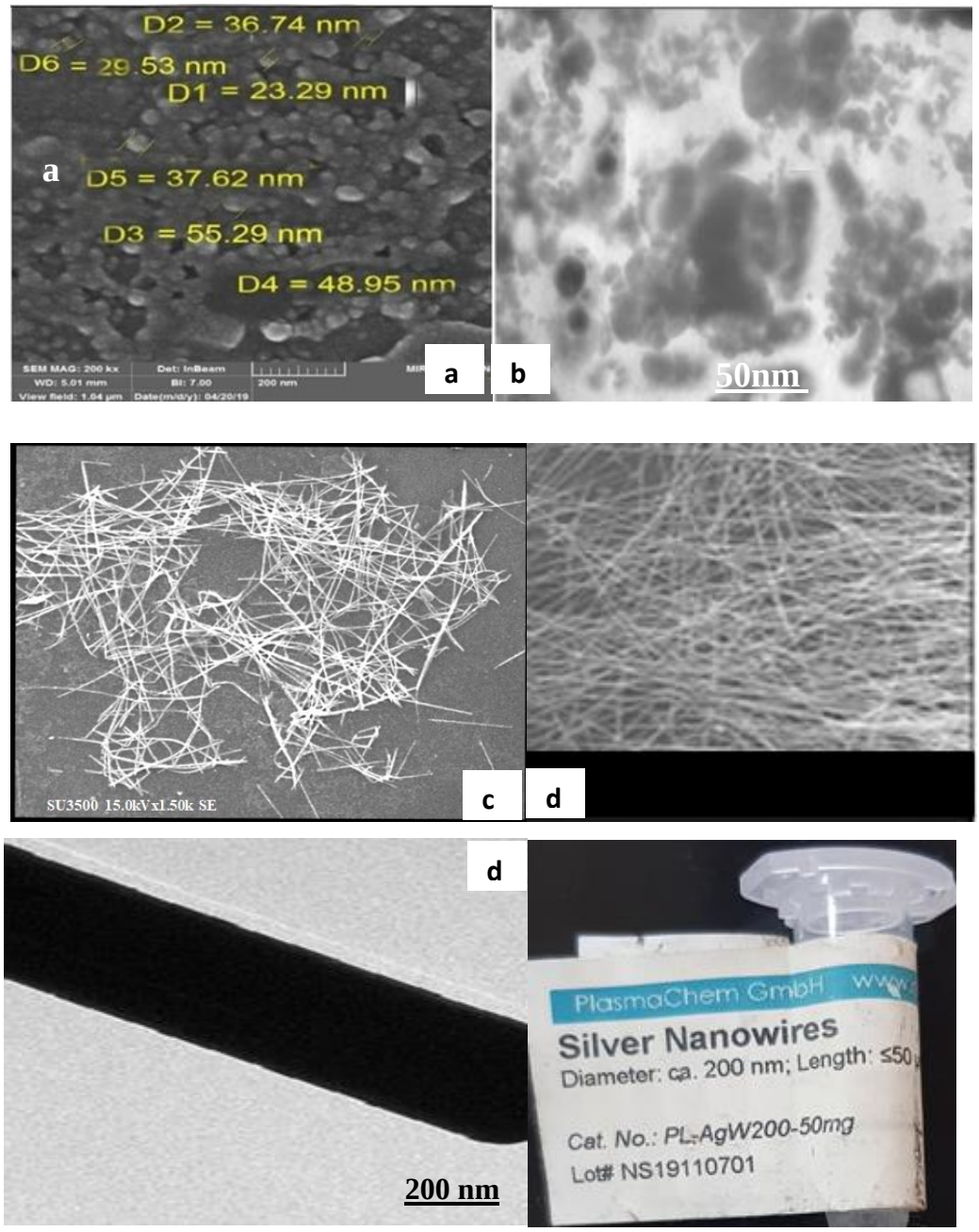

Fig. (4.27) (a) FE-SEM image Au NPs (b)TEM images of Au NPs (c) FE-SEM image of Ag nanowires (b)TEM images of Ag nanowires,in addition to real images .of boxe as received from the supplier company

4.6.5 Lasing characteristics

The laser chamber was formed to an annular resonator plus an external reflective surface in addition to the main resonator of the random laser consisting of (dye RhB in deionized water mixed with 0.03 mg/ml PVP polymer + AgNWe which were placed inside the chamber with different concentration of AgNWe)

The emission spectra of different for five random laser samples SA, SB, SC , Sd, Sf pumped by 532 nm have been investigated. Fig.(4.28) exhibits that the scattering centers of these media which were fabricated evince enough optical feedback, and the influence of the pumping energies on the emission spectra of these media was also prominent. From Fig. (4.28a) one can see the emission spectra of the sample SA at low pumping energy typically in the region 0.17 mJ, there is a broad emission of the SA with peak (λmax) at 603 nm and FWHM about 10 nm can be observed. With increasing the incident photons energy, the spectrum emission becomes narrower, showing a small bandwidth of about 9.2 nm at 0.51 mJ. Yet more pumping energy, the spectrum reaches its threshold where the gain is balanced with loss, and it can be observed that this spectrum is more narrowed until FWHM reaches 8.83 nm at 0.68 mJ and its intensity increases rapidly. Later on, when the pumping energy exceeds the threshold, i.e. photon generation rate becomes higher than its loss, the emission spectrum is narrowed more than the previous one and reaches its lowest value for this sample around 7.5 nm and then stabilizes at this value even if the pumping energy continues increasing, while its intensity of the emission spectrum continues to increase very rapidly and is subjected to a state of broken up in the emission spectrum announcing the appearance of spikes on its top of the spectrum which represent the state of closed paths

(the standing wave) that occurs inside the random medium, indicating the emergence of the coherent random laser. In addition to that

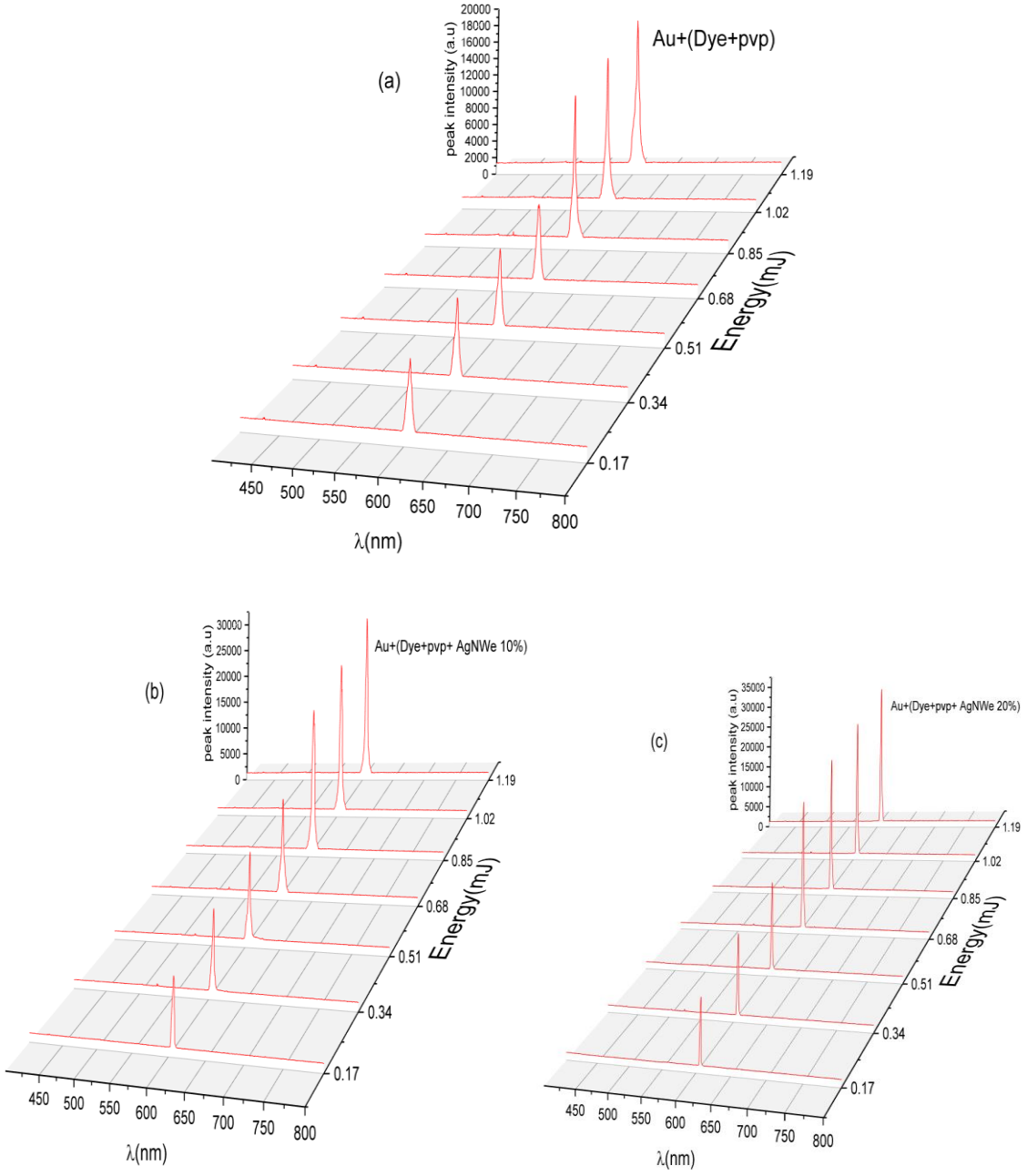

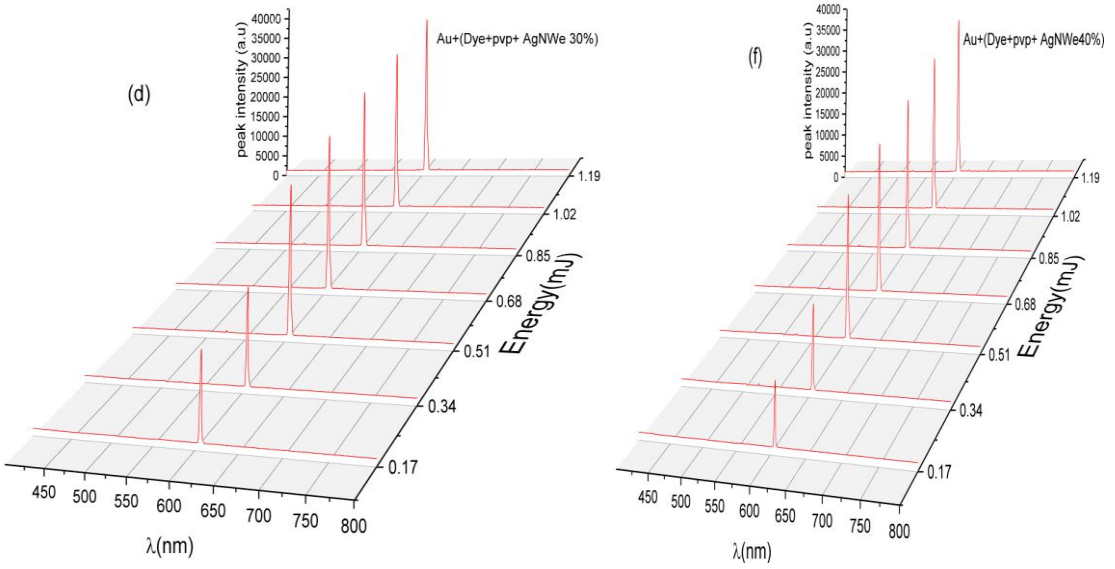

Fig.(4.28) The emission intensity of the five samples S_A, S_B, S_C, S_d, S_f, as function of the pumping energy

Fig.(4.28) shows of the effect of pumping power on the emission intensity of the random laser, it also indicates the extent to which the emission spectrum is affected due to the difference in the concentration of the (Ag NWe) of the five media. There is an improvement and increase in emission intensity and decrease in FWHM with increasing concentration(Ag NWe).By comparing the emission spectrum of the five samples, which differ only according to the concentration of the (Ag NWe), it is noted that sample Sd, in which the at a concentration of Ag NWe 30% has the greatest emission intensity 39420.64 a.u., while the other four samples be less, we note with increasing Ag concentration the intensity continued to increase Finally, at greater concentration which is (Ag NWe 40%)the quenching process is clear in Sf where the intensity decreased to be (37823,23) a.u.

Fig.(4.29) illustrates the peak emission intensity and FWHM as a function of the pumping energy, and this provides an opportunity to compare the laser threshold for the three samples SA, SB, Sc,Sd and Sf. Data show that the sample Sd (0.34 mJ) has a lower threshold than the sample SA(0.68 mJ) ,SB (0.68 mJ) , and sample Sc (0.51 mJ). Since the high light scattering

efficiency and large local-field enhancement can occur by increasing the concentration (AgNWe), then the medium that contains the (AgNWe) with large concentration will have a much lower threshold than the medium that the concentration with less .

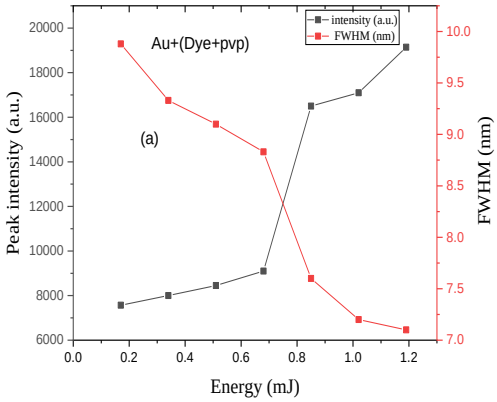

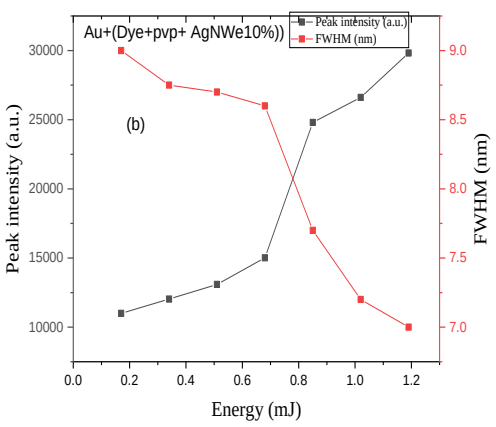

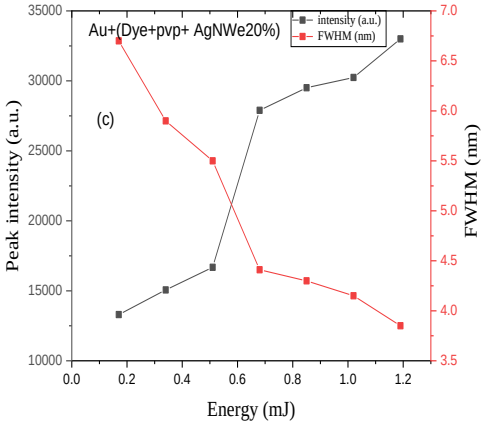

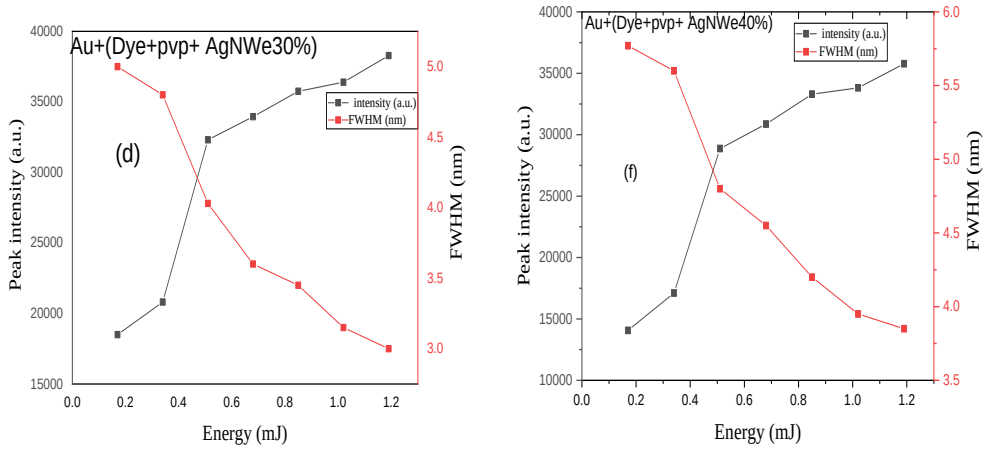

Fig.(4.29) (a) The emission peak of random laser and FWHM as function of pumping energy)

observed from the figure that the FWHM of theemission spectrum of the five samples decreases with increasing the pumping energy to reach approximately 3 nm, , from the sample at a small concentration to the large one. Also, it can be seen from the figure that the pulse width stabilizes at these values despite the continuous increase in pumping energy respectively, from the sample at a small concentrationto the large one. Also, it can be seen from the figure that the pulse width stabilizes at these values despite the continuous increase in pumping energy.

Fig (4.30) represents in support of the results obtained regarding the emission intensity and the laser threshold by changing the concentration of the as the figure shows that the intensity of the random laser increases with increasing the concentration (AgNWe) at a certain limit.

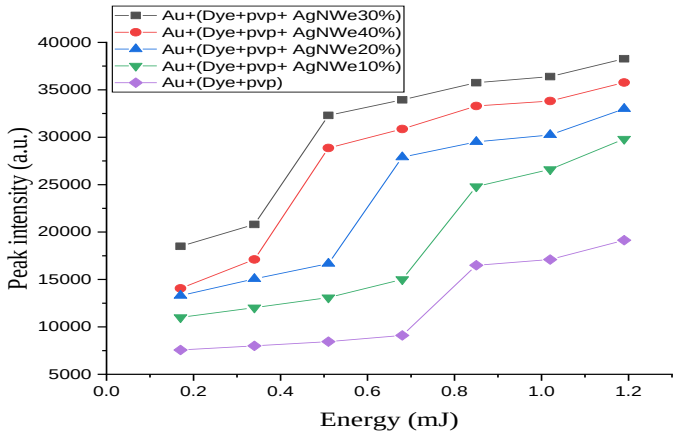

Fig.(4.30) The emission peak of random laser as function of pumping energy

it can be concluded that as the concentration increases within a certain range, FWHM and threshold mproves, As shown in the table (4.3), the times of the stay of the photon inside the random medium will be longer and thus the possibility of amplifying it and obtaining a coherent laser output increases,

Table (4.3) Random laser parameters for the five samples

Samples	λ_{peak} (nm)	FWHM (nm)	Lasing threshold)	Intensity (a.u.)
Au+(Dye+pvp)	603	7.4	0.68	19141
Au+(Dye+pvp+ AgNWe10%)	605	7	0.68	29823
Au+(Dye+pvp+ AgNWe20%)	602	3.85	0.51	33001
Au+(Dye+pvp+ AgNWe30%)	604	3	0.34	39420.64
Au+(Dye+pvp+ AgNWe40%)	603	3.45	0.34	37823.23

Chapter Five
Conclusions and Future Works

Chapter Five Conclusions and Future Works

5.1 The Conclusions

1-This study confirmed that the most common method of thermal cavitation generation involves focusing a continuous wave (CW) of laser beam on a liquid medium including nanoparticles and controlling the thermal cavity parameters and bubble formation by controlling the concentration of nanoparticles and power of the incident laser.

2- The properties of the random laser are significantly affected by the thermal cavity, as it was observed that the peak emission intensity reached its best value in the presence of composite thermal cavities. As for the FWHM and the laser threshold, their values decreased as well.find the Ag NWs effective more than Fe2O3 MNp

3- At random lasing composed of two-dimensional glass plasmonic nanostructures through surfaces, it was observed that the result of the convex surface inward was better than the outside in terms of intensity and pulse width FWHM, as well as the laser threshold from 0.85 to 0.35 mJ.

4-Random lasers fabricate Magento plasmonics based on a two-dimensional structured FeB Square array containing a thin layer of gold and an Rh6G dye. Our results show the possibility of improving the random laser parameters in the presence of the magnetic field. It was found that the emission intensity increases with the growth in the density of the scattering centres in each motif's corner of the two-dimensional structure.

5-The efficiency of this triplet -cavity random laser can be controlled by increasing the concentration of AgNw. observed the higher lasing efficiency in the sample with increasing the concentration AgNw in the internal gain medium and the irregular edges is considered a major factor in influencing the properties of the random laser, The study showed that irregular edges provide the scattered reflection of both the pumping beam and the radiation generated by the dye.

5.2 Suggestions for Future Works

1. We propose using other nanoparticles, such as Au nanostars, and a different CW laser, such as a high-power laser diode with a wavelength of 808 nm, to create hot spots and produce microbubbles

2- We propose that the active medium of the random laser should have a hemispherical shape in order to control the directions of the random laser emission directions.

3- Study the effect of change in temperature of the active medium of a random laser on the lasing characteristics

4.Fabricating sandwich structure by two MgF_2 plates and a highly transparent liquid active layer embedded with nanoparticles. This active media provides optical confinement by nanoparticle scattering and waveguide structure

5-Other cavities, such as optical cavities based on two grains of sand and capillary-tube liquid polymer, can be utilised alone or in combination with the ones presented in this study to enhance the random laser's capabilities

6. Choosing other active medium such as light emitting polymers to get coherent lasing in the multi wavelength spectral region.

References

References

[1] Kedia, Sunita, and Sucharita Sinha. "Random laser emission at dual wavelengths in a donor-acceptor dye mixture solution." Results in Physics 7 (2017), 697-704. doi:10.1016/j.rinp.2017.01.028.

[2] Wan, Yuan, Yashuai An, and Luogen Deng. "Plasmonic enhanced low-threshold random lasing from dye-doped nematic liquid crystals with TiN nanoparticles in capillary tubes." Scientific Reports 7, no. 1 (2017). doi:10.1038/s41598-017-16359-5.

[3] Fallert, J., R.J.B. Dietz, M. Hauser, F. Stelzl, C. Klingshirn, and H. Kalt. "Random lasing in ZnO nanocrystals." Journal of Luminescence 129, no. 12 (2009), 1685-1688. doi:10.1016/j.jlumin.2009.02.022.

[4] Ismail, Wan Z., Thanh P. Vo, Ewa M. Goldys, and Judith M. Dawes. "Plasmonic enhancement of Rhodamine dye random lasers." Laser Physics 25, no. 8 (2015), 085001. doi:10.1088/1054-660x/25/8/085001.

[5] Zhai, Tianrui, Zhiyang Xu, Songtao Li, and Xinping Zhang. "Red-green-blue plasmonic random laser." Optics Express 25, no. 3 (2017), 2100. doi:10.1364/oe.25.002100.

[6] Shivakiran Bhaktha, B. N., Nicolas Bachelard, Xavier Noblin, and Patrick Sebbah. "Optofluidic random laser." Applied Physics Letters 101, no. 15 (2012), 151101. doi:10.1063/1.4757872.

[7] Lee, Ya-Ju, Chun-Yang Chou, Zu-Po Yang, Thi B. Nguyen, Yung-Chi Yao, Ting-Wei Yeh, Meng-Tsan Tsai, and Hao-Chun Kuo. "Flexible

random lasers with tunable lasing emissions." Nanoscale 10, no. 22 (2018), 10403-10411. doi:10.1039/c8nr00229k.

[8] Zhai, Tianrui, Zhiyang Xu, Xiaofeng Wu, Yimeng Wang, Feifei Liu, and Xinping Zhang. "Ultra-thin plasmonic random lasers." Optics Express 24, no. 1 (2016), 437. doi:10.1364/oe.24.000437.

[9] Smetanin, Sergei N., and Tasoltan T. Basiev. "Random lasing in a nanocomposite medium." Quantum Electronics 43, no. 1 (2013), 63-70. doi:10.1070/qe2013v043n01abeh014944.

[10] Chen, Y. K., D. G. Zhang, X. X. Wang, C. Liu, P. Wang, and H. Ming. "Launching plasmonic Bloch waves with excited dye molecules." Nanotechnology 23, no. 47 (2012), 475202. doi:10.1088/0957-4484/23/47/475202.

[11] Wang, Zhuoxian, Xiangeng Meng, Alexander V. Kildishev, Alexandra Boltasseva, and Vladimir M. Shalaev. "Nanolasers Enabled by Metallic Nanoparticles: From Spasers to Random Lasers." Laser & Photonics Reviews 11, no. 6 (2017), 1700212. doi:10.1002/lpor.201700212.

[12] R. G. S. El-Dardiry and A. Lagendijk, “Tuning random lasers by engineered absorption,” *Appl. Phys. Lett.*, vol. 98, no. 16, pp. 1–4, 2011, doi: 10.1063/1.3571452.

[13] A. K. Tiwari, “Coherent random lasing in a disordered array of amplifying microresonators.” 2018.

[14] D. Van Hoang, N. Thi Phuong, and N. Van Phu, “Random Lasers: Characteristics, Applications and Some Research Results,” *Computational Methods in Science and Technology*, vol. Special Is,

no. 02. pp. 47–51, 2010, doi: 10.12921/cmst.2010.si.02.47-51.

[15] C. S. Wang, Y. L. Chen, H. Y. Lin, Y. T. Chen, and Y. F. Chen, "Enhancement of random lasing through fluorescence resonance energy transfer and light scattering mediated by nanoparticles," *Appl. Phys. Lett.*, vol. 97, no. 19, pp. 1–4, 2010, doi: 10.1063/1.3515913.

[16] Chua, Song-Liang, Yidong Chong, A. D. Stone, Marin Soljacic, and Jorge Bravo-Abad. "Low-threshold lasing action in photonic crystal slabs enabled by Fano resonances." *Optics Express* 19, no. 2 (2011), 1539. doi:10.1364/oe.19.001539.

[17] Zhai, Tianrui, Jie Chen, Li Chen, Jieyu Wang, Li Wang, Dahe Liu, Songtao Li, Hongmei Liu, and Xinping Zhang. "A plasmonic random laser tunable through stretching silver nanowires embedded in a flexible substrate." *Nanoscale* 7, no. 6 (2015), 2235-2240. doi:10.1039/c4nr06632d.

[18] Long, Li, Daisi He, Weiying Bao, Menglei Feng, Peng Zhang, Dingke Zhang, and Shijian Chen. "Localized surface plasmon resonance improved lasing performance of Ag nanoparticles/organic dye random laser." *Journal of Alloys and Compounds* 693 (2017), 876-881. doi:10.1016/j.jallcom.2016.09.246.

[19] Wang, Zhaona, Xiaoyu Shi, Sujun Wei, Yanyan Sun, Yanrong Wang, Jing Zhou, Jinwei Shi, and Dahe Liu. "Two-threshold silver nanowire-based random laser with different dye concentrations." *Laser Physics Letters* 11, no. 9 (2014), 095002. doi:10.1088/1612-2011/11/9/095002.

[20] Qian, Xiang-zhong. "Tunable Liquid Crystal Random Laser Radiation Based on Photonic Crystal Micro-Cavity." *2011 Symposium on*

Photonics and Optoelectronics (SOPO), 2011. doi:10.1109/sopo.2011.5780721.

[21] Shasti, M., P. Coutino, S. Mukherjee, A. Varanytsia, T. Smith, A. P. Luchette, L. Sukhomlinova, T. Kosa, A. Munoz, and B. Taheri. "Reverse mode switching of the random laser emission in dye doped liquid crystals under homogeneous and inhomogeneous electric fields." *Photonics Research* 4, no. 1 (2016), 7. doi:10.1364/prj.4.000007.

[22] Lee, Chia-Rong, Shih-Hung Lin, Jin-Wei Guo, Jia-De Lin, Hong-Lin Lin, Yang-Chen Zheng, Chia-Lien Ma, Chi-Ting Horng, Han-Ying Sun, and Shuan-Yu Huang. "Electrically and thermally controllable nanoparticle random laser in a well-aligned dye-doped liquid crystal cell." *Optical Materials Express* 5, no. 6 (2015), 1469. doi:10.1364/ome.5.001469.

[23] Song, Qinghai, Liying Liu, Lei Xu, Yonggang Wu, and Zhanshan Wang. "Electrical tunable random laser emission from a liquid-crystal infiltrated disordered planar microcavity." *Optics Letters* 34, no. 3 (2009), 298. doi:10.1364/ol.34.000298.

[24] Chen, Peiliang, Xiangyang Ma, Dongsheng Li, Yuanyuan Zhang, and Deren Yang. "Electric-field-induced random lasing from ZnO and Mg_01Zn_09O films optically pumped with an extremely low intensity." *Optics Express* 17, no. 21 (2009), 18513. doi:10.1364/oe.17.018513.

[25] Ferjani, Sameh, Valentin Barna, Antonio De Luca, Carlo Versace, and Giuseppe Strangi. "Random lasing in freely suspended dye-doped nematic liquid crystals." *Optics Letters*33, no. 6 (2008), 557.

doi:10.1364/ol.33.000557.

[26] Chen, Ziping, Dechun Hu, Xingwu Chen, Deren Zeng, Yungjui Lee, Xiaoxian Chen, and Jiangang Lu. "Templated Sphere Phase Liquid Crystals for Tunable Random Lasing." *Nanomaterials* 7, no. 11 (2017), 392. doi:10.3390/nano7110392.

[27] Mujumdar, Sushil, Stefano Cavalieri, and Diederik S. Wiersma. "Temperature-tunable random lasing: numerical calculations and experiments." *Journal of the Optical Society of America B* 21, no. 1 (2004), 201. doi:10.1364/josab.21.000201.

[28] Mbarak, H., A.K. Kodeary, S.M. Hamidi, E. Mohajarani, and Y. Zaatar. "Control of nonlinear refractive index of AuNPs doped with nematic liquid crystal under external electric field." *Optik* 198 (2019), 163299. doi:10.1016/j.ijleo.2019.163299.

[29] T. Okamoto and S. Adachi, “Effect of particle size and shape on nonresonant random laser action of dye-doped polymer random media,” *Opt. Rev.*, vol. 17, no. 3, pp. 300–304, 2010, doi: 10.1007/s10043-010-0053-0.

[30] Murai, Shunsuke, Koji Fujita, Xiangeng Meng, and Katsuhisa Tanaka. "Random Dispersion of Metal Nanoparticles Can Form a Laser Cavity." *Chemistry Letters* 39, no. 6 (2010), 532-537. doi:10.1246/cl.2010.532

[31] L. Yang, G. Feng, J. Yi, K. Yao, G. Deng, and S. Zhou, “Effective random laser action in Rhodamine 6G solution with Al nanoparticles,” *Applied Optics*, vol. 50, no. 13. pp. 1816–1821, 2011, doi: 10.1364/AO.50.001816.

[32] Zhai, Tianrui, Xinping Zhang, and Zhaoguang Pang. "Polymer laser based on active waveguide grating structures." *Optics Express* 19, no. 7 (2011), 6487. doi:10.1364/oe.19.006487

[33] Lin, Ming C., Mong-Kai Wu, Miin-Jang Chen, Jer-Ren Yang, and Makoto Shiojiri. "Blue-shifted stimulated emission from ZnO films deposited on SiO2 by atomic layer deposition." *Materials Chemistry and Physics* 135, no. 1 (2012), 88-93. doi:10.1016/j.matchemphys.2012.04.027..

[34] Haque, Fozia Z., Vazid Ali, and M. Husain. "Synthesis and spectroscopic characterization of Kiton Red-620 dye doped silica gel rods." *Optik* 123, no. 11 (2012), 1010-1014. doi:10.1016/j.ijleo.2011.07.019.

[35] Heydari, Esmaeil, Roman Flehr, and Joachim Stumpe. "Influence of spacer layer on enhancement of nanoplasmon-assisted random lasing." *Applied Physics Letters* 102, no. 13 (2013), 133110. doi:10.1063/1.4800776

[36] Zhai, Tianrui, Jie Chen, Li Chen, Jieyu Wang, Li Wang, Dahe Liu, Songtao Li, Hongmei Liu, and Xinping Zhang. "A plasmonic random laser tunable through stretching silver nanowires embedded in a flexible substrate." *Nanoscale* 7, no. 6 (2015), 2235-2240. doi:10.1039/c4nr06632d.

[37] Wang, Zhaona, Xiaoyu Shi, Sujun Wei, Yanyan Sun, Yanrong Wang, Jing Zhou, Jinwei Shi, and Dahe Liu. "Two-threshold silver nanowire-based random laser with different dye concentrations." *Laser Physics Letters* 11, no. 9 (2014), 095002. doi:10.1088/1612-2011/11/9/095002.

[38] J. Ziegler, M. Djiango, C. Vidal, C. Hrelescu, and T. A. Klar, “Gold nanostars for random lasing enhancement,” *Optics Express*, vol. 23, no. 12. p. 15152, 2015, doi: 10.1364/oe.23.015152.

[39] Zhai, Tianrui, Zhiyang Xu, Xiaofeng Wu, Yimeng Wang, Feifei Liu, and Xinping Zhang. "Ultra-thin plasmonic random lasers." *Optics Express* 24, no. 1 (2016), 437. doi:10.1364/oe.24.000437.

[40] S. Ning, Z. Wu, N. Zhang, L. Ding, X. Hou, and F. Zhang, “Plasmonically enhanced lasing by different size silver nanoparticles-silver film hybrid structure,” *Org. Electron.*, vol. 50, pp. 403–410, 2017, doi: 10.1016/j.orgel.2017.08.018.

[41] Suja, Mohammad, Bishwajit Debnath, Sunayna B. Bashar, Longxing Su, Roger Lake, and Jianlin Liu. "Electrically driven plasmon-exciton coupled random lasing in ZnO metal-semiconductor-metal devices." *Applied Surface Science* 439 (2018), 525-532. doi:10.1016/j.apsusc.2018.01.075

[42] Zhang, Shuai, Junhua Tong, Chao Chen, Fengzhao Cao, Chengbin Liang, Yanrong Song, Tianrui Zhai, and Xinping Zhang. "Controlling the Performance of Polymer Lasers via the Cavity Coupling." *Polymers* 11, no. 5 (2019), 764. doi:10.3390/polym11050764

[43] Z. Ren, N. Zheng, K. Ge, G. Zhang, and S. Li, “Investigation of the LSPR on a wavelength-tunable random laser,” *Physica Scripta*, vol. 94, no. 10. 2019, doi: 10.1088/1402-4896/ab07df.

[44] Haddawi, S.F., A.K. Kodeary, N.S. Shnan, N. Roostaei, S.M. Hamidi, and Hammad R. Humud. "Vertically emitted dual wavelength random

laser based on light emitting polymers and silver nanowires double cavity structure." *Optik* 219 (2020), 165256. doi:10.1016/j.ijleo.2020.165256.

[45] Zhang, Naming, Shuya Ning, Kang Dai, Yifan Zhang, Yuan Wu, Fang Yuan, and Fanghui Zhang. "Random lasing based on a nanoplasmonic hybrid structure composed of (Au core)-(Ag shell) nanorods with Ag film." *Optical Materials Express* 10, no. 5 (2020), 1204. doi:10.1364/ome.392623

[46] V. S. Gummaluri, R. Gayathri, C. Vijayan, and V. M. Murukeshan, “Gold nano-urchins for plasmonic enhancement of random lasing in a dye-doped polymer,” *J. Opt. (United Kingdom)*, vol. 22, no. 6, 2020, doi: 10.1088/2040-8986/ab896b.

[47] Sato, Rodrigo, Joel Henzie, Boyi Zhang, Satoshi Ishii, Shunsuke Murai, Ken Takazawa, and Yoshihiko Takeda. "Random Lasing via Plasmon-Induced Cavitation of Microbubbles." *Nano Letters* 21, no. 14 (2021), 6064-6070. doi:10.1021/acs.nanolett.1c01321no. 13. pp. 1816–1821, 2011, doi: 10.1364/AO.50.001816.

[48] Pramanik, Ashim, Subrata Biswas, Arindam Dey, and Pathik Kumbhakar. "Optically Transparent Graphene Flakes as Nanogenerator of Microbubbles for Random Lasing in Weakly Scattering Regime." *Advanced Photonics Research* 2, no. 8 (2021), 2100063. doi:10.1002/adpr.202100063.

[49] Haddawi, S.F., N. Roostaei, and S.M. Hamidi. "Coupled modes enhance random lasing in plasmonic double grating structure." *Optics & Laser Technology* 156 (2022), 108577. doi:10.1016/j.optlastec.2022.108577..

[50] Li, Songtao. "The Film Random Laser Doped with Core-Shell Structure Ag Spheres." *Annals of Chemical Science Research* 3, no. 5 (2023). doi:10.31031/acsr.2023.03.000574

[51] H. Cao, “Random lasers: development, features and applications,” *Opt. Photonics News*, vol. 16, no. 1, pp. 24–29, 2005.

[52] B. Redding, M. A. Choma, and H. Cao, “Speckle-free laser imaging using random laser illumination,” *Nat. Photonics*, vol. 6, no. 6, pp. 355–359, 2012, doi: 10.1038/nphoton.2012.90.

[53] Song, Qinghai, Zhengbin Xu, Seung H. Choi, Xuanhao Sun, Shumin Xiao, Ozan Akkus, and Young L. Kim. "Detection of nanoscale structural changes in bone using random lasers." *Biomedical Optics Express* 1, no. 5 (2010), 1401. doi:10.1364/boe.1.001401.

[44] M. S. Dawood, E. G. Khalil, and H. H. Saleh, “Detection of tumor mass based on laser scanning imaging,” *Al-Nahrain J. Eng. Sci.*, vol. 20, no. 1, pp. 176–182, 2017.

[55] Q. Song Qinghai, Zhengbin., “Random lasing in bone tissue,” *Opt. Lett.*, vol. 35, no. 9, pp. 1425–1427, 2010.

[56] W. Z. W. Ismail, G. Liu, K. Zhang, E. M. Goldys, and J. M. Dawes, “Dopamine sensing and measurement using threshold and spectral measurements in random lasers,” *Opt. Express*, vol. 24, no. 2, pp. A85–A91, 2016.

[57] R. C. Polson and Z. V Vardeny, “Cancerous tissue mapping from random lasing emission spectra,” *J. Opt.*, vol. 12, no. 2, p. 24010, 2010.

[58] W. Z. W. Ismail, D. Liu, S. Clement, D. W. Coutts, E. M. Goldys, and J. M. Dawes, “Spectral and coherence signatures of threshold in random lasers,” *J. Opt. (United Kingdom)*, vol. 16, no. 10, 2014, doi: 10.1088/2040-8978/16/10/105008.

[59] G. Van Soest, F. J. Poelwijk, R. Sprik, and A. Lagendijk, “Dynamics of a random laser above threshold,” *Phys. Rev. Lett.*, vol. 86, no. 8, pp. 1522–1525, 2001, doi: 10.1103/PhysRevLett.86.1522.

[60] orazio Sevelto, “principles of lasers.” Springer, 2010.

[61] G. Thomas and R. Isaacs, “Basic principles of lasers,” *Anaesth. Intensive Care Med.*, vol. 12, no. 12, pp. 574–577, 2011, doi: 10.1016/j.mpaic.2011.09.013.

[62] S. Black, “Physical principles of LASER,” *Anaesth. Intensive Care Med.*, vol. 15, no. 11, pp. 530–532, 2014, doi: 10.1016/j.mpaic.2014.08.003.

[63] H. Cao, “Lasing in random media,” *Tutorials in Complex Photonic Media*. pp. 301–358, 2009, doi: 10.1117/3.832717.Ch11.

[64] J. Andreasen, N. Bachelard, S. B. N. Bhaktha, H. Cao, P. Sebbah, and C. Vanneste, “Partially pumped random lasers,” *International Journal of Modern Physics B*, vol. 28, no. 5. 2014, doi: 10.1142/S0217979214300011.

[65] F. Luan, B. Gu, A. S. L. Gomes, K. T. Yong, S. Wen, and P. N. Prasad, “Lasing in nanocomposite random media,” *Nano Today*, vol. 10, no. 2, pp. 168–192, 2015, doi: 10.1016/j.nantod.2015.02.006.

[66] L. Ye, Y. Feng, C. Lu, G. Hu, and Y. Cui, “Coherent random lasing from liquid waveguide gain layer containing silica nanoparticles,”

Laser Phys. Lett., vol. 13, no. 10, 2016, doi: 10.1088/1612-2011/13/10/105002.

[67] Wang, Zhuoxian, Xiangeng Meng, Seung H. Choi, Sebastian Knitter, Young L. Kim, Hui Cao, Vladimir M. Shalaev, and Alexandra Boltasseva. "Controlling Random Lasing with Three-Dimensional Plasmonic Nanorod Metamaterials." *Nano Letters* 16, no. 4 (2016), 2471-2477. doi:10.1021/acs.nanolett.6b00034.

[68] D. S. Wiersma, "The physics and applications of random lasers," *Nat. Phys.*, vol. 4, no. 5, pp. 359–367, 2008, doi: 10.1038/nphys971.

[69] C.-R. Lee, S.-H. Lin, C.-H. Guo, S.-H. Chang, T.-S. Mo, and S.-C. Chu, "All-optically controllable random laser based on a dye-doped polymer-dispersed liquid crystal with nano-sized droplets," *Opt. Express*, vol. 18, no. 3, p. 2406, 2010, doi: 10.1364/oe.18.002406.

[70] H. Zhang, G. Feng, J. Y. Yi, J. Mu, K. Yao, and S. Zhou, "Coherent random laser based on liquid waveguide gain channels," *J. Mod. Opt.*, vol. 62, no. 10, pp. 865–868, 2015, doi: 10.1080/09500340.2015.1009953.

[71] G. D. Dice and A. Y. Elezzabi, "Random lasing from a nanoparticle-based metal-dielectric-dye medium," *J. Opt. A Pure Appl. Opt.*, vol. 9, no. 2, pp. 186–193, 2007, doi: 10.1088/1464-4258/9/2/012.

[72] Lee, Ya-Ju, Chun-Yang Chou, Zu-Po Yang, Thi B. Nguyen, Yung-Chi Yao, Ting-Wei Yeh, Meng-Tsan Tsai, and Hao-Chun Kuo. "Flexible random lasers with tunable lasing emissions." *Nanoscale* 10, no. 22 (2018), 10403-10411. doi:10.1039/c8nr00229k.

[73] M. A. T. Khan, “Spatial coherence measurement of random laser.” 2016.

[74] R. Tang, “RANDOM LASER IN DISORDERED SOLUTIONS,” no. December. 2017.

[75] M. Pang, X. Bao, L. Chen, Z. Qin, Y. Lu, and P. Lu, “Frequency stabilized coherent Brillouin random fiber laser: theory and experiments,” *Opt. Express*, vol. 21, no. 22, p. 27155, 2013, doi: 10.1364/oe.21.027155.

[76] D. Wiersma, “Laser physics: The smallest random laser,” *Nature*, vol. 406, pp. 132–133, 2000.

[77] Y. Nastishin and T. H. Dudok, “Optically pumped mirror less lasing. A review. part I. random lasing,” *Ukr. J. Phys. Opt.*, vol. 14, no. 3, pp. 146–170, 2013, doi: 10.3116/16091833/14/3/146/2013.

[78] A. Ghasempour Ardakani, A. R. Bahrampour, S. M. Mahdavi, and M. Golshani Gharyeh Ali, “Numerical study of random lasing in three dimensional amplifying disordered media,” *Opt. Commun.*, vol. 285, no. 6, pp. 1314–1322, 2012, doi: 10.1016/j.optcom.2011.10.018.

[79] X. WU, “Study of Lasing in Random and Periodic Systems.” 2007.

[80] L. Li and L. Deng, “Low threshold and coherent random lasing from dye-doped cholesteric liquid crystals using oriented cells,” *Laser Phys.*, vol. 23, no. 8, 2013, doi: 10.1088/1054-660X/23/8/085001.

[81] R. C. Polson, M. E. Raikh, and Z. V. Vardeny, “Random Lasing from Weakly Scattering Media: Universality in the Emission Spectra from Pi-Conjugated Polymer Films,” no. September 2013, 2001.

[82] H. Cao, Y. Ling, J. Y. Xu, C. Q. Cao, and P. Kumar, “Photon statistics of random lasers with resonant feedback,” *Physical Review Letters*, vol. 86, no. 20. pp. 4524–4527, 2001, doi: 10.1103/PhysRevLett.86.4524.

[83] W. Z. W. Ismail, D. Liu, S. Clement, D. W. Coutts, E. M. Goldys, and J. M. Dawes, “Spectral and coherence signatures of threshold in random lasers,” *J. Opt. (United Kingdom)*, vol. 16, no. 10, 2014, doi: 10.1088/2040-8978/16/10/105008.

[84] R. G. S. El-Dardiry, A. P. Mosk, O. L. Muskens, and A. Lagendijk, “Experimental studies on the mode structure of random lasers,” *Phys. Rev. A - At. Mol. Opt. Phys.*, vol. 81, no. 4, pp. 1–8, 2010, doi: 10.1103/PhysRevA.81.043830.

[85] R. M. Ziff, G. E. Uhlenbeck, and M. Kac, “The ideal Bose-Einstein gas, revisited,” *Phys. Rep.*, vol. 32, no. 4, pp. 169–248, 1977, doi: 10.1016/0370-1573(77)90052-7.

[86] L. Florescu and S. John, “Photon statistics and coherence in light emission from a random laser,” *Phys. Rev. Lett.*, vol. 93, no. 1, pp. 013602–1, 2004, doi: 10.1103/PhysRevLett.93.013602.

[87] G. D. Dice, S. Mujumdar, and A. Y. Elezzabi, “Plasmonically enhanced diffusive and subdiffusive metal nanoparticle-dye random laser,” *Applied Physics Letters*, vol. 86, no. 13. pp. 1–3, 2005, doi: 10.1063/1.1894590.

[88] H. Cao, J. Y. Xu, S. H. Chang, and S. T. Ho, “Transition from amplified spontaneous emission to laser action in strongly scattering media,” *Phys. Rev. E - Stat. Physics, Plasmas, Fluids, Relat.*

Interdiscip. Top., vol. 61, no. 2, pp. 1985–1989, 2000, doi:

[89] A. Tulek and Z. V. Vardeny, "Studies of random laser action in π-conjugated polymers," *J. Opt. A Pure Appl. Opt.*, vol. 12, no. 2, 2010, doi: 10.1088/2040-8978/12/2/024008.

[90] X. Zhao, Z. Wu, S. Ning, S. Liang, D. Wang, and X. Hou, "Random lasing from granular surface of waveguide with blends of PS and PMMA," *Opt. Express*, vol. 19, no. 17, p. 16126, 2011, doi: 10.1364/oe.19.016126.

[91] L. Sznitko, J. Mysliwiec, and A. Miniewicz, "The role of polymers in random lasing," *J. Polym. Sci. Part B Polym. Phys.*, vol. 53, no. 14, pp. 951–974, 2015, doi: 10.1002/polb.23731.

[92] D. Wiersma, "Light in strongly scattering and amplifying random media," *Thesis*, no. november, p. 59, 1995.

[93] P. W. Anderson, "Absence of diffusion in certain random lattices," *Phys. Rev.*, vol. 109, no. 5, pp. 1492–1505, 1958, doi: 10.1103/PhysRev.109.1492.

[94] Z. Shang, M. Yang, and L. Deng, "Low–threshold and high intensity random lasing enhanced by MnCl2," *Materials (Basel).*, vol. 9, no. 9, p. 725, 2016.

[95] H. Cao, "Lasing in random media," *Waves in random media*, vol. 13, no. 3, p. R1, 2003.

[96] M. Li M. Yang., "Ultralow-threshold multiphoton-pumped lasing from colloidal nanoplatelets in solution," *Nat. Commun.*, vol. 6, no. 1, pp. 1–8, 2015.

[97] R. K. Thareja and A. Mitra, “Random laser action in ZnO,” *Appl. Phys. B*, vol. 71, no. 2, pp. 181–184, 2000.

[98] Yi, Jiayu, Guoying Feng, Liling Yang, Ke Yao, Chao Yang, Yingsong Song, and Shouhuan Zhou. "Behaviors of the Rh6G random laser comprising solvents and scatterers with different refractive indices." *Optics Communications* 285, no. 24 (2012), 5276-5282. doi:10.1016/j.optcom.2012.06.094.

[99] W. Z. W. Ismail, T. P. Vo, E. M. Goldys, and J. M. Dawes, “Plasmonic enhancement of Rhodamine dye random lasers,” *Laser Phys.*, vol. 25, no. 8, 2015, doi: 10.1088/1054-660X/25/8/085001.

[100] N. A. I. M. Kamil, “Principles and characteristics of random lasers and their applications in medical, bioimaging and biosensing,” *AIP Conf. Proc.*, vol. 2203, no. January, 2020, doi: 10.1063/1.5142109.

[101] Xia, Jiangying, Kang Xie, Jiajun Ma, Xianxian Chen, Yaxin Li, Jianxiang Wen, Jingjing Chen, et al. "The transition from incoherent to coherent random laser in defect waveguide based on organic/inorganic hybrid laser dye." *Nanophotonics* 7, no. 7 (2018), 1341-1350. doi:10.1515/nanoph-2018-0034.

[102] H. Cao, “Random Lasers with Coherent Feedback,” *Optical Properties of Nanostructured Random Media*. pp. 303–330, 2007, doi: 10.1007/3-540-44948-5_14.

[103] Hu, Zhijia, Qun Zhang, Bo Miao, Qiang Fu, Gang Zou, Yang Chen, Yi Luo, et al. "Coherent Random Fiber Laser Based on Nanoparticles Scattering in the Extremely Weakly Scattering Regime." *Physical Review Letters* 109, no. 25 (2012).

doi:10.1103/physrevlett.109.253901.

[104] J. Azkargorta, I. Iparraguirre, J. Fernández, R. Balda, S. García-Revilla, and M. Barredo-Zurriarrain, “ Random laser properties of Nd 3+ crystal powders ,” *Opt. Express*, vol. 26, no. 9, p. 11787, 2018, doi: 10.1364/oe.26.011787.

[105] A. Consoli and C. López, “Decoupling gain and feedback in coherent random lasers: Experiments and simulations,” *Sci. Rep.*, vol. 5, pp. 1–10, 2015, doi: 10.1038/srep16848.

[106] A. Sarkar, B. N. S. Bhaktha, and J. Andreasen, “Replica Symmetry Breaking in a Weakly Scattering Optofluidic Random Laser,” *Sci. Rep.*, vol. 10, no. 1, pp. 1–12, 2020, doi: 10.1038/s41598-020-59575-2.

[107] C. Sönnichsen, “Plasmons in metal nanostructures,” *Dissertation*, vol. 27, no. June, p. 134, 2001, doi: 10.1017/CBO9781107415324.004.

[108] V. G. Kravets, A. V. Kabashin, W. L. Barnes, and A. N. Grigorenko, “Plasmonic Surface Lattice Resonances: A Review of Properties and Applications,” *Chem. Rev.*, vol. 118, no. 12, pp. 5912–5951, 2018, doi: 10.1021/acs.chemrev.8b00243.

[109] Liu, Jianxun, Huilin He, Dong Xiao, Shengtao Yin, Wei Ji, Shouzhen Jiang, Dan Luo, Bing Wang, and Yanjun Liu. "Recent Advances of Plasmonic Nanoparticles and their Applications." *Materials* 11, no. 10 (2018), 1833. doi:10.3390/ma11101833.

[110] K. Okamoto, I. Niki, A. Shvartser, Y. Narukawa, T. Mukai, and A. Scherer, “Surface-plasmon-enhanced light emitters based on InGaN

quantum wells," *Nat. Mater.*, vol. 3, no. 9, pp. 601–605, 2004, doi: 10.1038/nmat1198.

[111] O. Popov, A. Zilbershtein, and D. Davidov, "Random lasing from dye-gold nanoparticles in polymer films: Enhanced gain at the surface-plasmon-resonance wavelength," *Appl. Phys. Lett.*, vol. 89, no. 19, 2006, doi: 10.1063/1.2364857.

[112] A. Yadav, L. Zhong, J. Sun, L. Jiang, G. J. Cheng, and L. Chi, "Tunable random lasing behavior in plasmonic nanostructures," *Nano Converg.*, vol. 4, no. 1, pp. 1–8, 2017, doi: 10.1186/s40580-016-0095-5.

[113] C. Noguez, "Surface plasmons on metal nanoparticles: The influence of shape and physical environment," *J. Phys. Chem. C*, vol. 111, no. 10, pp. 3606–3619, 2007, doi: 10.1021/jp066539m.

[114] P. Taylor and R. G. W. Brown, "Absorption and Scattering of Light by Small Particles," no. May 2012, 2010.

[115] E. Dulkeith, "Fluorescence Quenching of Dye Molecules near Gold Nanoparticles: Radiative and Nonradiative Effects," *Phys. Rev. Lett.*, vol. 89, no. 20, pp. 12–15, 2002, doi: 10.1103/PhysRevLett.89.203002.

[116] S. Ning R. Flehr., "Enhancement of amplified spontaneous emission in organic gain media by the metallic film," *Org. Electron.*, vol. 15, no. 9, pp. 2052–2058, 2014, doi: 10.1016/j.orgel.2014.05.022.

[117] E. Heydari, R. Flehr, and J. Stumpe, "Influence of spacer layer on enhancement of nanoplasmon-assisted random lasing," *Appl. Phys. Lett.*, vol. 102, no. 13, 2013, doi: 10.1063/1.4800776.

[118] Ruby, Stanley L. "Induced Currents in Multiple Resonant Scattering." 1998. doi:10.2172/9931.

[119] "LIGHT OPTICS, ELECTRON OPTICS AND WAVE MECHANICS." *Principles of Optics*, 1980, 738-746. doi:10.1016/b978-0-08-026482-0.50023-2.

[120] "Absorption and Scattering by an Arbitrary Particle." *Absorption and Scattering of Light by Small Particles*, 2007, 57-81. doi:10.1002/9783527618156.ch3.

[121] "Lasers with Nonresonant Feedback and Laserlike Emission from Powders: Early Ideas and Experiments." *Solid-State Random Lasers* (n.d.), 1-9. doi:10.1007/0-387-25105-7_1.

[122] "Multiple scattering of laser light from turbid water." *Joint Conference on Sensing of Environmental Pollutants*, 1971. doi:10.2514/6.1971-1098.

[123] "Scattering in Random Media, General scattering in random media scattering in random media." *Formulas of Acoustics*, 2008, 238-241. doi:10.1007/978-3-540-76833-3_77.

[124] A. Ishimara "Wave Propagation and Scattering in Random Media." 1978. doi:10.1016/b978-0-12-374701-3.x5001-7.

[125] Wiersma, Diederik S., Paolo Bartolini, Ad Lagendijk, and Roberto Righini. "Localization of light in a disordered medium." *Nature* 390, no. 6661 (1997), 671-673. doi:10.1038/37757.

[126] Tishkovets, V.P. "Multiple scattering of light by a layer of discrete random medium: backscattering." *Journal of Quantitative*

Spectroscopy and Radiative Transfer 72, no. 2 (2002), 123-137. doi:10.1016/s0022-4073(01)00059-0.

[127] Olga, Korotkova. "Weak scattering of random beams." *Random Light Beams*, 2017, 319-353. doi:10.1201/b15471-8.

[128] Van der Mark, Martin B., Meint P. Van Albada, and Ad Lagendijk. "Light scattering in strongly scattering media: Multiple scattering and weak localization." *Physical Review B* 37, no. 7 (1988), 3575-3592. doi:10.1103/physrevb.37.3575.

[129] Hitchen, Christopher J. "The Effect of Suspension Medium Refractive index on the particle size analysis of quartz by laser diffraction." *Particle & Particle Systems Characterization* 9, no. 1-4 (1992), 171-175. doi:10.1002/ppsc.19920090123.

[130] Balachandran, R. M., N. M. Lawandy, and J. A. Moon. "Theory of laser action in scattering gain media." *Optics Letters* 22, no. 5 (1997), 319. doi:10.1364/ol.22.000319.

[131] K.L. Chopra, Mc. Graw Hill (1969) ISBN: 978-0070107991.

[132] C.N.R. Rao, S.R.C. Vivekchand, K. Biswas and A. Govindaraj, Dalton Trans. 34 (2007) 3728–3749.

[133]Karasinski, P. Sol-gel derived optical waveguide films for planar sens ors with phase modulation. Opt. Appl. 2004, 34, 467–475.

[134]Karasinski, P.; Tyszkiewicz, C.; Rogozinski, R. Rib waveguides base d on the sol-gel derived SiO2:TiO2 films. Photonics Lett. Pol. 2010, 2, 40–42.

[135]Matsui, T.; Komatsu, K.; Sugihara, O.; Kaino, T. Simple process for f abricating a monolithic polymer optical waveguide. Opt. Lett. 2005, 3 0, 970–972.

[136] D.M. Mattox, Handbook of physical vapor deposition (PVD) processing: Film formation, Adhesion, surface preparation and contamination control, Noyes publications (1998) ISBN: 0-8155-1422-0.

[137] K.S. Harsha, Principles of Physical vapor deposition of thin films, Wiley publication house (2006) ISBN: 978-0-08-04469-8.

[138] V. Ramakrishna, A.S. Oberai, P.A. Farrar, D.W. Kemmer, P.A. Totta, N.G. Koopman and M.B. Small, Proc. 4th IEEE VLSI Multilevel Interconnec. Conf. (1987) 27.

[139] N.T. Nguyen, Chapter 4 - Fabrication technologies, Micromixers (Second Edition) Fundamentals, Design and Fabrication Micro and Nano Technologies (2012) 113-161.

[140] M. Eslamian and F.S. Kordshuli, J. Coat. Technol. Res., 15 (2) (2018) 271–280

[141]Brinker, C.J.; Ashley, C.S.; Cairncross, R.A.; Chen, K.S.; Hurd, A.J.; Reed, S.T.; Samuel, J.; Schunk, P.R.; Schwartz, R.W.; Scotto, C.S. So l-gel derived ceramic films-fundamentals and applications. In Metallu rgical and Ceramic Protective Coatings; Stern, K.H., Ed.; Springer: D ordrecht, The Netherlands, 1996.

[142]Jaglarz, J.; Dulian, P.; Karasinski, P.; Winkowski, P. Scattering pheno mena in porous sol-gel-derived silica films. Coatings 2020, 10, 509.

[143]Faustini, M.; Louis, B.; Albouy, P.; Kuemmel, M.; Grosso, D. Prepara tion of sol−gel films by dip-coating in extreme conditions. J. Phys. Ch em. C 2010, 114, 7637–7645

[144] F.P. Schafer, W. Schmidt, J. Volze, Organic dye solution laser. Appl. Phys. Lett. 9(8), 306 (1966)

[145]. D. Moses, High quantum efficiency luminescence from a conducting polymer in solution—a novel polymer laser-dye. Appl. Phys. Lett. 60(26), 3215–3216 (1992)

[146]. R.E. Hermes et al., High-efficiency pyrromethene doped solid-state dye-lasers. Appl. Phys. Lett. 63(7),

[147] R. Bornemann, U. Lemmer, E. Thiel, Continuous-wave solid-state dye laser. Opt. Lett. 31(11), 1669–1671 (2006

[148] Okamoto, K., Fundamentals of Optical Waveguides, 2nd edn. (Academic Press, London, 2005)

[149] H. Kogelnik, C.V. Shank, J. Appl. Phys. 43, 2327 (1972) 17. W. Holzer, Corrugated neat thin-film conjugated polymer distributed-feedback lasers. Appl. Phys. B-Lasers Opt. 74(4–5), 333–342 (2002) 18.

[150] Sahar, E., D. Treves, and I. Wieder. "Fluorescence quenching in laser dyes by absorption from an excited singlet state." *Optics Communications* 16, no. 1 (1976), 124-127. doi:10.1016/0030-4018(76)90066-3.

[151] Petukhov, V. A., M. B. Popov, and A. I. Krymova. "Determination of the quantum efficiency of the fluorescence of the solutions of organic dyes by diffraction on a thermal phase grating induced by laser radiation." *Soviet Journal of Quantum Electronics* 16, no. 4 (1986), 503-509. doi:10.1070/qe1986v016n04abeh006528.

[152]Jagtap, Krishna K., Alok K. Ray, S. K. Pardeshi, and K. Dasgupta. "Kiton red S dye: Photophysical, photostability, photothermal and narrow-band laser performances using different solvents." *Pramana* 75, no. 5 (2010), 991-998. doi:10.1007/s12043-010-0186-5.

[153] Rai, V. N. "Optical properties of Rhodamine B and Rhodamine 6G on silver surfaces." *Pramana* 31, no. 4 (1988), 313-322. doi:10.1007/bf02847749.

[154] Vrehen, Q.H.F. "Spectral distribution of the stimulated emission of a rhodamine B dye laser." *Optics Communications* 3, no. 3 (1971), 144-146. doi:10.1016/0030-4018(71)90165-9.

[156] Yang, Fuyong, Ying Chu, Lei Huo, Yang Yang, Yang Liu, and Jinglin Liu. "Preparation of uniform rhodamine B-doped SiO2/TiO2 composite microspheres." *Journal of Solid State Chemistry* 179, no. 2 (2006), 457-463. doi:10.1016/j.jssc.2005.11.006.

[157] Arbeloa, I.Lopez, and K.K. Rohatgi-Mukherjee. "Solvent effect on photophysics of the molecular forms of rhodamine B. Solvation models and spectroscopic parameters." *Chemical Physics Letters* 128, no. 5-6 (1986), 474-479. doi:10.1016/0009-2614(86)80656-x.

[158] O'Neil, Michael P. "Synchronously pumped visible laser dye with twice the efficiency of Rhodamine 6G." *Optics Letters* 18, no. 1 (1993), 37. doi:10.1364/ol.18.000037.

[159] Kurian, Achamma, Nibu A. George, Binoy Paul, V. P. Nampoori, and C. P. Vallabhan. "Studies on Fluorescence Efficiency and Photodegradation of Rhodamine 6G Doped PMMA Using a Dual Beam Thermal Lens Technique." *Laser Chemistry* 20, no. 2-4 (2002), 99-110. doi:10.1080/02786270215153.

[160] Sathy, P., Reji Philip, V. P. Nampoori, and C. P. Vallabhan. "Fluorescence quantum yield of rhodamine 6G using pulsed photoacoustic technique." *Pramana* 34, no. 6 (1990), 585-590. doi:10.1007/bf02846435.

[161] Beija, Mariana, Carlos A. Afonso, and José M. Martinho. "Synthesis and applications of Rhodamine derivatives as fluorescent probes." *Chemical Society Reviews* 38, no. 8 (2009), 2410. doi:10.1039/b901612k.

[162] Scavennec, Andre, and Norris S. Nahman. "Active and passive mode locking of continuously operating rhodamine 6G dye lasers." 1974. doi:10.6028/nbs.ir.73-347.

[163] N. Sharma, G. Bhatt, and P. Kothiyal, “Gold nanoparticles synthesis, properties, and forthcoming applications-a review,” *Indian J. Pharm. Biol. Res.*, vol. 3, no. 2, p. 13, 2015.

[164] C. Etrich, S. Fahr, M. K. Hedayati, F. Faupel, M. Elbahri, and C. Rockstuhl, “Effective optical properties of plasmonic nanocomposites,” *Materials (Basel).*, vol. 7, no. 2, pp. 727–741, 2014.

[165] P. Zijlstra, M. Orrit, and A. F. Koenderink, “Metal nanoparticles for microscopy and spectroscopy,” in *Nanoparticles*, Springer, 2014, pp. 53–98.

[166] A. Di Giuseppe, *Metrology and Physical Constants*, vol. 185. IOS Press, 2013.

[167] M. A. Mahmoud, M. Chamanzar, A. Adibi, and M. A. El-Sayed, “Effect of the dielectric constant of the surrounding medium and the substrate on the surface plasmon resonance spectrum and sensitivity factors of highly symmetric systems: silver nanocubes,” *J. Am. Chem. Soc.*, vol. 134, no. 14, pp. 6434–6442, 2012.

[168] Resch-Genger, Ute, Markus Grabolle, Sara Cavaliere-Jaricot, Roland Nitschke, and Thomas Nann. "Quantum dots versus organic dyes as fluorescent labels." *Nature Methods* 5, no. 9 (2008), 763-775. doi:10.1038/nmeth.1248.

[169] Grabolle, Markus, Peter Kapusta, Thomas Nann, Xu Shu, Jan Ziegler, and Ute Resch-Genger. "Fluorescence Lifetime Multiplexing with Nanocrystals and Organic Labels." *Analytical Chemistry* 81, no. 18 (2009), 7807-7813. doi:10.1021/ac900934a.

[170] Ghosh Chaudhuri, Rajib, and Santanu Paria. "Core/Shell Nanoparticles: Classes, Properties, Synthesis Mechanisms, Characterization, and Applications." *Chemical Reviews* 112, no. 4 (2011), 2373-2433. doi:10.1021/cr100449n.

the Delivery of Erythropoietin," *bioRxiv*, p. 44875, 2016.

[171] A. A. Ashkarran, S. Estakhri, M. R. H. Nezhad, and S. Eshghi, "Controlling the geometry of silver nanostructures for biological applications," *Phys. Procedia*, vol. 40, pp. 76–83, 2013, doi: 10.1016/j.phpro.2012.12.011.

[172] X. K. Meng, S. C. Tang, and S. Vongehr, "A Review on Diverse Silver Nanostructures," *J. Mater. Sci. Technol.*, vol. 26, no. 6, pp. 487–522, 2010, doi: 10.1016/S1005-0302(10)60078-3.

[173] B. Wiley and Y. Sun, "Synthesis of Silver Nanostructures with Controlled Shapes and Properties," vol. 40, no. 10, pp. 1067–1076, 2007.

[174] X. Huang and M. A. El-Sayed, "Gold nanoparticles: Optical properties and implementations in cancer diagnosis and photothermal therapy," *J. Adv. Res.*, vol. 1, no. 1, pp. 13–28, 2010, doi: 10.1016/j.jare.2010.02.002.

[175] S. W. Verbruggen, M. Keulemans, J. A. Martens, and S. Lenaerts, "Predicting the surface plasmon resonance wavelength of gold-silver alloy nanoparticles," *J. Phys. Chem. C*, vol. 117, no. 37, pp. 19142–19145, 2013, doi: 10.1021/jp4070856.

[176] K. Wongwailikhit and S. Horwongsakul, “The preparation of iron (III) oxide nanoparticles using W/O microemulsion,” *Mater. Lett.*, vol. 65, no. 17–18, pp. 2820–2822, 2011.

[177] Laurent, Sophie, Delphine Forge, Marc Port, Alain Roch, Caroline Robic, Luce Vander Elst, and Robert N. Muller. "Magnetic Iron Oxide Nanoparticles: Synthesis, Stabilization, Vectorization, Physicochemical Characterizations, and Biological Applications. " *Chemical Reviews* 108, no. 6 (2008), 2064-2110. doi:10.1021 /cr068445e.

[178] A. M. Abu-Dief and S. M. Abdel-Fatah, “Development and functionalization of magnetic nanoparticles as powerful and green catalysts for organic synthesis,” *Beni-Suef Univ. J. Basic Appl. Sci.*, vol. 7, no. 1, pp. 55–67, 2018.

[179] Ali, Arbab, Tufail Shah, Rehmat Ullah, Pingfan Zhou, Manlin Guo, Muhammad Ovais, Zhiqiang Tan, and YuKui Rui. "Review on Recent Progress in Magnetic Nanoparticles: Synthesis, Characterization, and Diverse Applications." *Frontiers in Chemistry* 9 (2021). doi:10.3389/fchem.2021.629054.

[180] V. A. J. Silva, P. L. Andrade, M. P. C. Silva, A. D. Bustamante, L. De Los Santos Valladares, and J. Albino Aguiar, “Synthesis and characterization of Fe3O4 nanoparticles coated with fucan polysaccharides,” *J. Magn. Magn. Mater.*, vol. 343, pp. 138–143, 2013, doi: 10.1016/j.jmmm.2013.04.062.

[181] Bocarsly, Joshua D., Emily E. Levin, Samuel A. Humphrey, Tom Faske, Wolfgang Donner, Stephen D. Wilson, and Ram Seshadri. "Magnetostructural Coupling Drives Magnetocaloric Behavior: The

Case of MnB versus FeB." *Chemistry of Materials* 31, no. 13 (2019), 4873-4881. doi:10.1021/acs.chemmater.9b01476.

[182].Haynes, William M. Handbook of Chemistry and Physics (91 edition.). 2010, Boca Raton, Florida: CRC Press. ISBN 978-1439820773

[183] M. F. Al-Kadhemy, I. F. Alsharuee, and A. A. D. Al-Zuky, "Analysis of the effect of the concentration of rhodamine B in ethanol on the fluorescence spectrum using the 'Gauss Mod' function," *J. Phys. Sci.*, vol. 22, no. 2, pp. 77–86, 2011.

[184] A. K. Kodeary, "Energy transfer studies in binary laser dye Mixtures

[185] M. F. Al-Kadhemy, I. F. Alsharuee, and A. A. D. Al-Zuky, "Analysis of the effect of the concentration of rhodamine B in ethanol on the fluorescence spectrum using the 'Gauss Mod' function," *Journal of Physical Science*, vol. 22, no. 2. pp. 77–86, 2011.

[186] "Study of the Effect of Concentration on the Absorption Spectrum of Copper-Phthalocyanine Dye (CuPc)," *Australian Journal of Basic and Applied Sciences*. pp. 407–412, 2015.

[187] Ejbarah, R. A., J. M. Jassim, and S. M. Hamidi. "The effect of dye concentration and cell thickness on dye–polymer random laser action." *Optical and Quantum Electronics* 53, no. 2 (2021). doi:10.1007/s11082-021-02742-0.

[188] Li, Yunyang, Ujitha Abeywickrema, and Partha Banerjee. "Dynamics of laser-induced microbubbles in an absorbing liquid." *Optical Engineering* 58, no. 08 (2019), 1. doi:10.1117/1.oe.58.8.084107.

[189] Nguyen, Minh D., Hung-Vu Tran, Shoujun Xu, and T. R. Lee. "Fe3O4 Nanoparticles: Structures, Synthesis, Magnetic Properties,

Surface Functionalization, and Emerging Applications." *Applied Sciences* 11, no. 23 (2021), 11301. doi:10.3390/app112311301.

[190]. Mosleh, M., Ranjbaran, M., Hamidi, S. M., Tehranchi, M. M.,“Ellipsometric spectroscopy of rubidium vapor cell at near-normal incidence”, Scientific Reports 10 (1), 1-9, 2020.

[191]. Chauhan, Sumanyu, Souptik Mukherjee, Andrii Varanytsia, Chien Tsung Hou, Lu Zou, and Liang-Chy Chien. "Efficient random lasing in topologically directed assemblies of blue-phase liquid crystal microspheres." *Optical Materials Express* 10, no. 9 (2020), 2030. doi:10.1364/ome.399169.

[192]. Redding, Brandon, Michael A. Choma, and Hui Cao. "Spatial coherence of random laser emission." *Optics Letters* 36, no. 17 (2011), 3404. doi:10.1364/ol.36.003404.

[193]. Perumbilavil, Sreekanth, Armando Piccardi, Raouf Barboza, Oleksandr Buchnev, Martti Kauranen, Giuseppe Strangi, and Gaetano Assanto. "Beaming random lasers with soliton control." *Nature Communications* 9, no. 1 (2018). doi:10.1038/s41467-018-06170-9.

الخلاصة

في هذه الدراسة ، تم تناول وسائط انبعاث الليزر العشوائية السائلة والصلبة في شكل تجاويف مركبة على أداء أنظمة الليزر العشوائية ، ولا سيما شدة طيف انبعاثها ، وعرض طيف الانبعاث (FWHM) ، و عتبة الليزر.

تمت في الجزء الأول من العمل دراسة تأثير التجاويف المركبة السائلة على أداء الليزرات العشوائية. وقد ناقش العامل الأول ظاهرة التفتح الحراري باستخدام ليزر CW بطول موجي 405 نانومتر وقوة ضوئية 100 ميغاواط عمودياً. ركز الباحثون على كوفيت كوارتز يحتوي على محلول صبغي يحتوي على جسيمات نانوية مختلفة، لتوليد التجويف الحراري. لاحظنا أن حلقات المجال البعيد النموذجية لـ SPM تحولت فجأة إلى نمط حيود مختلف تمامًا عندما تم تسخين محلول الصبغة بما يتجاوز تعديل الطور الذاتي(SPM) ، وينشأ هذا التغيير في أنماط الحيود الجديدة عن طريق تكوين الفقاعات. بالإضافة إلى ذلك، لاحظنا تأثير(Ag, Fe_2O_3 وAg: Fe_2O_3 NPs) على سرعة تكوين الفقاعات وعددها. ويزداد مع زيادة تركيز المواد النانوية . بعد ذلك تمت دراسة تأثير التجويف الحراري على خصائص الليزر العشوائي، وأظهرت النتائج أن خصائص الليزر العشوائي تتأثر بالتجويف الحراري بشكل كبير،

كما تمت دراسة أفلام الجسيمات النانوية المنتشرة في ركيزة زجاجية باستخدام الترسيب الفيزيائي للبخار مع الطلاء الدوراني بالتراكيز الثلاثة المختلفة M(10^{-5}, 10^{-4}, 10^{-3}) من خليط صبغ رودامين G6 وبوليمر PVP. . أظهرت النتائج أن الوسط النشط للصبغة ذو التركيز المتوسط (10^{-4}) كان له أفضل تأثير وأطوال موجية متعددة منفصلة مقارنة مع التراكيز المنخفضة والعالية بسبب الاقتران الصلب الذي يظهر في التركيز المتوسط. أدى ذلك إلى تعزيز كثافة الذروة وتقليل عتبة الليزر وFWHM،

بعد ذلك، تم الحصول على الليزر الأحمر والأخضر من خلال بنية ثنائية الأبعاد متعددة الطبقات على ركيزة زجاجية منحنية وبنية نانوية ذهبية مع صبغة الرودامين. ولهذا الغرض، تم ربط طبقة من شريط كابتون بجهاز CCD عن طريق الضغط للحصول على هيكل ثنائي الأبعاد ونقله على الزجاج، ثم تمت تغطية الهيكل النانوي الذهبي داخل تلك المادة الزجاجية. تمت دراسة خصائص الليزر العشوائي من جوانب مختلفة، وأظهرت النتائج عشوائية متماسكة فعالة، وكانت نتيجة السطح المحدب إلى الداخل أفضل من الخارج من حيث الشدة وعرض النبضة، وكذلك عتبة الليزر من 0.85 إلى . 0.35 مللي جول. وهذا يدل على أن الفوتونات متناثرة من السطح الداخلي وهذا مؤشر

واضح على زيادة الكسب في هذا الوسط. علاوة على ذلك، يُعزى هذا التحسن في مخرجات الليزر إلى التغير في نمط المربع الدوري ثنائي الأبعاد، مما يؤدي إلى تقليل المسافة بينهما، بحيث يمكن للفوتونات البقاء في الوسط لأطول فترة ممكنة. يتكون التجويف من بنية مغناطيسية بلازمونية ثنائية الأبعاد تعتمد على FeB والتي تغطي طبقة رقيقة من الذهب وروداميين G6 من الأسفل والأعلى على التوالي، مما يقترح كنوع جديد من مادة الليزر العشوائية تحت المجال المغناطيسي الخارجي. أظهرت النتائج كثافة أعلى في أطياف الانبعاث مع عتبة أقل لليزر وعرض كامل عند نصف الحد الأقصى (FWHM) تبعاً لتأثيرات المجال المغناطيسي الخارجي على العينة، كما لوحظ تحسن في أطياف الانبعاث الناتج مع انخفاض عتبة الليزر من 0.66. مللي جول إلى 0.35 مللي جول، وكذلك انخفض FWHM من 7.8 إلى 4 نانومتر.

تم تصنيع الرنان الحلقي على قاعدة زجاجية لتشكيل تجاويف مركبة. تم استخدام مادة زجاج السيليكا بسماكة (2 ملم)، وتم حفر ثقب دائري بقطر (9 ملم) وعمق (2 ملم)، ثم تم وضع هذا الرنان الحلقي على ركائز زجاجية لتكوين تجويف. . ثم تم طلاء هذا التجويف الحلقي بالذهب بطريقة (dip Coating) في محلول نانو مكون (ماء + ذهب) 10 مرات، ثم تم ملء هذا التجويف الحلقي بصبغة (RhB مذابة في ماء نقي مع بوليمر (pvp) مع Ag بتركيزات مختلفة، وقد وجد زيادة في كثافة انبعاث (من 19141 الى 39420.64)، والانخفاض عتبة ليزر (من0.68 الى 0.34 مللي جول)، ووالانخفاض في FWHM (من 7.4الى 3نانومتر) بزيادة تركيز Ag nanowires .

Publications

Journal articles

1. Haddawi, Majid F., Jassim M. Jassim, N. Roostaei, and S.M. Hamidi. "Red and green plasmonic-induced random laser in two-dimensional square array onto glass substrate." ***Optik*** 283 (2023), 170929. doi:10.1016/j.ijleo.2023.170929.

2. Haddawi, Majid F., Jassim M. Jassim, and S. M. Hamidi. "Plasmonic multi-wavelength random laser by gold nanoparticles doped into glass substrate." Journal of Optics, 2023. doi:10.1007/s12596-023-01315-6

Under publications

1. Kiton red dye solution-based nanomaterials under continuous wave laser as generators of thermal cavitation for random lasing

2. Magneto-Plasmonic-Induced Random Laser in Two-dimensional FeB Square Array

3. triple compound cavity random lasing: fabrication and characterizatization

جمهورية العراق
وزارة التعليم العالي والبحث العلمي
جامعة بابل
كلية العلوم للبنات

دراسة معلمات عمل الليزر العشوائي للتجويف المركب

أطروحة

مقدمة الى قسم فيزياء الليزر في كلية العلوم للبنات- جامعة بابل
كجزء من متطلبات نيل درجة الدكتوراه في فيزياء الليزر وتطبيقاته

من قبل

ماجد فليح حداوي الجبوري

(بكالوريوس فيزياء – جامعة بغداد 2001 م)

(ماجستير علوم فيزياء الليزر– جامعة بابل 2017 م)

بإشراف

الاستاذ الدكتور

جاسم محمد جاسم

جامعة بابل \كلية علوم البنات

الاستاذ الدكتور

مهري حميدي

جامعة الشهيد بهشتي

1445 هـ

2023 م